



Carlos Alberto Toloza Toloza

Spectroanalytical methods using graphene quantum dots as photoluminescent probes for the determination of analytes of biological and pharmacological interest

Tese de Doutorado

Thesis presented to the Programa de Pós-graduação em Química of PUC-Rio in partial fulfillment of the requirements for the degree of Doutor em Química.

Advisor: Prof. Ricardo Queiroz Aucélio

Co-Advisor: Prof. Sarzamin Khan

Rio de Janeiro
March 2018



Carlos Alberto Toloza Toloza

Spectroanalytical methods using graphene quantum dots as photoluminescent probes for the determination of analytes of biological and pharmacological interest

Thesis presented to the Programa de Pós-graduação em Química of PUC-Rio in partial fulfillment of the requirements for the degree of Doutor em Química. Approved by the undersigned Examination Committee

Prof. Ricardo Queiroz Aucélio

Advisor
Departamento de Química - PUC-Rio

Prof. Maurício Lanznaster

UFF

Prof. Eric Cardona Romani

SENAI

Prof^a. Andrea Rosane da Silva

CEFET/RJ

Prof^a. Aurora Perez Gramatges

Departamento de Química - PUC-Rio

Prof. Márcio da Silveira Carvalho

Vice Dean of Graduate Studies Centro Técnico Científico –
PUC-Rio

Rio de Janeiro, March 2nd 2018

All rights reserved

Carlos Alberto Toloza Toloza

Doctorate candidate in Chemistry of the Pontifical Catholic University of Rio de Janeiro (PUC-Rio). He holds a Master's degree in Chemistry from the National University of Colombia (2011). He holds a degree in Chemistry from the University of Atlantic in (2008). He has experience in the field of Organic Chemistry and Instrumental Analytical Chemistry.

Bibliographic data

Toloza, Carlos Alberto Toloza

Spectroanalytical methods using graphene quantum dots as photoluminescent probes for the determination of analytes of biological and pharmacological interest / Carlos Alberto Toloza Toloza; advisor: Ricardo Queiroz Aucélio; co-advisor: Sarzamin Khan – 2018.

158 f. : il. color. ; 30 cm

1. Tese (doutorado) – Pontifícia Universidade Católica do Rio de Janeiro, Departamento de Química.

Inclui bibliografia

1. Química – Teses. 2. Pontos quânticos de grafeno. 3. Fotoluminescência. 4. Captopril. 5. Histamina. 6. Sulfato de canamicina. I. Aucélio, Ricardo Queiroz. II. Khan, Sarzamin. III. Pontifícia Universidade Católica do Rio de Janeiro. Departamento de Química. IV. Título.

CDD: 540

Acknowledgments

To God, for the strength of culminating this dream;

To Dr. Ricardo Queiroz Aucélio, from PUC-Rio, for the confidence he had in accepting me in his research group, for always correct orientation, motivation in the most difficult moments of the research, friendship and also dedication;

To my co-mentor Dr. Sarzamin Khan for dedicated help, contribution to work and friendship;

To Dr. Andrea Rosane da Silva for her collaboration and support in the development of the research;

To my students of scientific initiation, Renan and Yasmin, for the support in the realization of the research, the seriousness with which they treated the project and the affection established during the period of work together.

To the examining members, for their availability and for accepting the invitation.

To my parents and my brothers for their unconditional love and their support to fulfill this goal.

To all my family who have always been by my side in the most difficult moments;

My wife and life-mate Maira, for your understanding and support, over these four years, as she was a motivation of my effort every day;

To all the friends of the postgraduate course, especially to my great friends Joseany Almeida, Juan Garcia and Luis Miguel Gutierrez;

To Dr. Alessandra Licursi Cerqueira da Cunha for all the teachings transmitted in the field of chromatography and for her dedication, support and friendship;

To the friends and technicians of LEEA Claudiomar, Igor, Ana Paula, Larissa, Sônia Gomes, Leila, Júnior and Paulo Santos, always willing to help me in the laboratory;

To my friends, Marlin, Jessica, Lina, Rafael Celin, Stefany, Wendy, Jarol, Oliver, Luis Maqueira, Maria Fernanda, Mauricio and Jeferson;

To Prof. Dr. Aurora for her availability and support, during the development of the work.

Prof. Dr. Dunieskys and Prof. Dr. Eric for the support in the morphological and characterization analysis of the nanomaterials synthesized in this work and for the support that allowed a better realization of this work;

To the graduate Department of Chemistry at PUC-Rio, for the opportunity and the support of the research; and of course, to the professors of the department whose teachings gave me great academic growth, and especially to Fatima, who has always demonstrated personal and professional availability during this work;

To the Brazilian Agencies CNPq, CAPES and FAPERJ for grants and doctoral scholarship;

Finally, I thank all the people who have passed through my life and influenced me in some way, but, eventually, were not mentioned in here.

Abstract

Toloza, Carlos Alberto Toloza; Aucélio, Ricardo Queiroz (Advisor); Khan, Sarzamin (Co-advisor). **Spectroanalytical methods using graphene quantum dots as photoluminescent probes for the determination of analytes of biological and pharmacological interest.** Rio de Janeiro, 2018. 158p. Tese de doutorado - Departamento de Química, Pontifícia Universidade Católica do Rio de Janeiro.

The objective of the present work was the development of spectroanalytical methods capable of indirectly determining analytes of biological and pharmacological interest that present inherent weak optical activity in UV-vis (in this case, captopril, histamine and kanamycin sulfate). Although many methods to quantify these analytes are reported, many of these depend on chemical derivatization, a procedure considered complex and laborious to promote UV-vis absorption and luminescence. Therefore, the proposed use of photoluminescent quantum dots is interesting since they allow, under adjusted conditions, analytical responses that allow the indirect determination of the analytes of interest in concentrations of the order of down to 10^{-8} mol L⁻¹. The determination of captopril was proposed using graphene quantum dots aminofunctionalized using glutathione as a precursor (GQDs-amino). Captopril induced photoluminescence suppression and spectral red-shift from the aqueous dispersion of GQDs-amino. In contrast, when Fe³⁺ is used as a mediator, it generates a suppression of the photoluminescence of the GQD-amino dispersion and the addition of captopril restored the original photoluminescence of the quantum dots. In adjusted experimental conditions, photoluminescence suppression of the GQDs-amino, as a function of the captopril concentration, can be related both to the magnitude of the suppression and to the spectral shift. In both cases, the linearized response covered three orders of magnitude (10^{-6} to 10^{-4} mol L⁻¹). In contrast, the probe signal restoration of the previously Fe³⁺ suppressed photoluminescent GQDs, also proved to be analytically useful. The proposed approaches were tested by the determination of captopril in simulated samples and in commercial pharmaceutical formulations. Spectral shift from the GQDs-amino probe and the

photoluminescence on/off approach (using GQDs-amino-Fe³⁺ probe) resulted in satisfactory recoveries, showing the quantitative capability of the method. In the work concerning histamine, the photoluminescent behavior of the aqueous dispersion of GQDs-amino in the presence of this amino acid was studied in function of different interaction mediators (metal ions). The results revealed that strong and selective interaction existed in the presence of Eu³⁺, Fe³⁺ and Cu²⁺. The sensitivity of normalized photoluminescence (K_s) suppression curves indicated a ten-fold stronger interaction of histamine with the surface of GQDs in the presence of Fe³⁺. The linear response observed in the GQDs-amino-Fe³⁺ (luminescence measured at 345/435 nm) covered the histamine concentration of 4.3×10^{-7} mol L⁻¹ (quantification limit) to 3.2×10^{-5} mol L⁻¹. The GQDs-amino-Fe³⁺ was applied as a probe in the analysis of tuna fish samples after solid phase extraction (SPE) of the analyte using a cationic solid phase. The analytical results were statistically similar to those obtained with a method based on liquid chromatography with fluorimetric detection (after chemical derivatization of histamine). The determination of kanamycin sulfate was made by measuring the effect it exerts on the photoluminescence of gold nanoparticles (AuNPs) associated GQDs, that were produced by the reduction of AuCl₄ with NaBH₄ in an aqueous dispersion of GQDs-amino (obtained by pyrolysis of citric acid and glutathione) also containing the cationic surfactant CTAB. The AuNPs-GQDs-amino-CTAB system showed a suppressed photoluminescence, which was amplified in the presence of kanamycin. Under adjusted experimental conditions, the magnification of the photoluminescence of the nanomaterial as a function of the analyte concentration was linear and covered three orders of magnitude (10^{-7} to 10^{-5} mol L⁻¹). The use of solid phase extraction with a cartridge packed with a molecularly imprinted polymer (selective for aminoglycosides) ensured selectivity in the determinations made in yellow fever vaccine and in veterinary pharmaceutical formulations. The analytical results were statistically similar to those obtained with an HPLC based method with fluorimetric detection (after chemical derivatization of kanamycin). The proposed methods for quantification present simple procedure, are very sensitive and selective, not involving the use of toxic reagents used for chemical derivatization.

Keywords

Graphene quantum dots; Photoluminescence; Captopril; Histamine; Kanamycin sulfate.

Resumo

Toloza, Carlos Alberto Toloza; Aucélio, Ricardo Queiroz; Khan, Sarzamin. **Métodos espectroanalíticos utilizando pontos quânticos de grafeno como sondas fotoluminescentes para a determinação de analitos de interesse biológico e farmacológico.** Rio de Janeiro, 2018. 158p. Tese de Doutorado - Departamento de Química, Pontifícia Universidade Católica do Rio de Janeiro.

O presente trabalho teve como objetivo o desenvolvimento de métodos espectroanalíticos capazes de determinar indiretamente analitos de interesse biológico e farmacológico que possuem fraca atividade óptica no UV-vis (no caso, captopril, histamina e sulfato de canamicina). Embora muitos métodos para quantificar esses analitos estejam reportados, muitos dependem da derivatização química do analito, procedimento considerado complexo e trabalhoso para fazer tais analitos absorverem e emitirem no UV-vis. Por isso, a proposta de uso de pontos quânticos fotoluminescentes é interessante, pois permitem, em condições ajustadas, respostas analíticas que proporcionam a determinação indireta dos analitos de interesse em concentrações da ordem de até 10^{-8} mol L⁻¹. A determinação do captopril foi proposta utilizando pontos quânticos de grafeno aminofuncionalizados com uso de glutationa (GQDs-amino). O captopril induziu a supressão e o deslocamento espectral (para o vermelho) da fotoluminescência da dispersão aquosa dos GQDs-amino. Por outro lado, quando Fe³⁺ foi usado como um mediador que gera uma supressão da fotoluminescência da dispersão de GQDs-amino, a adição de captopril restabelece a fotoluminescência original dos pontos quânticos. Em condições experimentais ajustadas, a magnitude da supressão ou de deslocamento espectral da fotoluminescência dos GQDs-amino pode ser relacionada com a concentração de captopril. Em ambos os casos, a resposta linearizada abrangeu três ordens de grandeza (10^{-6} a 10^{-4} mol L⁻¹). Em contrapartida, a abordagem de restauração do sinal da sonda, previamente suprimida com Fe³⁺, também se mostrou útil do ponto de vista analítico. As abordagens propostas foram testadas com a determinação de captopril em amostras simuladas e em formulações farmacêuticas comerciais. O deslocamento

espectral a partir da sonda GQDs-amino e ativação/desativação da fotoluminescência utilizando GQDs-amino-Fe³⁺ resultou em recuperações satisfatórias, mostrando o potencial de detecção quantitativo do método. No estudo com a histamina, avaliou-se o comportamento fotoluminescente da dispersão aquosa de GQDs-amino na presença de histamina com interação mediada por diferentes íons metálicos. Os resultados revelaram que uma interação mais forte e seletiva existia na presença de Eu³⁺, Fe³⁺ e Cu²⁺. A sensibilidade das curvas de supressão de fotoluminescência normalizada (K_s) indicou uma interação dez vezes mais forte da histamina com a superfície dos GQDs na presença de Fe³⁺. A resposta linear observada nos GQDs-amino-Fe³⁺ (luminescência medida a 345/435 nm) abrangeu a concentração de histamina de $4,3 \times 10^{-7}$ mol L⁻¹ (limite de quantificação) até $3,2 \times 10^{-5}$ mol L⁻¹. A dispersão de GQDs-amino-Fe³⁺ foi usada como sonda na análise de amostras de atum após extração do analito em cartucho fase sólida catiônica. Os resultados analíticos foram estatisticamente semelhantes aos obtidos com um método baseado na cromatografia líquida com detecção fluorimétrica (após derivatização química da histamina). A determinação do sulfato de canamicina foi feita medindo o efeito que ela exerce sobre a fotoluminescência dos GQDs-amino associados às nanopartículas de ouro (AuNPs), que foram produzidas pela redução de AuCl₄ com NaBH₄ em uma dispersão aquosa de GQDs-amino (obtido pela pirólise de ácido cítrico e glutatona) contendo também o agente tensoativo catiônico CTAB. O sistema AuNPs-GQDs-amino-CTAB apresentou fotoluminescência suprimida, que foi amplificada na presença de canamicina. Sob condições experimentais ajustadas, a ampliação da fotoluminescência do nanomaterial em função da concentração de analito se mostrou linear e abrangeu três ordens de grandeza (10^{-7} a 10^{-5} mol L⁻¹). O uso de extração em fase sólida com um cartucho empacotado com um polímero molecularmente impresso (seletivo para aminoglicosídeos) assegurou a seletividade nas determinações de sulfato de canamicina feitas em vacina da febre amarela e em formulações farmacêuticas veterinárias. Os resultados analíticos foram estatisticamente semelhantes aos obtidos com um método baseado em HPLC com detecção fluorimétrica (após derivatização química da canamicina). Os métodos propostos para a quantificação apresentaram procedimento simples, são muito sensíveis e seletivos, não envolvendo uso de reagentes tóxicos empregados para derivatização química.

Palavras-chave

Pontos quânticos de Grafeno; Fotoluminescência; Captopril; Histamina; Sulfato de canamicina.

Table of contents

1	Introduction	26
1.1	Contextualization of work	26
1.2	Thesis structure	28
1.3	Objective of this work	29
1.3.1	General Objective	29
1.3.2	Specific objectives	29
2	Theoretical fundamentals	31
2.1	Photoluminescence from molecules	31
2.2	Use of nanomaterials as photoluminescent probes	32
2.2.1	Quantum dots	33
2.2.2	Graphene quantum dots and their optical properties	37
2.2.3	Synthesis of graphene quantum dots	38
2.2.4	Functionalization of graphene quantum dots	40
2.3	Analytical approaches through the direct use of graphene quantum dots as nanosensors	41
2.4	Graphene quantum dots as photoluminescent probe with metal ion mediation	44
2.5	Approaches using graphene quantum dots coupled with gold nanoparticles	46
3	Experimental	48
3.1	Apparatus	48
3.2	Reagents and materials	49
3.3	Aqueous synthesis of nanomaterials	50
3.3.1	Synthesis of graphene quantum dots	50
3.3.2	Synthesis of AuNPs.	51
3.3.3	Synthesis of AuNPs-GQDs-amino.	51
3.4	Characterization procedures	52
3.4.1	Quantum yield determination	52
3.4.2	Raman, AFM, XPS and STEM measurements.	53
3.4.3	Time resolved luminescence measurements	53

3.5 Preparation of molecular imprinted polymer for group-selective recognition of aminoglycosides	54
3.6 Photoluminescence measurements and preparation of samples	56
3.6.1 Procedures for captopril	56
3.6.1.1 Analytical probes, standard solutions and photoluminescence measurements for captopril	56
3.6.1.2 Determination of captopril in tablets	57
3.6.1.3 The Ellman's method for determination of captopril	57
3.6.2 Procedures for histamine	58
3.6.2.1 Analytical probes, standard solutions and photoluminescence measurements for histamine	58
3.6.2.2 Procedure for preparation of tuna samples	59
3.6.2.3 Solid phase extraction of histamine	59
3.6.2.4 Chromatographic method for the determination of histamine	60
3.6.3 Procedures for kanamycin	61
3.6.3.1 Analytical probes, standard solutions and photoluminescence measurements for kanamycin.	61
3.6.3.2 Solid phase extraction of kanamycin using MIP	61
3.6.3.3 Sample preparation for analysis of kanamycin in pharmaceutical formulation and yellow fever vaccine	62
3.6.3.4 Chromatographic method for the determination of kanamycin sulfate	62
3.6.3.5 Study of the catalytic reduction of 4-nitrophenol with AuNPs	63
4 Characterization of the nanomaterials	64
4.1 Optical properties of the GQDs and GQDs-amino	64
4.2 Structural characterizations of the GQDs and GQDs-amino	66
4.3 Characterization of AuNPs	70
5 Different approaches for sensing captopril based on functionalized graphene quantum dots as photoluminescent probe	72
5.1 Captopril and analytical methods for its determination	72
5.2 Results and Discussion	75

5.2.1 Preliminary studies of the interaction between captopril and graphene quantum dots	75
5.2.2 GQDs-amino photoluminescence quenching and spectral displacement induced by captopril	76
5.2.2.1 Stability of photoluminescence signal in function of time and pH	76
5.2.2.2 Effect of Temperature	79
5.2.2.3 Photoluminescence time-decay	80
5.2.2.4 Analytical sensing of captopril using GQDs-amino aqueous probe	81
5.2.3 GQDs-amino-Fe ³⁺ switch on/off photoluminescence probe for captopril	83
5.2.3.1 Captopril response in the GQDs-amino and Fe ³⁺ probe	84
5.2.3.2 Stability of photoluminescence signal in function of time	85
5.2.3.3 Photoluminescence time-decay	86
5.2.3.4 Effect of temperature	87
5.2.3.5 Analytical sensing of captopril using the switching on/off GQDs-amino-Fe ³⁺ aqueous probe	88
5.2.4 Effect of coexisting substances	89
5.2.5 Comparative sensing performance	90
5.3 Partial conclusion	92
6 Photoluminescence suppression effect caused by histamine on amino-functionalized graphene quantum dots with the mediation of Fe ³⁺ , Cu ²⁺ , Eu ³⁺ : Application in the analysis of spoiled tuna fish	94
6.1 Histamine and analytical methods for its determination	94
6.2 Results and Discussion	96
6.2.1 Studies of the interaction between GQDs-amino and metal ions	96
6.2.1.1 The effect of cations on the photoluminescence of GQDs-amino	96
6.2.1.2 Evaluation of the interaction between histamine and GQDs-amino mediated by Cu ²⁺ , Fe ³⁺ and Eu ³⁺	98
6.2.1.3 Electrokinetic measurements	102
6.2.1.4 Evaluation of photoluminescence quenching mechanism	103

6.2.2 GQDs-amino response towards histidine mediated by Cu ²⁺ , Fe ³⁺ and Eu ³⁺ .	105
6.2.3 Analytical characteristics of the GQDs-amino-Fe ³⁺ for sensing histamine	107
6.2.4 Selectivity studies	108
6.2.5 Application in tuna fish samples	110
6.3 Partial conclusions	112
7 Determination of kanamycin using photoluminescent amino-functionalized graphene quantum dots coupled with gold nanoparticles in organized medium and solid phase extraction using an aminoglycoside-selective molecular imprinted polymer	114
Manuscript submitted to <i>Anal. Chim. Acta</i>	114
7.1 Kanamycin and analytical methods for its determination	114
7.2 Results and Discussion	117
7.2.1 Preliminary studies	117
7.2.2 Study of the conditions to produce the AuNPs-GQDs-amino analytical probe for kanamycin	119
7.2.3 Optimized experimental parameters for the analytical probe	127
7.2.3.1 Amount of AuNPs-GQDs-amino-CTAB of the probe	127
7.2.3.2 Influence of pH on the photoluminescence amplification induced by kanamycin	128
7.2.3.3 Stability of photoluminescence intensity and reaction time	129
7.2.4 The nature of the photoluminescence	130
7.2.5 Analytical characteristics of the AuNPs-GQDs-amino-CTAB aqueous probe for the sensing kanamycin sulfate	132
7.2.6 Selectivity studies and solid phase extraction with a cartridge packed with a molecularly imprinted polymer	134
7.2.7 Application of the method	136
7.3 Partial conclusions	137
8 General Conclusion	139
9 Future work	142
10 References	143

11 Attachment	155
A Published papers	155
B Participation in Congress	157

List of figures

Figure 2. 1. Jablonski diagram	32
Figure 2. 2. Schematic of excitation and emission of quantum dots with the typical energy band structure of semiconductor. V_B is the valence band, C_B is the conduction band, ΔE is the Stokes shift, E_g is the band gap energy, E_{ex} is the excitation energy, $E_{em 0-4}$ are the various emission energies	35
Figure 3.1. Synthesis procedure aqueous dispersion of GQDs-amino	51
Figure 3.2. Image of the gold nanoparticle synthesis (AuNPs-GQDs-amino) made in the reactor. (A) Mixing the reactants before of addition of $NaBH_4$. (B) AuNPs after addition of $NaBH_4$	52
Figure 3. 3 Infrared spectrum of kanamycin sulfate (red) and kanamycin MIP after clean-up to remove the kanamycin template	55
Figure 3.4. Scanning electron microscopy of the sol-gel matrix kanamycin-MIP (fraction collected in the sieve of $150 \mu m$) using different enlargements: (A) 35 times, (B) 50 times, C) 140 times and D) 7000 times.	55
Figure 4.1. (A) Absorption spectra of aqueous dispersion GQDs-amino; (B) Photoluminescence spectrum of excitation and emission GQDs-amino	66
Figure 4. 2. FE-STEM images and size distribution of: a) GQDs in $NaOH$ and b) GQDs-amino in pure water	67
Figure 4. 3. Raman spectra of GQDs, GQDs-amino, GSH and citric acid (10 times amplification for GSH and citric acid spectra)	68
Figure 4.4. Characterization of GQDs-amino: (A) Raman spectra; (B) FE-STEM images and size distribution; (C) AFM topography image	69
Figure 4.5. (A) XPS general survey scan of GQDs-amino. (B) High resolution C 1s peaks with a, b, and c corresponding to C-C sp^2 e sp^3 , C-N (-O), and COOH groups, respectively. (C) High resolution N 1s peaks with a and b corresponding to C-N pyridinic and graphitic respectively.	70
Figure 4.6. (A) AuNPs synthesized from $HAuCl_4$ (5 fold dilution) with $NaBH_4$ as the reducing agent (B) FE-STEM images and size distribution of AuNPs aqueous dispersion.	71

Figure 5. 1. Captopril structure.	73
Figure 5. 2. Study of pH (adjusted with HCl 0.01 mol L ⁻¹) to evaluate the effect of the photoluminescence quenching of GQDs-amino in the presence of 5.0 × 10 ⁻⁵ mol L ⁻¹ captopril, where L ₀ and L are the photoluminescence measurements before and the addition of analyte.	77
Figure 5.3. Spectral shift observed from GQDs-amino the in the presence of of captopril (5.0 × 10 ⁻⁵ mol L ⁻¹) in function of pH (adjusted with HCl 0.01 mol L ⁻¹).	78
Figure 5. 4. Effect of pH (adjusted with NaOH 0.01 mol L ⁻¹) of the GQDs-amino aqueous dispersion: (A) quenching of signal of GQDs-amino in the presence of captopril (5.0 × 10 ⁻⁵ mol L ⁻¹), where L ₀ and L are the photoluminescence measured before and after the addition of analyte. (B) relative spectral shift (λ ₀ - λ) of the photoluminescence maximum of the in the presence of captopril (5.0 × 10 ⁻⁵ mol L ⁻¹), where λ ₀ and λ are the wavelength measured before and the addition of analyte.	79
Figure 5. 5. Effect of temperature on the photoluminescence from aqueous GQDs-amino probe: (A) the quenching effect in the presence of 5.0 × 10 ⁻⁵ mol L ⁻¹ captopril, where L ₀ and L are the photoluminescence measurements before and the addition of captopril and (B) the spectral red-shift in the presence of 5.0 × 10 ⁻⁵ mol L ⁻¹ of captopril.	80
Figure 5.6. Photoluminescence time decay of: A) (a) GQDs-amino and (b) GQDs-amino in the presence of captopril (5.0 × 10 ⁻⁵ mol L ⁻¹).	81
Figure 5.7. (A) Photoluminescent spectral response from the GQDs-amino probe for different concentrations of captopril: (a) 0; (b) 1.7 × 10 ⁻⁵ ; (c) 2.5 × 10 ⁻⁵ ; (d) 3.3 × 10 ⁻⁵ ; (e) 5.0 × 10 ⁻⁵ ; (f) 8.3 × 10 ⁻⁵ ; (g) 1.2 × 10 ⁻⁴ and (h) 1.7 × 10 ⁻⁴ mol L ⁻¹ . (B) Stern-Volmer curve. (C) analytical curve based on the spectral red-shift.	83
Figure 5.8. GQDs-amino photoluminescence spectrum with excitation at 345 nm: A) GQDs-amino with addition of Fe ³⁺ : (a) 0 mol L ⁻¹ ; (b) 1.7 × 10 ⁻⁵ ; (c) 3.3 × 10 ⁻⁵ ; (d) 5.0 × 10 ⁻⁵ ; (e) 6.7 × 10 ⁻⁵ ; (f) 1.0 × 10 ⁻⁴ ; and (g) 1.3 × 10 ⁻⁴ mol L ⁻¹ and B) GQDs-amino-Fe ³⁺ after edition of captopril: (a) 0 mol L ⁻¹ to (b) 1.0 × 10 ⁻⁴ mol L ⁻¹ .	84
Figure 5.9. Photoluminescence intensity studies in function of time: A) GQDs-amino dispersion after addition of Fe ³⁺ (3.0 × 10 ⁻⁴ mol L ⁻¹) B) GQDs-amino-Fe ³⁺ dispersion after addition of captopril (5.0 × 10 ⁻⁵ mol L ⁻¹).	86

- Figure 5.10. Photoluminescence time decay of: (a) GQDs-amino, (b) GQDs-amino-Fe³⁺ and (c) GQDs-amino-Fe³⁺ plus addition of captopril ($5.0 \times 10^{-5} \text{ mol L}^{-1}$). 87
- Figure 5.11. Effect of temperature on the photoluminescence GQDs-amino-Fe³⁺ aqueous dispersion: (A) absence of captopril and (B) presence of captopril ($5.0 \times 10^{-5} \text{ mol L}^{-1}$). 88
- Figure 5. 12. A) Photoluminescence from the GQDs-amino-Fe³⁺ probe with increasing concentrations of captopril: (a) 0 (b) 8.3×10^{-6} , (c) 5.0×10^{-5} , (d) 8.2×10^{-5} , (e) 1.3×10^{-4} , (F) 1.6×10^{-4} , (g) 2.1×10^{-4} , (h) 2.8×10^{-4} , (i) $3.9 \times 10^{-4} \text{ mol L}^{-1}$. B) analytical curve based on the photoluminescence enhancement induced by captopril. 89
- Figure 6.1. Histamine structure. 95
- Figure 6.2. Photoluminescence quenching of GQDs-amino by metal ions. The concentration of the metal ions is $1.0 \times 10^{-4} \text{ mol L}^{-1}$. L_0 and L represent the intensities in the absence and presence of tested metal ions. 98
- Figure 6.3. Study of pH (adjusted with HCl 0.01 mol L^{-1} and NaOH 0.01 mol L^{-1}) to evaluate the effect of the photoluminescence quenching of GQDs-amino mediated by A) Cu²⁺; B) Eu³⁺ and C) Fe³⁺ ions in the presence of $5.0 \times 10^{-5} \text{ mol L}^{-1}$ histamine, where L_0 and L are the photoluminescence measurements before and the addition of analyte respectively. 99
- Figure 6.4. Reaction time of the GQD-amino-Mⁿ⁺ dispersion after addition of histamine ($1.0 \times 10^{-5} \text{ mol L}^{-1}$), where Mⁿ⁺ is A) Eu³⁺, B) Cu²⁺ and C) Fe³⁺. 100
- Figure 6.5. Photoluminescent response of the GQD-amino in the presence of increasing concentrations of histamine mediated by: A) Fe³⁺ (a) blank, (b) 4.3×10^{-7} , (c) 2.0×10^{-6} , (d) 4.0×10^{-6} , (e) 8.0×10^{-6} , (f) 1.6×10^{-5} , (g) $3.2 \times 10^{-5} \text{ mol L}^{-1}$. B) Eu³⁺ (a) blank, (b) 5.0×10^{-6} , (c) 1.0×10^{-5} , (d) 2.0×10^{-5} , (e) 5.0×10^{-5} , (f) 7.0×10^{-5} , (g) $1.2 \times 10^{-4} \text{ mol L}^{-1}$. B) Cu²⁺ (a) blank, (b) 2.0×10^{-5} , (c) 1.0×10^{-4} , (d) 2.0×10^{-4} , (e) 4.5×10^{-4} , (f) $6.0 \times 10^{-4} \text{ mol L}^{-1}$ Inserts: The normalized plots for the GQDs-amino photoluminescence quenching mediated by respectively Fe³⁺, Eu³⁺, and Cu²⁺. 101
- Figure 6.6. UV-vis absorption spectra of GQDs-amino, GQDs-amino-Mⁿ⁺, GQDs-amino-Mⁿ⁺-histamine complex, where Mⁿ⁺ is A) Eu³⁺, B) Fe³⁺ and C) Cu²⁺. 102
- Figure 6.7. A) Photoluminescence time decay of: (a) GQDs-amino; (b) GQDs-amino-Fe³⁺ and (c) GQDs-amino-Fe³⁺ plus addition of histamine ($5 \times 10^{-6} \text{ mol L}^{-1}$); B) Normalized curve

for GQDs-amino-Fe³⁺ in the presence of histamine mediated by Fe³⁺ at 20 °C (a) 25 °C (b) 30 °C (c) and 35 °C (d) in aqueous system. 104

Figure 6.8. Liquid chromatogram of a tuna fish spoiled sample extract showing the main histamine peak at about 1 min retention time. (B) Mass spectrum of the histamine peak. 112

Figure 7. 11. A) Photoluminescence from the AuNPs-GQDs-amino-CTAB probe with increasing concentrations of kanamycin: (a) 0 (b) 2.5×10^{-7} , (c) 7.5×10^{-7} , (d) 1.5×10^{-6} , (e) 3.0×10^{-6} , (f) 4.0×10^{-6} , (g) 5.0×10^{-6} , (h) 6.0×10^{-6} , (i) 7.0×10^{-6} mol L⁻¹, (j) 8.0×10^{-6} , (k) 9.0×10^{-6} mol L⁻¹, (l) 1.0×10^{-5} mol L⁻¹. B) Analytical curve based on the photoluminescence enhancement of AuNPs-GQDs-amino-CTAB (expressed as $L-L_0/L_0$ in function of the concentration of kanamycin). 133

Figure 7. 1. Kanamycin sulfate structure. 114

Figure 7.2. Photoluminescence spectra measured at 345/425 nm from: A) GQDs-amino in the presence of increasing amounts of added AuNPs dispersion (in mol L⁻¹): (a) 0; (b) 3.7×10^{-11} ; (c) 7.5×10^{-11} ; (d) 1.2×10^{-10} ; (e) 1.5×10^{-10} ; (f) 1.9×10^{-10} ; (g) 2.3×10^{-10} ; (h) 2.8×10^{-10} ; (i) 3.0×10^{-10} ; (j) 3.5×10^{-10} mol L⁻¹; (k) 3.8×10^{-10} ; (l) 4.3×10^{-10} and (m) 4.5×10^{-10} . B) Mixture of aqueous dispersions of AuNPs (4.5×10^{-10} mol L⁻¹) and GQDs-amino before (a) and after (b) addition of kanamycin (1.0×10^{-5} mol L⁻¹); C) Dispersion prepared by producing AuNPs by reducing HAuCl₄ directly in an aqueous dispersion of GQDs-amino before (a) and after (b) the addition of kanamycin (1.0×10^{-5} mol L⁻¹). 118

Figure 7. 3. A) Evaluation of the amount of GQDs-amino dispersion in the preparation of the synthesis of the AuNPs-GQDs-amino probe and B) Photoluminescence spectra of the AuNPs-GQDs-amino dispersion synthesized in the presence of CTAB at concentrations of: (a) 0 (b) 2.0×10^{-3} , (c) 5.0×10^{-3} , (d) 1.0×10^{-3} and (d) 5.0×10^{-4} mol L⁻¹ (final concentration in the synthesis dispersion). C) Evaluation of the effect of CTAB concentration on the probe response towards a kanamycin (concentration in the working dispersion of 1×10^{-5} mol L⁻¹). D) Photoluminescence spectra from the AuNPs-GQDs-amino probe with increasing concentrations of CTAB: (a) 0 (b) 1.0×10^{-4} , (c) 4.0×10^{-4} , (d) 7.0×10^{-4} mol L⁻¹ (final concentration in the probe). 120

Figure 7.4. Proposal of interaction between AuNPs and GQDs-amino mediated by CTAB. 122

- Figure 7. 5. Histograms regarding the size distribution obtained by DLS of the synthesized AuNP dispersions: (A) control AuNPs (B) AuNPs in CTAB $5.0 \times 10^{-4} \text{ mol L}^{-1}$, (C) AuNPs-GQDs-amino, (D) AuNPs- GQDs-amino in CTAB $5.0 \times 10^{-4} \text{ mol L}^{-1}$. 123
- Figure 7.6. UV-vis spectra of dispersions (5 fold dilution): (a) control AuNPs in ultrapure water (b) AuNPs-GQDs-amino, AuNPs in CTAB $5.0 \times 10^{-4} \text{ mol L}^{-1}$, (c) AuNPs in CTAB $5.0 \times 10^{-4} \text{ mol L}^{-1}$, (d) AuNPs-GQDs-amino in CTAB $5.0 \times 10^{-4} \text{ mol L}^{-1}$ 124
- Figure 7.7. (A) FE-STEM images and size distribution of AuNPs-GQDs-amino-CTAB aqueous dispersion. Histograms referring to the process of images of AuNPs-GQDs-amino-CTAB (B) Aspect ratio and (C) Circularity. 125
- Figure 7. 8. UV-vis spectra of 4-nitrophenol and 4-nitrophenolate ion 126
- Figure 7. 9. Time profile of the absorbance of 4-phenolate ion absorption (measured at 410 nm) in the presence of: A) AuNPs-CTAB and B) AuNPs-GQDs-amino-CTAB, both sintetized in CT AB ($5 \times 10^{-4} \text{ mol L}^{-1}$ final concentration) 127
- Figure 7. 10. A) Effect of amount of the AuNPs-GQDs-amino-CTAB on the photoluminescence intensity (measured as $\Delta L = L - L_0$, where L_0 and L are respectively the photoluminescence of the quantum dots dispersion before and after the addition of $5.0 \times 10^{-6} \text{ mol L}^{-1}$ of kanamycin). B) Influence of the pH on the photoluminescence amplification (measured as $L - L_0$, where L_0 is AuNPs-GQDs-amino dispersion in the absence of kanamycin and L in the presence of kanamycin at $5.0 \times 10^{-6} \text{ mol L}^{-1}$) 128
- Figure 7. 11. A) Stability of the photoluminescence intensity of the AuNPs-GQDs-amino-CTAB dispersion. B) Stability of the photoluminescence of the AuNPs-GQDs-amino-CTAB after mixing kanamycin (final concentration in dispersion $5.0 \times 10^{-6} \text{ mol L}^{-1}$). C) Effect of the temperature on the photoluminescence enhancement of the aqueous AuNPs-GQDs-amino-CTAB working dispersion after addition of kanamycin ($3.0 \times 10^{-6} \text{ mol L}^{-1}$ final concentration) 130
- Figure 7. 12. UV-vis extinction spectra (5-fold dilution) of the: A) AuNPs in CTAB $5.0 \times 10^{-4} \text{ mol L}^{-1}$ and B) AuNPs-GQDs-amino in CTAB $5.0 \times 10^{-4} \text{ mol L}^{-1}$ before (a) and after (b) the addition of kanamycin sulfate (final concentration on the probe $5.0 \times 10^{-6} \text{ mol L}^{-1}$). 132

Figure A.1. Published paper: Chapter 4.	155
Figure A. 2. Published paper: Chapter 5.	156

List of tables

Table 4. 1. Normalized photoluminescence from GQDs and GQDs-amino aqueous dispersions obtained by the pyrolysis, using pure water and using solutions with different solutes (signals normalized by the one obtained from GQDs in pure water)	65
Table 5. 1. Experimental conditions for the GQDs-amino probe and GQDs-amino-Fe ³⁺ probe used for the sensing of captopril	82
Table 5. 2. Effect of co-existing substances on the photoluminescence of GQDs-amino and GQDs-amino-Fe ³⁺ aqueous dispersion	90
Table 5. 3. Analytical figures of merit for the captopril sensing using the GQDs-amino probe and the GQDs-amino-Fe ³⁺ probe	91
Table 6. 1. Electrokinetic potential (ζ -potential) values obtained of GQDs-amino in aqueous dispersion and in the presence of Eu ³⁺ , Fe ³⁺ and Cu ²⁺ ions.	103
Table 6. 2. Evaluation the interference imposed by histidine in the histamine ($1.0 \times 10^{-5} \text{ mol L}^{-1}$) photoluminescence signal.	106
Table 6. 3. Evaluation of the quenching effect of histamine ($5.0 \times 10^{-6} \text{ mol L}^{-1}$) in the presences of amino acids	110
Table 6. 4. Recovery results (n =3) for histamine fortified fresh tuna fish samples	111
Table 6. 5. Application of method developed for the determination of histamine in three samples of tuna fish after up to 24 h of storage at room temperature	111
Table 7. 1. Electrokinetic potential (ζ -potential) values obtained of nanostructures under different conditions	121
Table 7. 2. Experimental conditions for the AuNPs-GQDs-amino probe used for the quantification of kanamycin sulfate	133
Table 7. 3. Recovery results (n = 3) for kanamycin sulfate in fortified vaccine samples and a sample of actual pharmaceutical formulation	137

List of abbreviations

ACE – acetylcholinesterase
AFM - atomic force microscopy
AMG – Aminoglycosides
APTMS - 3-(aminopropyl) trimethoxysilane
AuNPs- gold nanoparticles
CB - conduction band
CE - capillary electrophoresis
CQDs - carbon quantum dots
CTAB- hexadecyltrimethylammonium bromide
CZE - capillary zone electrophoresis
DLS- Dynamic light scattering
DTNB - 5,5-dithio (bis-2-nitrobenzoic acid)
ECL- electrochemiluminescence
EIS - electrochemical impedance spectroscopy
FE-SEM - field emission scanning electron microscopy
FIA- flow injection analysis
GO - graphene oxide
GQDs- graphene quantum dots
GQDs-amino – amino-functionalized graphene quantum dots
GSH – glutathione
HPLC- high performance liquid chromatography
HPLC-MS - high performance liquid chromatography with mass spectrometry
ISC - intersystem crossing
LED – lighting emitting diode
LOD – limit of detection
LOQ – limit of quantification
LSPR - localized surface plasmon resonance
MIP - molecularly imprinted polymer
MOF – molecular organic framework
N-GQDs – nitrogen doped graphene quantum dots
4-NP – paranitrophenol

OPA- o-phthalaldehyde
QDs – quantum dots
RCF- relative centrifugal force
rGQDs - reduced graphene quantum dots
RSD- relative standard deviation
SPE- solid phase extraction
LSPR- surface plasmon resonance
STEM - scanning transmission electron microscopy
TCA - trichloroacetic acid
TEOS - tetraethyl orthosilicate
THF- tetrahydrofuran
UPLC - ultra-performance liquid chromatography
UV-vis - ultraviolet visible
VB - valence band
XPS - X-ray photoelectron spectroscopy
ZIF-8C - zeolitic imidazolate frameworks

1 Introduction

1.1 Contextualization of work

The main objective of the use of optical active nanomaterials in analytical chemistry is to explore their peculiar properties in the development of analytical methods for the determination of several types of analytes in various samples. Since different types of nanoparticles have become available through their photoluminescent properties, they have been increasingly proposed as photoluminescent probes. The development of analytical procedures based on these nanomaterials may provide advantages to analytical detection in terms of selectivity, sensitivity and reliability. Recently, carbon nanomaterials so called graphene quantum dots (GQDs) have had important use as analytical sensors, attracting great interest in the research field as an important and promising nanomaterial of the carbon family. In analytical chemistry GQDs have been used to enable indirect detection of chemical species since their photoluminescent properties can be altered by functionalization allowing them, to interact selectively with the species of interest.

Captopril is a drug widely used in the treatment of hypertension and congestive heart failure that blocks the conversion of angiotensin II causing a contraction of the blood vessels. It was the first acetylcholinesterase (ACE) inhibitor drug in the market. Although several other efficient ACE inhibitors have been developed, captopril has the best cost-effectiveness and therefore is widely indicated for the population in general. Biogenic amines or biologically active amines such as histamine and histidine are organic bases with aliphatic, aromatic or heterocyclic structures, produced mainly by microbial decarboxylation of aminoacids in various foods. They may be of endogenous origin, coming in low concentrations in unfermented foods such as fruits, vegetables, meat, milk and fish. They act as natural substances for the growth of microorganisms and plants (nitrogen reserve) and play an important role in various physiological functions in

humans and animals, participating in the regulation of gastric secretion, contraction and relaxation of smooth muscle. Some crucial cellular activities are also dependent on biogenic amines. Aminoglycosides (AMG) are a class of antibiotics that inhibit bacteria growth acting on their ribosomes causing the production of anomalous proteins. They have activity especially against gram negative and aerobic bacteria and act synergistically against gram positive organisms. Kanamycin is a polybasic AMG antibiotic that has activity against a variety of pathogenic bacteria. Because it is poorly absorbed by the gastrointestinal mucosa, kanamycin is most commonly administered parenterally (intramuscularly and intravenously) reaching the maximum serum levels after 1 h of administration. It is indicated mainly for systemic diseases (septicemia) or localized (meningitis, infections of the urinary tract) caused by Gram-negative bacilli.

Currently the analytical methods used for the determination and quantification of biogenic amines, aminoglycoside and captopril are based on capillary electrophoresis chromatographic methods with optical detection after chemical derivatization of these analytes. Chemical derivatization use expensive and toxic chemical reagents and these procedures tend to be complex and time-consuming. Therefore, alternative analytical approaches based on the use of highly photoluminescent nanoprobe are attractive since they enable indirect determination of analytes in a simple way, commonly leading to limits of detection in the range of $\mu\text{g L}^{-1}$ and ng L^{-1} , in addition reducing the cost and time of analyzes. The direct interaction of GQDs dispersed in aqueous solution (analytical probe) with analytes or through the action of mediators may lead to variations of probe's photoluminescence emission (enhancement, quenching or spectral shifting), providing useful quantitative relationship. This concept provides the basis for simple, low cost, sensitive and, sometimes, selective detection of molecules that do not have strong chromophore groups.

Since 2009, the Laboratory of Applied Spectro-analytical and Electro-analytical methods (LEEA) at PUC-Rio has devoted a considerable part of its scientific effort to the application of nanomaterials (semiconductor quantum dots, graphene quantum dots and gold nanoparticles) in analytical chemistry. These aims the development of analytical methods taking advantage of nanomaterials special properties concerning the analytical detection, sample preparation,

separation of species, etc. The present thesis is the first of this research group that relies exclusively on the use of graphene quantum dots as photoluminescent probes in analytical chemistry.

1.2

Thesis structure

This thesis is structured in seven chapters. In Chapter 2, a bibliographical review is made to present the theoretical basis on carbon nanomaterials, called in this Thesis as graphene quantum dots, focusing on the characteristics optical properties and functionalization, besides indicating other relevant information about these nanomaterials, as well as the current use of these nanomaterials as nanosensors for different types of analytes.

Chapter 3 contains detailed information on instrumentation and materials used in this work and procedures for preparing solutions, production of graphene quantum dots dispersed in aqueous solutions. The detailed procedures involving the developed analytical methods are also presented.

The results are presented in three chapters (4, 5 and 6) each referring to one of the papers published aiming the development of photoluminescent probes for the determination of the chosen analytes. A brief introduction on each of the analytes and the goals intended are presented at the beginning of each of these chapters before the full description of the results. A partial conclusion regarding each chapter is also presented.

Chapter 4 is referred to the overall studies (optimization of different experimental conditions, and understanding of interaction mechanism), the method developed concerning captopril using Fe^{3+} as a mediator of the interaction between the dispersed amino-functionalized graphene quantum dots (GQDs-amino) with the analyte and the method validation and application in pharmaceutical samples.

In Chapter 5 the results concerning the determination of histamine using GQDs-amino as photoluminescent probe is presented, showing a preliminary study of mediation using Fe^{3+} , Cu^{2+} and Eu^{3+} . The following main points are presented: (i) the optimization of the experimental conditions for the

photoluminescent determination of histamine; (ii) the analytical figures of merit and (iii) the application of the proposed method in the analysis of tuna samples using a developed solid phase extraction procedure.

The development of the analytical method for the determination of kanamycin using GQDs-amino coupled with gold nanoparticles as photoluminescent probe is presented in Chapter 6. Preliminary studies to obtain and to characterize the nano-system used as analytical probe are described. In addition, studies of optimization of experimental parameters to achieve proper analytical response, analytical figures of merit and the application of the method in the analysis of yellow fever vaccine and in veterinary pharmaceutical formulations are described. Concerning analysis, the procedure using a molecularly imprinted polymer is shown, guaranteeing selectivity in the measurements through a solid phase extraction.

Finally, in chapter 7 the overall conclusion of the thesis is made along with the suggestions for the continuation of the work.

1.3

Objective of this work

1.3.1

General Objective

Development of spectrometric methods based on functionalized graphene quantum dots (GQDs) systems for the determination of analytes of biological and pharmaceutical interest (captopril, histamine and kanamycin) that present weak inherent optical activity in the UV-vis.

1.3.2

Specific objectives

- ✓ Adjust conditions for the synthesis of graphene quantum dots (GQDs); amino functionalized graphene quantum dots (GQDs-amino) and amino

functionalized graphene quantum dots coupled gold nanoparticle (AuNPs-GQDs-amino) in aqueous dispersion;

- ✓ Characterization of the nanomaterials by different spectroscopic techniques and microscopic techniques;
- ✓ Evaluation of the GQDs and GQDs-amino photoluminescence response in the presence of captopril, histamine and kanamycin.
- ✓ Adjusting experimental parameters (concentration of quantum dots, pH of dispersion, time and temperature, etc.) for probing of captopril, histamine, and kanamycin;
- ✓ Study the interactions between quantum dots and the analytes evaluated;
- ✓ Evaluation of the analytical potential of the optical probes;
- ✓ Study of selectivity in terms of possible interfering substances that may exist in samples of interest;
- ✓ Applications of proposed approaches in the analysis of diverse samples.

2 Theoretical fundamentals

2.1 Photoluminescence from molecules

Photoluminescence depends primarily on the ability of a chemical species to absorb energy from incident photons with appropriate energy [1]. Taking molecules as example, by absorbing energy, electrons are transferred to higher energy orbitals, causing the molecule (or population of molecules) to pass from the ground state to the excited state. Photoluminescence occurs when these excited molecules return to the ground state producing a radiative event (emitting a photon with less energy than the one absorbed during excitation). The radiative emission from a population of molecules (emission spectrum) provides useful information for qualitative or quantitative purposes. Fluorescence is a result of the return of the population of molecules between energy states of the same multiplicity (singlet-singlet, usually from S_1 , the first excited state, to S_0 which is the ground state). Thus, the process occurs with a typical lifetime in the order of ns. In phosphorescence, an inversion in multiplicity occurs during the time when the molecule is in the excited state, in a phenomenon called intersystem crossing. In this process, because of spin-orbital coupling, the spin of the electron is reversed, and the excited state becomes a triplet-excited state (e.g., T_1). Spin-orbital coupling is more likely to occur in molecules containing heteroatoms in their structure or vicinities. Therefore, phosphorescence is the radiant emission that occurs when the population returns from T_1 to S_0 . Phosphorescence is a type of radiant transition less likely to occur, since it involves states of different multiplicities, and has a high lifetime (above μs) which makes, unless exceptional conditions, non-radiant deactivation (internal crossing due to collisions and vibrations) to be more likely to bring molecules to ground state. These processes can be observed in the Jablonski diagram (Figure 2.1).

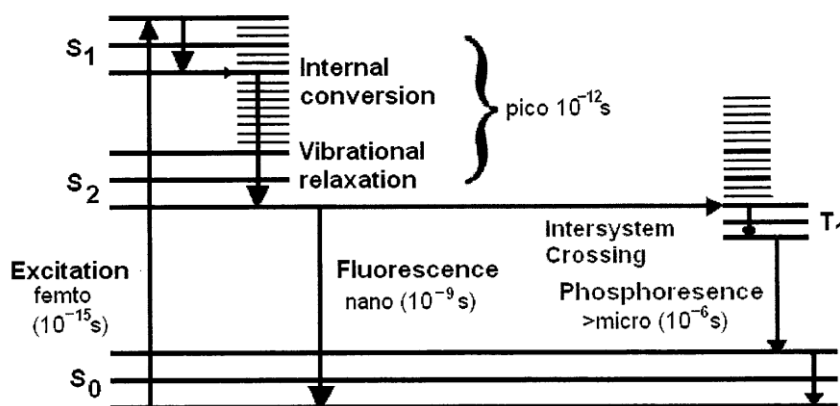


Figure 2. 1. Jablonski diagram. Source: KHAN, 2013 [2].

2.2

Use of nanomaterials as photoluminescent probes

The preparation of highly luminescent nanoparticles intend to be applied to the detection of different kind of analytes (molecules, metal ions, even microorganisms) has been one of the most important fields of study of nanotechnology [3,4]. Several techniques have been developed for the preparation of nanoparticles such as quantum dots (QDs) [5,6] and doped silica, which are attractive to be used in analytical sensing due to its high photostability and strong luminescence [7].

In the last decade, water-dispersed nanoparticles such as quantum dots have received great attention because their electronic states are very sensitive to surface changes induced by the presence of nearby chemical species. This indicates that the surface phenomenon is very important to use such nanoparticles dispersions as analytical probes. Therefore, the presence of different molecules near the surface and edges of the nanostructure can be expected to cause changes in its luminescent properties and these modifications can be used for analytical purposes [8].

The discovery of these luminescent nanoparticles enabled a promising new approach for photoluminescent chemical detection in important applications [9] since the suppression or amplification of photoluminescence may be observed after the interaction of the analyte with QDs. Research involving QDs has gained relevance in the early 1990s with the use of QDs-bioconjugate systems as fluorescent markers for bio-imaging, attracting significant interest in the

biomedical field. Today, a great scientific effort has been made to control synthesis, modify surfaces and edges, understand and enhance special properties aiming different technological applications.

2.2.1

Quantum dots

Quantum dots, also known as monocrystalline colloidal semiconductors, are one of several types of nanomaterials that are promoting a significant impact in many areas such as the biological sciences in physics and chemistry. The inorganic QDs generally have spherical shape and diameters ranging from about 1 to 20 nm [10] whose optical properties suffer the effect of the quantum confinement, which is a fundamental factor that justifies the luminescence characteristics of these QDs [11]. The QDs were discovered in the early 1980s by Alexei Ekimov [12], using a vitreous matrix and by Louis Brus [13] using colloidal dispersions. The most common QDs are those consisting of the groups II-VI, III-V and IV-VI of the periodic table, the QDs, being the most common the ones consisting of elements of group II-VI atoms such as CdS, CdSe, CdTe. These nanomaterials have peculiar optical and electronic properties [14]. In terms of optical properties, they have high quantum yields (the quantum yield is the ratio between the numbers of photons emitted as photoluminescence with respect to the number of absorbed photons), wide extinction spectra and strong resistance to photodegradation, which makes them very attractive in the area of sensing. The QDs are recognized for providing better luminescent intensity and photo stability compared to conventional fluorescent dyes, and they are more suitable for multicolor applications [15].

The attractive photophysical properties of quantum dots are consequence of a phenomenon known as quantum confinement [16]. The quantum confinement effect is observed when the size of the material is small enough to be comparable to the wavelength associated to the moving electron. In bulk materials (macroscopic semiconductors), the energy levels are very close to each other resulting in small difference between them, thus behaving as continuous distribution of energy (non-quantized). In this way, the energy levels become quantized and the valence band (VB) and conduction band (CB) unfold in a set of

discrete levels similar to the atomic energy levels [17]. In QDs, as in any semiconductor, the promotion of electrons from a quantized energy level of the VB to one quantized level of the CB leaves a vacancy behind (called hole, which has no electron). Electrons (negative charge) and holes (positive charge as it indicates electron deficiency) attract themselves by electrostatic force, forming a system called excitonic and a transitory excited state. The lower the diameter of the QDs, the greater the quantum confinement suffered by the system, with the consequent increase in the energy difference (band gap) between the highest energy level of VB and the lower energy level of CB as illustrated in the Figure 2.2 [18]. Due to the small dimensions of the QDs, when the exciton is created, the physical dimensions of the particle confine the energy similarly to the quantum mechanics model of the particle in the box [19]. Photoluminescence from QDs occurs when the electron-hole (excitonic) pair return to the original situation (recombination of the excitonic) releasing energy as radiant process with photons energy corresponding to the energy gap. The process may also involve non-radiant stages (loss of energy by heat, through vibrations of the crystalline lattice). As the bandgap energy increases with decreasing of QDs size, the photons emitted by the semiconductors tend to blue (decrease in wavelength) as the size of the nanoparticle decreases. Ordinarily, electrons upon returning to VB trigger a combination of both processes (radiant and non-radiant). Electrons can move rapidly through the energy levels of CB through small non-radiant decays and the final transition through bandgap is via radiant decay. Non-radiant processes occur from defects present on the surface of the nanocrystal or in the crystalline structure, where electrons and holes can recombine in the traps formed in these defects [20], reducing the efficiency of the photoluminescence. Since a part of the energy is lost through non-radiative decays, the photon energy emitted in the radiative decay is smaller than that of the energy of the incident photons, with consequent difference in the excitation and emission wavelengths (Stokes displacement) [21].

Brus has developed a popular effective mass model that relates particle size (neglecting spatial correlation effects) to the bandgap energy of a semiconductor quantum dot (Equation 2.1):

$$E_g(\text{quantum dot}) = E_g(\text{Bulk}) + \left(\frac{h^2}{8R^2}\right) \left(\frac{1}{m_e} + \frac{1}{m_h}\right) - \frac{1.8e^2}{4\pi\epsilon_0\epsilon R} \quad (\text{Equation 2.1})$$

In the Equation 2.1, E_g represents the bandgap energy of the quantum dots or solid in bulk, h is Planck's constant, R is the radius of the quantum dots, m_e is the effective mass of the electron in the solid, m_h is the effective mass of the hole in the solid, e is the charge on the electron and ϵ is the dielectric constant of the solid. The second term of Equation 2.1 is a particle in a box like for the exciton, while the third term of the equation represents the coulombic attraction of the pair electron-hole, mediated by the solid. Implicit in this equation is that the quantum dots are spherical and that the effective masses of charge carriers and the dielectric constant of the solid are constant as a function of size. In particular, some workers refer to quantum dots as “artificial atoms” because their quantized electronic states bear many analogies to atomic electronic states [22].

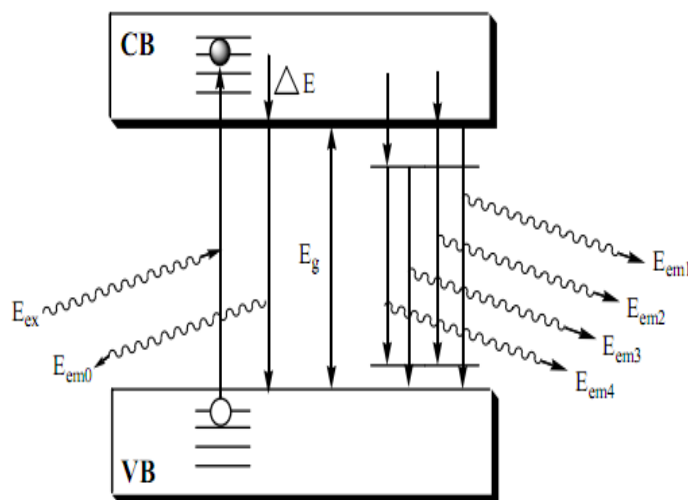


Figure 2. 2. Scheme of excitation and emission of quantum dots with the typical energy band structure of semiconductor. VB is the valence band, CB is the conduction band, ΔE is the Stokes shift, E_g is the band gap energy, E_{ex} is the excitation energy, $E_{em\ 0-4}$ are the various emission energies.

It is important to point out that inorganic quantum dots must be capped with ligands that acquire electrical charges, under specific pH ranges, that keep individual QDs separated, hindering the natural tendency of these nanoparticles to

coalesce forming bulk material, thus losing special properties related to the small size and large surface-size relationship.

Carbon quantum dots (CQDs) are a new form of zero-dimensional (materials with all of their dimensions in the nanometric scale) carbonaceous nanomaterials [23], which were first obtained during purification of single walled carbon nanotubes *via* preparative electrophoresis [24]. They are quasi-spherical carbon nanoparticles with typical diameters of less than 10 nm [25,26]. Compared to inorganic QDs, CQDs are superior in terms of low cytotoxicity and biocompatibility [27]. CQDs are emerging new type of photoluminescent nanomaterials that present similar optical attributes to inorganic QDs such as extensive optical extinction, which in this case may cover even the near infrared region [28-31]. CQDs have a strong photoluminescence but, in general, lower quantum yields when compared to inorganic QDs however also characterized by size-wavelength dependence. In contrast, CQDs present fascinating optical properties, such as electrochemiluminescence (ECL) and photo-induced electron-transfer. The ECL mechanism of CQDs is suggested to involve the formation of an excited-state CQDs via electron-transfer annihilation of negatively charged and positively charged CQDs [32]. The photoluminescence from CQDs can be quenched efficiently by either electron acceptor or electron donor molecules in solution. These interesting photoinduced-electron transfer properties offer new opportunities in using CQDs for light energy conversion and related applications [33].

CQDs have been obtained using different and less-exhaustive synthetic routes than the ones used for inorganic QDs. Synthesis of CQDs may be simple as a partial combustion of carbon materials [34] or by laser ablation of carbon based materials [35]. CQDs are produced from cheap and abundant carbon based precursors and, in principle, present lower environmental and biological toxicity [35,36]. The produced CQDs naturally present functional groups (electrically charged in aqueous dispersions) that promote long-term colloidal stability. These groups are bridges to enable functionalization or chemical complexation, promoting luminescence changes and the possibility for selective interactions with nearby chemical species.

Recently, efforts have been made to understand the photoluminescence of CQDs. Although photoluminescence origins are still not completely understood, it

is reported that the photoluminescence properties of the CQDs are attributed to: i) the effect of quantum confinement or conjugated π -domains, which are determined by the carbon core; ii) by surface state, which is determined by hybridization of the carbon backbone and to the attached chemical groups; iii) the molecule state, which is determined solely by the photoluminescence molecules connected on the surface or interior of CQDs; and iv) the crosslink enhanced emission effect. Due to the variety of mechanisms that can be presented for these types of carbon nanomaterials, a wide range of approaches (top-down cutting and bottom-up carbonization) already exist to producing CQDs with controllable characteristics. The investigation of the photoluminescence properties of CQDs includes the different emission centers, excitation dependence, and pH and solvent sensitivity [25,32, 35,37].

2.2.2

Graphene quantum dots and their optical properties

"CQDs" is a comprehensive term for various nanocarbon materials. In a broad sense, all nano materials that are composed primarily of carbon may be called CQDs, which include graphene quantum dots (GQDs) and carbon nanotubes [34].

Graphene is an allotropic, form of carbon with two-dimensional structure with thickness of a single atom, has attracted enormous attention due to its extraordinary electronic, mechanical, thermal and chemical stability properties [38, 39]. When a graphene flake is small enough to be under the influence of quantum confinement effect, it becomes a semi-conductor and present the special properties of CQDs, including the optical ones. These structures, called graphene quantum dots, have sizes typically smaller than 100 nm [40,41] but, in general, the mean GQDs size is below 10 nm, and the largest diameter of the GQDs reported so far is 60 nm [42]. Similar to the size, the GQDs height depends on the preparation method and conditions used but, in most of cases, ranges from 0.5 to 5 nm. However, the heights of GQDs prepared by different methods are not monotonously related to their sizes, since most GQDs structures consist of layers, but no more than 5 layers [42-44]. GQDs, in fact, are the simplest of CQDs, having one or a few layers of graphene, usually bearing chemical groups attached

to the edges of the structure. They are anisotropic with lateral dimensions larger than their height. Due to the existence of a carbon in the core, GQDs present certain crystallinity, with an average lattice parameter of 0.24 nm, which correspond to (100) spacing of single graphene dots on lacey support film [45].

The theory of functional density and time-dependent functional density theory provides systematic theoretical investigations to show that the emission of GQDs can be widely observed through ultraviolet to near infrared, depending on their size, configuration, functional groups, defects and the heterogeneous hybridization of the carbon network. The unique photoluminescence of GQDs can be effectively tuned by doping heteroatoms to the π - π conjugated system which may be controlled by stepwise reactions of small molecules [46-48]. Their high photoluminescence is due to quantum confinement and edge effects [49,50]. The presence of oxygen-containing groups, structural defects and doping elements also affect considerably their photoluminescent properties [40]. Although the exact mechanism is still an enigma, some theories propose that photoluminescence from GQDs is due to electron-hole recombination, quantum size effect, doping, structural edge, and surface defects of functional groups of GQDs.

The maximum extinction of the GQDs depends on the approach used for their preparation and the size of their quantum confinement effect. The GQDs generally exhibit a characteristic extinction peaks around 230 nm, attributed to the π - π^* transition of the C = C bonds present in the graphene structure, with a tail extending beyond the visible range [51,52]. Some GQDs have extinction peaks in the 270-360 nm range due to the number of π - π^* transition bonds of C = O [44, 53, 54]. For example, GQDs with 60 nm size exhibit poor extinction at 280 nm [42], compared to GQDs of size 2-3 nm functionalized with N (nitrogen) obtained through the electrochemical method, which present spectral features at about 270 nm [55].

2.2.3

Synthesis of graphene quantum dots

The technological applications of GQDs are still a field to be explored and many studies are required to understand the most influential factors in synthesis and how to control them to obtain the desired properties. Contradictory

hypotheses may arise from experimental observations because of the great heterogeneity of the GQDs and due to the fact that their properties depend on numerous parameters (e.g. size, chemical portions, and defects). In terms of photoluminescence, these parameters affect quantum efficiency and color that ranges from deep ultraviolet [56] to blue [52] and red [6] under UV light at 365 nm.

Different methods have been proposed for the preparation of what is generally reported as graphene quantum dots, despite the fact that some procedures probably produce multilayered structures, aiming excellent photoluminescent properties. Approaches of size adjustment can generally be classified into top-down and bottom-up methods. Top-down methods include cutting large graphene-based materials in nanometric systems, while bottom-up approaches involve the preparation of GQDs from organic molecules as carbon source. Approaches based on surface chemistry include surface functionalization [41,53,57-59] and doping with variety of elements [54,55,60,61].

Pan *et al.*, [52] have employed hydrothermal cutting and reduction of graphene oxide (GO) producing a photoluminescent water dispersed GQDs with maximum emission at 430 nm. Shen *et al.* [41] produced GQDs from polyethylene glycol surface-passivated GO, using a reduction with hydrazine hydrate. The nanomaterial presented up-conversion (with excitation at lower energies than the emitted photons). GQDs were also prepared from graphene under concentrated acid and ultrasound followed by pyrolysis. Photoluminescence up-conversion was achieved by modifying the GQDs with TiO₂ [62]. Zhou *et al.*, have produced GQDs from the reaction of GO with the Fenton reagent under UV light. The produced photoluminescent nanomaterial presented carboxylic acid groups on their surface [63]. Electrochemical preparation of GQDs was performed by using cyclic voltammetry, within ± 3000 mV, of a graphene film [64]. GQDs were also prepared by microwave assisted oxidation [65] that cleaved GO under acidic reduction conditions [66, 67]. Dong *et al.* produced aqueous dispersed GQDs by submitting an amount of citric acid to an incomplete carbonization before it was added to an alkaline aqueous solution. The process resulted in a photoluminescent dispersion where carbon nanosheets containing small sp² clusters were isolated within the incomplete carbonized precursor [51].

Phama *et al.*, 2011 have developed a green and easy approach to producing graphene nanosheets using an environmentally friendly reagent, i.e., L-glutathione as a reducing agent. Graphene was prepared by a step of reducing the graphene oxide in aqueous solution. Synthesized graphene was characterized using a variety of analytical techniques such as Fourier transform; infrared spectroscopy and X-ray photoelectron spectroscopy were used to study the changes in surface functionalities. X-ray diffraction was used to investigate the crystallinity of graphene nanosheets while high-resolution transmission electron microscopy and atomic force microscopy were used to investigate the graphene morphologies obtained. The thermogravimetric analysis was used to characterize the thermal stability of the samples in the heating. Digital images provided a clear observation of the stable dispersions of graphene in aqueous medium and in polar aprotic solvents [68].

2.2.4

Functionalization of graphene quantum dots

The functional modification and assembly of GQDs are essential for applications related to their technological use [69]. In principle, GQDs contain carboxylic acid radicals on their surface, so they can be functionalized by covalent bondings and by non-covalent interactions with various inorganic, organic or biological species [53]. When functionalization occurs with organic molecules covalently bound to the GQDs, a disturbance may result in increased optical properties [70]. Non-covalent functionalization offers the possibility of interactions between functional groups without affecting the optical properties. Therefore, the coupling of GQDs with biomolecules can promote important and attractive interactions for the development of sensors with high analytical performance in biomolecular recognition [71].

The functionalization of GQDs may improve their photoluminescence and provide some selectivity in interaction with the target chemical species. In addition, such carbon-based structures are non-toxic, can be better stabilized when dispersed in water, being more photo-stable when compared to inorganic QDs. Recent studies show that doping of GQDs with heteroatoms such as nitrogen [55,46,72,73], boron [74,43], sulfur [48,75], fluorine [61] and chlorine [76] may

effectively adjust its band gap and electron density as well as improve quantum yield and chemical activity [77]. Besides, the assembly of surface chemical groups, for instance containing either O or N, the presence of structural defects, edges and surface doping with metal ions considerably affect the photoluminescence of such carbon nanostructures [40,50,78,79].

Feng *et al.*, reported a simple and effective chemical method to increase the photoluminescence of GQDs. GQDs were prepared by the solvothermal method from graphene oxide, which are chemically reduced by hydrazine hydrate to produce reduced GQDs (rGQDs). The results showed that the reduction of hydrazine hydrate not only decreases the atomic ratio O/C of the GQDs, but also altered the type of nitrogen atoms binding. Functionalization of GQDs through reduction by hydrazine hydrate (rGQDs) increased by two-fold the photoluminescence intensity compared to crystalline GQDs [80]. Xu *et al.*, synthesized nitrogen-doped GQDs (N-GQDs) with the objective of improving photoluminescent performance and amplifying their applications in photocatalysis, such as sensors, bio-image, etc. The authors were able to obtain N-GQDs by using molecular organic framework (MOF) derived carbon zeolitic imidazolate frameworks (ZIF-8C) as a new source of well-crystallized and water-compatible graphene sheets. The preparation was considered fast and environmentally friendly due to the efficient cutting strategy of acid vapor being different from the other reported chemical routes [81]. Jin *et al.* have also found peculiar photoluminescence in amine-functionalized GQDs produced from the reduction of GO and then reacted with alkyl amine groups [59].

2.3

Analytical approaches through the direct use of graphene quantum dots as nanosensors

GQDs have been applied in several fields of physics, chemistry, materials science, and biological area. Currently the researches are mainly focused on theoretical studies, chemical preparation and study of the optical properties of GQDs. In contrast, analytical applications related to their photoluminescent properties are few [82]. The interaction between GQDs and target chemical species (analytes) in solution may cause suppression, amplification and/or spectral shift of the GQDs characteristic photoluminescence. Such optical effects have

been recently used to enable chemical detection of different ions and molecules [9,69].

Analytical sensors based on the optical characteristics of nanomaterials may bring advantages in detecting molecules that do not present relevant inherent optical properties in the UV and visible range of the spectrum. One of such nanomaterials is the so called graphene quantum dots (GQDs) that produce photoluminescence (due to confinement effect that generates quantum size properties), which can be tuned by modifying size, by functionalization and by changing its nearby environment [49,50,83-87].

He *et al.* developed a highly sensitive and specific photoluminescent biosensor from the functionalization of the GQDs with hemin through glucose oxidation for the monitoring of blood glucose. The GQDs prepared simply by citric acid pyrolysis showed strong photoluminescence and good solubility in water. Due to the non-covalent bonding between hemin and GQDs, the addition of hydrogen peroxide (H_2O_2) to destroy the passivated surface of the GQDs, caused extinction of the significant photoluminescent GQDs. Based on this effect, a new photoluminescent method was proposed for the detection of glucose. Under optimized conditions, the linear glucose range was 9 to 300 μM , and the detection limit (LOD) was 0.1 μM . The synthesized biosensor showed photoluminescence in the green, in addition to simplicity in use, cost efficiency, and was successfully applied for the determination of glucose in human serum. In addition, the proposed method provided a new pathway for the development of biosensors based on the functionalization of GQDs with hemin for the detection of biomolecules [71].

Xu *et al.*, obtained a rapid synthesis of nitrogen-doped graphene quantum dots (N-GQDs) with a carbon derived from zeolitic imidazolate frameworks (ZIF-8C) as the starting material. The N-GQD is photoluminescent and exhibited an excitation-independent behavior. Due to the presence of O-functional groups on the surface of the obtained N-GQD, it was possible to use it as a photoluminescent probe for the highly selective determination of Fe^{3+} ions [81]. GQDs functionalized with glutathione were prepared by pyrolysis in a single step with a quantum yield of 33.6% and used as a photoluminescent probe to estimate the level of adenosine triphosphate ATP in cell lysates and human blood serum. The

LOD was 22 μM and the method developed was successfully applied in the samples [69].

In 2014, Wang *et al.*, used GQDs as a highly effective sensor for determination of Cu^{2+} with luminescence intensity inversely proportional to the concentration of the target ion, enabling linear analytical response up to 15 $\mu\text{mol L}^{-1}$, with LOD of 0.226 $\mu\text{mol L}^{-1}$ [88]. Chakraborti *et al.*, determined Hg^{2+} in aqueous solution through the quenching of the GQDs photoluminescence, enabling the LOD of 3.4 $\mu\text{mol L}^{-1}$ [89]. Fan *et al.*, proposed the determination of 2,4,6-trinitrotoluene based on the photoluminescence quenching of the unmodified GQDs, leading to the detection of 2.2 $\mu\text{mol L}^{-1}$ [90], probably due to the formation of a non-luminescent complex.

In 2013, Wang *et al.*, used GQDs as probes to determine kinase protein [91] using Zr^{4+} as a mediator of the process in aqueous solution. The decreasing of the optical signal of the GQDs-peptide complex was due to the aggregation of the phosphorylated peptide triggered by Zr^{4+} . Wu *et al.*, [49] used GQDs to develop a method to determine GSH, cysteine and homocysteine based on the mediation of Hg^{2+} that quenches the intense blue photoluminescence from the GQDs. As these analytes were added in the aqueous buffered GQDs- Hg^{2+} dispersion, the removing the mercuric ion from the GQDs occurred, restoring photoluminescence. The method enabled LOD down to 2.5 nmol L^{-1} .

Zhou *et al.*, 2014 developed a molecularly imprinted polymer (MIP) photoluminescent GQD composite sensor for the photoluminescent detection of paranitrophenol (4-NP) in water samples, in which the MIP was incorporated into GQDs. The silica-coated hydrothermal method was used to synthesize the GQDs. The final composite was developed to anchor a layer of MIP in the silica-coated GQDs using 3-aminopropyltriethoxysilane as the functional monomer and tetraethoxysilane as the crosslinking agent. The method presented selectivity and linearity in the range of 0.02-3.00 $\mu\text{g mL}^{-1}$ and LOD of 9.00 ng mL^{-1} [92]. Zhang *et al.*, in 2013 deposited GQDs on the Au electrode using cysteamine as a cross-linking agent. The covalent reaction between GQDs and the Au electrode showed good stability and good analytical performance for detection of H_2O_2 . The GQD-modified Au electrode showed a rapid amperometric response for H_2O_2 determination and LOD of 0.7 $\mu\text{mol L}^{-1}$ in the 0.002-8 mmol L^{-1} concentration

range. Due to the good electrocatalytic activity and high stability, the modified GQD Au electrode was applied to detect H_2O_2 in biological systems [93].

Li *et al.*, in 2014 using GQDs, developed an efficient method for determining hydroquinone in water samples. The analytical variable, photoluminescence quenching, was generated from the formation of benzoquinone intermediates through the catalytic oxidation of hydroquinone by horseradish peroxidase. The reaction mechanism involved hydroquinone as an electron acceptor affected the surface state of the GQDs through an electron transfer effect. The water-compatible GQDs were directly prepared by pyrolysis of citric acid with the use of the hybrid enzyme system. The LOD for hydroquinone was $8.4 \times 10^{-8} \text{ mol L}^{-1}$. Other phenolic compounds and quinine, such as phenol, resorcinol and other quinines, did not interfere with the analysis. The method developed using GQD as a photoluminescent probe produced satisfactory results for hydroquinone analysis in different types of water samples [94].

2.4

Graphene quantum dots as photoluminescent probe with metal ion mediation

The mediation of metal ions, somehow affecting the interaction with GQDs with other chemical species, has been reported [95]. Literature reports that lanthanides (erbium, ytterbium and europium) are good to form composites with graphene [96] aiming the production of doped semiconductors. For instance, the GQDs doped with europium produced strong and intense emission at around 620 nm due to intra-4'-shell transitions of Eu^{3+} ions [97, 98]. The coordination of Eu^{3+} with carboxylate groups on the surface of GQDs [99] acts as a bridge to induce the aggregation of GQD, quenching photoluminescence through energy-transfer or electron-transfer processes. The system GQD- Eu^{3+} is dissociated by the introduction of phosphate ion, since Eu^{3+} has a higher affinity for oxygen-donor atoms than to the carboxylate groups on the surface of GQDs, thus, photoluminescence from GQDs were restored enabling the quantification of phosphate.

In 2014, Wang *et al.*, [88] used GQDs as a highly effective photoluminescent sensor for determination of Cu^{2+} . The preparation of the blue

photoluminescent GQDs was based on the hydrothermal method using reoxidized graphene oxide. According to the authors, the sensor developed for direct detection of Cu^{2+} was studied and exhibited a high sensitivity and selectivity compared to other metallic ions in aqueous solution. Photoluminescence intensity was inversely proportional to Cu^{2+} concentration, and the calibration curve exhibited linear regions up to the $15 \mu\text{mol L}^{-1}$ with a LOD of $0.226 \mu\text{mol L}^{-1}$. The results indicated that the GQDs used as a photoluminescence detection sensor meet the selectivity required by the biomedical area and can be applied by the environmental area with sufficient sensitivity to detect Cu^{2+} in water samples according to the United States Environmental Protection Agency.

In 2014, Wu *et al.* reported that Hg^{2+} is a more effective GQDs photoluminescence quencher when compared to other metal ions (Mg^{2+} , K^+ , Ca^{2+} , Al^{3+} , Zn^{2+} , Fe^{3+} , Fe^{2+} , Mn^{2+} , Cd^{2+} , Co^{2+} , Ni^{2+} and Pb^{2+}) [49]. Such a selective quenching can be attributed to the fact of the Hg^{2+} have strong affinity for carboxylic groups in the surface of GQDs than the other metal ions [100], promoting either electron or energy transfer from the GQDs to the Hg^{2+} [69]. Moreover, for GQDs synthesized in the presence of glutathione (GSH), the photoluminescence quenching promoted by Fe^{3+} (in aqueous systems) was more efficient than the one of Hg^{2+} . Synthesis in the presence of GSH produced GQDs with N and S in their structure that significantly affect properties of the nanomaterial.

Recently, Lin *et al.* [77] synthesized GQDs doped with europium (Eu-GQDs). Structure characterization revealed that the Eu^{3+} were complexed with the oxygen functional groups on the surface of the GQDs. The Eu-GQDs aqueous dispersion was used as a probe for the determination of either Cu^{2+} or L-cysteine as the photoluminescence intensity was quenched in the presence of Cu^{2+} (because of the coordination of Cu^{2+} with carboxyl groups on the surface of Eu-GQDs) with the restoring of signal by the addition of L-cysteine (due to the strong affinity of Cu^{2+} to this amino acid). Linear analytical responses were achieved with LOD of $0.056 \mu\text{mol L}^{-1}$ for Cu^{2+} and $0.31 \mu\text{mol L}^{-1}$ for L-cysteine. Liu *et al.* used amino-functionalized GQDs (synthesized in the presence of GSH) as a probe to estimate the ATP levels in cell lysates and in human blood serum [69]. Dong *et al.* [101] developed a fluorescent sensor branched polyethylenimine-carbon capped quantum dots (BPEI-GQDs) to detect cyanide ions. The amino groups on the

surface of BPEI-GQDs can capture selectively Cu^{2+} to form cupric amine absorbent species. The result is the attenuation of the BPEI-GQDs photoluminescence through an internal filter effect. The CN^- ions can combine strongly with Cu^{2+} forming complex ions, preventing Cu^{2+} to be captured by the amino groups of the BPEI-GQDs. Thus CN^- can amplify the photoluminescence from BPEI-GQDs- Cu^{2+} system enabling detection limits on the order of $0.65 \mu\text{mol L}^{-1}$ and a linear response up to $200 \mu\text{mol L}^{-1}$.

2.5

Approaches using graphene quantum dots coupled with gold nanoparticles

Gold nanostructures exhibit distinct properties that are governed by their surface atoms and electrons. Under the influence of electromagnetic radiation, a collective oscillation of electrons in the conduction band of nanoparticles is induced, leading to a periodic charge separation that generates oscillating dipoles. Coherent oscillation of electrons gives rise to localized surface plasmon resonance (LSPR) spectral bands, which show remarkable changes depending on the shape and size of gold nanoparticles (AuNPs) [102]. Surface plasmon oscillation alters drastically as AuNPs agglomerate, allowing the individual particles to electronically couple to each other, generating a new band encompassing a red shift and enlargement [103]. Such agglomeration can be induced by chemicals that interact with the surface of AuNPs by electrostatic or Van der Waals forces.

Very recently nanostructures containing both GQDs and AuNPs have been used as photoluminescent analytical probes and electrochemical sensors. Ting *et al.* developed a method based AuNPs functionalized GQDs for the electroanalytical detection of heavy metals Hg^{2+} and Cu^{2+} [104]. The authors attribute the detection performance to the synergistic cooperation between GQDs and AuNPs. Detection limits of 0.02 nmol L^{-1} for Hg^{2+} and 0.05 nmol L^{-1} for Cu^{2+} have been achieved. Ju *et al.* developed a strategy for the in situ growth of AuNPs in quantum dots of nitrogen-doped graphene. Such nanostructures exhibited high sensitivity and selectivity for the electrochemical detection of hydrogen peroxide with a limit of detection (LOD) of $0.12 \mu\text{mol L}^{-1}$ [105]. Huang *et al.* proposed a photoluminescent probe constituted of GQDs and AuNPs for the detection of L-cysteine. The photoluminescence of GQDs, previously suppressed by the

interaction with AuNPs due to resonance energy transfer, was gradually recovered as L-cysteine was added to the solution because of strongly binding of the thiol containing amino acid to AuNPs [106]. Such on-off luminescent probe produced signal changes directly proportional to the concentration of L-cysteine in the range of 0.32 to 4000 nmol L⁻¹ and applied in the analysis of urine and human blood plasma. Dong *et al.*, synthesized GQDs in a medium where hydrazine reduced AuCl₄ to form nanostructures employed to modify glassy carbon aiming to use it as an electro-chemiluminescent immuno-sensor for the carcinoembryonic antigen. The linear response range was between 0.02 and 80 ng mL⁻¹ [107].

3 Experimental

3.1 Apparatus

UV-vis absorption spectra were acquired on a Perkin-Elmer model Lambda 35 double beam spectrophotometer (Perkin-Elmer, UK) using 1000 nm min⁻¹ scan rate, 10 nm spectral bandpass and solutions/dispersions placed on 1 cm optical path length quartz cuvettes. Photoluminescence measurements were made on a model LS 55 luminescence spectrometer (Perkin-Elmer) using 1000 nm min⁻¹ scan rate, 10.0 nm spectral bandpass on 1 cm optical path length quartz cuvettes. A thermostatic system with stirring (PTP-1 Fluorescence Peltier System with a PCB1500 Water Peltier System, Perkin-Elmer) was used to keep the dispersions in the cuvette at specific constant temperatures during photoluminescence. Time resolved luminescence measurements were made on a spectrometer model HJY 5000 M (Horiba/Jobin-Yvon) with a 330 nm pulsed LED source.

Images from the GQDs were made using a field emission scanning electron microscope (JEOL, model JSM-6701F, Japan) operated in the scanning transmission electron microscopy (STEM) mode at 30 kV. Raman spectroscopy and atomic force microscopy (AFM) for topology were performed using a micro-Raman spectrometer (NT-MDT, NTEGRA SPECTRA, Russia) equipped with a charge coupled device detector and a solid-state laser. Raman measurements were obtained using a cooled charge couple device and 473 nm laser source and AFM images were obtained using tapping-mode diamond tip (7 × 7 microns). X-ray photoelectron spectroscopy (XPS) measurement were performed using a spectrometer equipped with a commercial hemispherical electron energy analyzer Alpha 110 with Mg K_α radiation (hν = 1253.6 eV). High-resolution XPS spectra were obtained (pass energy of 20 eV) and data were processed using the CasaXPS software. The reference energy was the C1s peak at 284.5 eV. Dynamic light scattering (DLS) and zeta potential measurements were made on a nanoparticle analyzer model SZ-100 (Horiba, Japan). Zeta potential measurement were made using an acrylic electrochemical cell containing a flat carbon electrode (6 mm

thickness) and DLS measurements were obtained using glass cuvettes with 1 cm optical path length. Total carbon measurements were made on a Carbon Analyzer model TOC-VCPN (Shimadzu, Japan).

Chromatographic analysis made on a high performance liquid chromatography system (Model 1200, Agilent Technologies, Japan) equipped with a multiwavelength fluorescence detector, a column oven (kept at 30°C) and a Agilent Eclipse XDB-C18 column (250 × 4.6 mm and 5 µm average particle size). The Acquity model ultra-performance liquid chromatography (UPLC) system (Waters, USA) was employed to evaluate selectivity of the solid phase extraction procedure. This system was operated with an Acquity UPLC BEH C₈ (100 mm x 2.1 mm, 1.7 µm) column. Detection was made on the Orbitrap XL mass spectrometer (Thermo Scientific, Germany) utilizing electrospray ionization (ESI) in positive mode. For the pH measurements was employed a pH-meter model MPA 210 Tecnoion (Brazil) with a glass membrane electrode combined with a reference Ag/AgCl(KCl_(sat)). The flow analytical system used to automatization of the solid-phase extraction procedure was a FIALab-2500 system (FIALab Instrument, USA). For the AuNPs synthesis, the Orb jacketed reactor system model R18 (Syrris Ltd, UK) was used.

3.2

Reagents and materials

Ultrapure water (18.2 MΩ cm) was obtained from the Milli-Q gradient A10 ultra-purifier (Millipore, USA). Histamine, histidine, valine, tyrosine, lysine, phenylalanine, threonine, methionine, tryptophan, cysteine, reduced L-glutathione (GSH), captopril, kanamycin sulfate, hydrogen tetrachloroaurate (III) hydrate, lactose, alanine, sorbitol, sodium bisulfite, (3-aminopropyl) trimethoxysilane (APTMS), tetraethyl orthosilicate (TEOS), sodium dodecyl sulfate (SDS), β-cyclodextrin, hexadecyltrimethylammonium bromide (CTAB), triethylamine, 2-mercaptoethanol, 5,5-dithio (bis-2-nitrobenzoic acid) (DTNB) europium (III) nitrate (Eu(NO₃)₃·5H₂O), 4-nitrophenol (4-NP) and nickel nitrate (NiCl₂·6H₂O) were from Sigma-Aldrich (USA). Sodium citrate, acetic acid, iron (III) chloride (FeCl₃·6H₂O), cadmium chloride (CdCl₂·H₂O) lead nitrate (Pb(NO₃)₂) and copper sulfate (CuSO₄·5H₂O) were from Vetec (Brasil). Iron (II)

sulfate ($\text{FeSO}_4 \cdot 7\text{H}_2\text{O}$) was from JT Baker (USA) and zinc sulfate ($\text{ZnSO}_4 \cdot 7\text{H}_2\text{O}$) was from Reagen (Brazil). Quinine sulfate were purchased from Fluka (Germany). The chemical derivatization agent *o*-phthalaldehyde (OPA), trichloroacetic acid (TCA), tetrahydrofuran (THF), methanol (HPLC-grade), acetonitrile (HPLC-grade), sodium hydroxide, sodium acetate, sodium chloride, hydrochloric acid, boric acid and citric acid were obtained from Merck (Germany). Syringe filters (0.22 μm) were from Whatman, UK. Nitrogen (99.999% purity) was from Lynde gases, Brazil. Captopril pharmaceutical tablets (União Química, containing 25 mg captopril per tablet) were purchased in a local drugstore. Dialysis membrane (retained molecular weight of 3.5 kDa) and ammonium acetate were purchased from Spectrum Laboratories Inc. (USA).

3.3

Aqueous synthesis of nanomaterials

3.3.1

Synthesis of graphene quantum dots

The amino functionalized GQDs (GQDs-amino) were produced by the pyrolysis of both citric acid and GSH. This synthesis was made according to a literature procedure with small modifications [69]. Briefly, 0.50 g of citric acid was first mixed with 0.15 g of GSH. The mixture was placed into a 5 mL beaker and heated to 240 °C using a heating mantle. As the mixture became molten (with color changing from colorless to pale yellow and then to brown) within 2 to 5 min, the hot liquid was added into 50 mL of ultrapure water at room-temperature in order to obtain (after filtering on a 0.22 μm syringe filter) a clear pale yellow aqueous sample that was further dialyzed for 24 h in order to obtain the GQDs-amino aqueous synthesis dispersion (Figure 3.1). The production of GQDs without GSH was carried out with the same procedure with pyrolysis of citric acid only. These GQDs-amino and GQDs dispersions were also prepared by adding the molten mixtures into CTAB ($1.0 \times 10^{-3} \text{ mol L}^{-1}$), HCl (0.1 mol L^{-1}) and NaOH (0.25 mol L^{-1}) aqueous solutions at room-temperature.

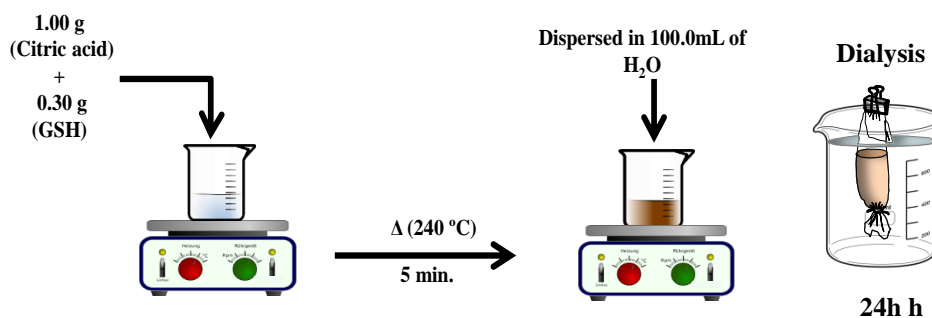


Figure 3.1. Synthesis procedure aqueous dispersion of GQDs-amino.

3.3.2 Synthesis of AuNPs.

AuNPs were produced based on the procedure reported by Feng *et al.* but changing surfactant and using different synthetic apparatus. AuNPs were prepared reducing of HAuCl_4 (3.25 mL of a 23 mmol L^{-1} solution) with the addition of 830 μL of a freshly prepared aqueous solution of NaBH_4 (0.4 mol L^{-1}) in a jacketed vessel containing 250 mL of water [108]. This mixture was mechanical stirred vigorously and continuously for 5 min. The reducing agent was added dropwise to promote reduction with the formation of AuNPs. AuNPs were synthesized in the presence and absence of the cationic surfactant CTAB previously added in the reactor at a concentration of 5.0×10^{-4} mol L^{-1} final concentration in the reactor.

3.3.3 Synthesis of AuNPs-GQDs-amino.

The AuNPs-GQDs-amino-CTAB dispersion was prepared by adding 3.25 mL of a 23 mmol L^{-1} aqueous solution of HAuCl_4 into the reactor glass vessel previously loaded with 125 mL of water with 125 mL of a CTAB (1.0 mmol L^{-1}) aqueous solution and 0.75 mL of the synthesis GQDs-amino dispersion. This mixture was mechanical stirred vigorously and continuously (5 min) using a Teflon rod stirrer before the addition of 830 μL of freshly prepared NaBH_4 (0.4 mol L^{-1}) aqueous solution to promote reduction with formation of AuNPs (Figure 3.2).

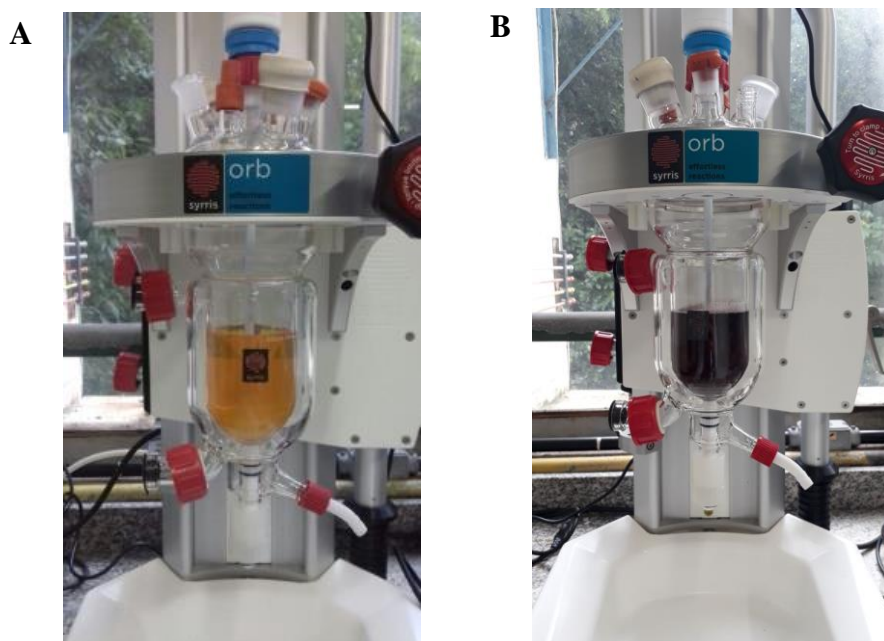


Figure 3.2. Image of the gold nanoparticle synthesis (AuNPs-GQDs-amino) made in the reactor. (A) Mixing the reactants before of addition of NaBH_4 . (B) AuNPs after addition of NaBH_4 .

3.4 Characterization procedures

3.4.1 Quantum yield determination

Photoluminescence quantum yields (ϕ) were determined by preparing the different dispersions of GQDs using quantities of the synthesized original dispersion in water and the reference standard solution of quinine sulfate ($1.0 \times 10^{-4} \text{ mol L}^{-1}$) prepared in sulfuric acid (0.5 mol L^{-1}). Photoluminescence measurements were recorded by exciting both (GQDs and quinine sulfate) at 345 nm. The integrated photoluminescence intensity was calculated by measuring the entire area under the emission spectrum. In order to minimize the self-absorption, the absorbance of the measured solution/dispersion was kept below 0.10. The measurement procedure involves the comparison of the reference ϕ_{ST} of the quinine sulfate (QY of 54%) [109] with the one of the GQDs dispersions, therefore, from the plot of absorbance in function of the integrated

photoluminescence of the standard and the dispersions, the ϕ_x value could be calculated as indicated in Equation 3.1.

$$\phi_x = \phi_{ST} \left[\frac{\text{Grad}_x}{\text{Grad}_{ST}} \right] \left[\frac{\eta_x^2}{\eta_{ST}^2} \right] \quad (\text{Equation 3.1})$$

Where ϕ , Grad and η represent respectively the luminescence quantum yield, the slope of the integrated photoluminescence intensity versus absorbance plot, and the refractive index of the solvent used to prepare quantum dots dispersion and standard solution. The sub-indexes X and ST refers respectively to the GQDs and reference standard. In this experiment, the diluted GQDs were dispersed in deionized water ($\eta_{\text{water}} = 1.33$) and the diluted solution of quinine sulfate was dissolved in in 0.5 mol L^{-1} sulfuric acid ($\eta_{\text{solution}} = 1.33$).

3.4.2

Raman, AFM, XPS and STEM measurements.

About 25 microliters of aqueous dispersions of GQDs-amino were deposited on a silicon substrate and left to dry at room-temperature and atmospheric pressure. The film obtained after drying was used to make measurements of Raman, AFM and XPS. It was probed by the 473 nm laser beam of the Raman spectrometer. For XPS measurements, the energy from the Mg K_{α} line (1253.6 eV) was used for excitation. Samples for the STEM analysis have not been submitted to any specific treatments. They were analyzed by placing a few microliters of the colloidal dispersions on carbon grids and allowed to dry at room temperature for further analysis by STEM.

3.4.3

Time resolved luminescence measurements

Lifetime measurements were obtained with excitation at 330 nm (pulsed nanoLED source). The luminescence decay profiles were fitted with a multi-exponential expression ($I(t) = \sum \alpha_i \tau_i$) using Horiba Jobin Yvon DAS6 software for

deconvolution that takes into account the excitation pulse profile. The average lifetime was calculated using each lifetime τ_i in the decay profile weighted with its relative amplitude f_i ($\langle\tau\rangle = \sum f_i\tau_i$, with $f_i = \alpha_i\tau_i / \sum \alpha_j\tau_j$).

3.5

Preparation of molecular imprinted polymer for group-selective recognition of aminoglycosides

The synthesis of the molecularly imprinted polymer (using kanamycin sulfate as template) was made using the sol-gel process [110]. Initially an amount of 500 mg of kanamycin sulfate was dissolved in 6 mL deionized water, where it was added 400 μL of HCl 1.0 mol L⁻¹ aqueous solution (as catalyst), 3200 μL of (3-aminopropyl) trimethoxysilane (APTMS) and 2650 μL of tetraethyl orthosilicate (TEOS). The mixture was heated to 40 °C until the appearance of turbidity and kept in this temperature under controlled stirring for 5 min. The obtained gel was cooled to room temperature and maintained at ambient temperature for 12 h to ensure dryness of the material. After this period, the MIP was crushed in a agate mortar and washed with 1 L of warm deionized water and then with 300 mL of methanol to remove the template molecule. This washing process was repeated for two more times to ensure complete removal of the template (kanamycin sulfate). The total extraction of kanamycin sulfate of the MIP was monitored through the photoluminescent response of the probe (AuNPs-GQDs-amino). The clean polymer was left to dry in a desiccator and then passed through a molecular sieve to obtain regular particles with diameters from 106 to 150 μm . The MIP was stored at room temperature. In Figure 3.3 the infrared spectra of the MIP are shown after the cleaning steps compared to the spectrum of the template molecule. In the infrared spectrum of the MIP it can be seen that the characteristic peaks of kanamycin (template molecule) are absent after cleaning, where the characteristic infrared bands of the polymer are dominant: 3307 cm⁻¹ (NH₂ from the APTMS); 2956-2889 cm⁻¹ (CH₂ from the APTMS); 1120 and 1033 cm⁻¹ (stretching of C-O from ether and Si-O-Si stretching) and 781 cm⁻¹ (Si-C stretching) [110]. The microscopy of produced MIP after cleaning is shown in Fig. 3.4. The microscopy corroborated the diameter of the fraction of MIP chosen to perform extraction.

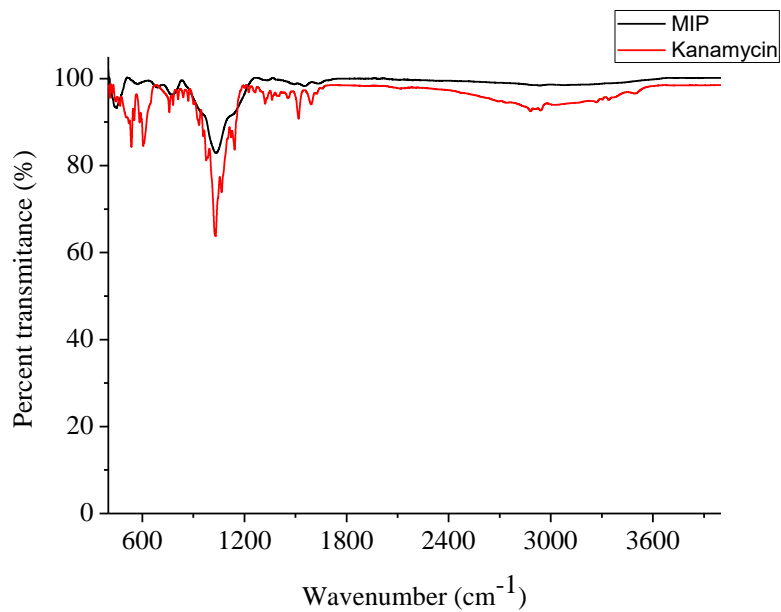


Figure 3.3. Infrared spectrum of kanamycin sulfate (red) and kanamycin MIP after clean-up to remove the kanamycin template.

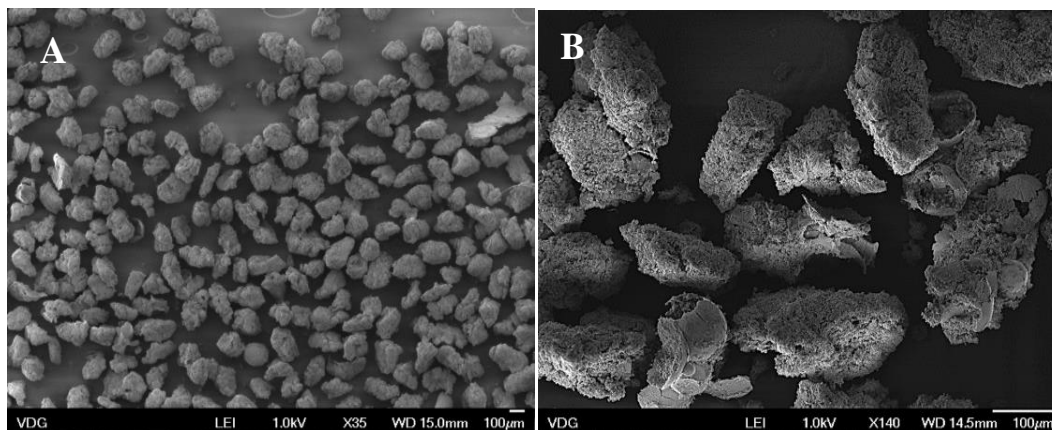


Figure 3.4. Scanning electron microscopy of the sol-gel matrix kanamycin-MIP (fraction collected in the sieve of 150 μm) using different enlargements: (A) 35x and (B) 140x.

3.6

Photoluminescence measurements and preparation of samples

3.6.1

Procedures for captopril

3.6.1.1

Analytical probes, standard solutions and photoluminescence measurements for captopril

Standard stock solutions at $1.0 \times 10^{-2} \text{ mol L}^{-1}$ and $1.0 \times 10^{-3} \text{ mol L}^{-1}$ were prepared by dissolving appropriate amounts of captopril or a specific co-existing substances (lactose, silicon dioxide, hydrochloro-thiazide, citric acid, ascorbic acid, SDS, β -cyclodextrin) in ultrapure water.

Working dispersions of GQDs and GQDs-amino (analytical probes) were prepared using 500 μL of the synthesis dispersion and placed to the 5.00 mL volumetric flask. Volume was adjusted with water. When including any additional component, the addition was made before adjusting the final volume with water. The dispersion of GQDs-amino with Fe^{3+} was prepared by mixing 400 μL of the stock aqueous dispersion of GQDs-amino and 1.2 mL of a solution of FeCl_3 ($1.0 \times 10^{-2} \text{ mol L}^{-1}$ at pH 2.0), at room temperature, and then adjusting the volume to 50.00 mL with water in volumetric flask. Volumes of captopril standards were added before the working dispersion had their volume adjusted, with water, to 5.00 mL. These dispersions were transferred to quartz cuvettes to measure photoluminescence at the maximum excitation/emission wavelength pairs either for the GQDs-amino (345/425 nm) or for GQDs-amino- Fe^{3+} (345/435 nm). Blank measurements were made in aqueous dispersions of GQDs-amino with and without Fe^{3+} (depending on the case) without addition of captopril. Working dispersions containing captopril or coexisting substances were left to rest at room temperature for 25 min (GQDs-amino- Fe^{3+}) and 3 min (GQDs-amino) before measurement. Photoluminescence measured from GQDs-amino dispersions containing captopril (L) were normalized by their respective blank signals (L_0) in order to establish an increasing relationship between normalized signal (L_0/L) and the concentration of captopril, with K_s (quenching constant) as the sensitivity factor (Equation 3.2). The quantitative potential of the spectral shift of photoluminescence were evaluated using the net spectral shifting ($\Delta\lambda$), measured

at the maximum of the shifted band and related to the one of the original spectrum in absence of captopril (Equation 3.3).

$$L_0/L = 1 + K_s [\text{captopril}] \quad (\text{Equation 3.2})$$

$$\Delta\lambda = m [\text{captopril}] + b \quad (\text{Equation 3.3})$$

Photoluminescence measured by system GQDs-amino-Fe³⁺ dispersions containing captopril were normalized using the net photoluminescence ($L - L_0$) and concentration de captopril (Equation 3.4).

$$(L - L_0) = m [\text{captopril}] + b \quad (\text{Equation 3.4})$$

3.6.1.2

Determination of captopril in tablets

Pharmaceutical formulation sample solutions were made using a powder obtained from 10 tablets (pulverized in a porcelain mortar). The required quantities were dissolved in water and placed in an ultrasound bath. The non-solubilized excipients were separated by passing the sample through a filter of 0.45 pore size.

3.6.1.3

The Ellman's method for determination of captopril

The Ellman's method was used as a comparative method for the determination of captopril with some modifications. The stock solution (2×10^{-3} mol L⁻¹) of DTNB was prepared in phosphate buffer (0.1 mol L⁻¹, pH 7). For the preparation of the calibration curve, 3 mL of deionized water, 200 μ L of DTNB solution and 400 μ L of phosphate buffer solution were mixed in a cuvette. After mixing, different amounts of standard captopril solution were added. The mixture was allowed to stand for 5 min and then the absorbance was monitored at 412 nm. The blank of the curve was prepared with the same procedure but in the absence of captopril.

3.6.2

Procedures for histamine

3.6.2.1

Analytical probes, standard solutions and photoluminescence measurements for histamine

Standard stock solutions at $1.0 \times 10^{-2} \text{ mol L}^{-1}$ and $1.0 \times 10^{-3} \text{ mol L}^{-1}$ were prepared by dissolving appropriate amounts of histamine or a specific amino acid in ultrapure water. Stock solutions from salts ($\text{NiCl}_2 \cdot 6\text{H}_2\text{O}$, $\text{CdCl}_2 \cdot \text{H}_2\text{O}$, $\text{Pb}(\text{NO}_3)_2$ and $\text{CuSO}_4 \cdot 5\text{H}_2\text{O}$, $\text{ZnSO}_4 \cdot 7\text{H}_2\text{O}$, $\text{FeSO}_4 \cdot 7\text{H}_2\text{O}$), were $1.0 \times 10^{-1} \text{ mol L}^{-1}$ and prepared by the dissolution of the salt in water. Europium nitrate and iron(III) chloride stock solutions were $1.0 \times 10^{-2} \text{ mol L}^{-1}$.

The GQDs-amino aqueous intermediary dispersions were prepared by diluting the synthesis dispersion with water to achieve a final ten-fold dilution (10% v/v). Then, 500 μL of this intermediary dispersion was placed on a 50.00 mL volumetric flask where appropriate volumes of salt stock solutions was added before adjusting final volumetric flask volume. These dispersions, named intermediary GQDs-amino- M^{n+} dispersions, contained one of the following metal ions (M^{n+}): Cu^{2+} at $3.0 \times 10^{-3} \text{ mol L}^{-1}$; Fe^{3+} at $2.0 \times 10^{-4} \text{ mol L}^{-1}$ or Eu^{3+} at $6.0 \times 10^{-4} \text{ mol L}^{-1}$.

The working dispersions (probes) were prepared by placing 4.00 mL of the GQDs-amino- M^{n+} dispersions into a 5.00 mL volumetric flask. Then appropriate volume of either histamine or an amino acid solution was added before adjusting the final volume with water. Blank dispersions had their final volume adjusted only with water. Working dispersions containing histamine or amino acids were left to rest at room temperature for 20 min before measurement.

Appropriate volumes of histamine or other amino acid standard solution were added before the working dispersion of either GQDs-amino or GQDs-amino- M^{n+} had their final volumes adjusted with water. These dispersions were transferred to quartz cuvettes to measure photoluminescence at the maximum excitation/emission wavelength pairs: GQDs-amino (345/425 nm); GQDs-amino- Fe^{3+} (345/435 nm); GQDs-amino- Cu^{2+} (345/428 nm) and GQDs-amino- Eu^{3+} (345/428 nm). Blank measurements (L_0) were made in aqueous dispersions of

GQDs-amino- M^{n+} without addition of histamine. Photoluminescence measured from dispersions containing histamine or a specific amino acid (L) were normalized by their respective blank signals (L_0) in order to establish an increasing relationship between normalized signal (L_0/L) and the concentration of histamine, with K_s (quenching constant) as the sensitivity factor (Equation 3.2).

$$L_0/L = 1 + K_s [\text{histamine}] \quad (\text{Equation 3.5})$$

3.6.2.2

Procedure for preparation of tuna samples

The histamine was extracted from the flesh of tuna samples following a procedure reported in the literature with minor modifications in terms of the amount of TCA used for the precipitation of proteins in the sample extract [111]. An amount of tuna (dorsal part of skinless fish) was macerated and homogenized for 5 min. Then, 5.0 g of it was transferred to a polypropylene centrifuge tube, mixed with 25 mL of an aqueous TCA 2.5% solution before performing SPE.

Fresh tuna extracts were fortified with histamine after neutralization and before the SPE procedure. The determination of the real content of histamine in tuna fish samples were conducted with the samples brought to the lab under refrigerated conditions. One aliquot of the refrigerated sample was taken and processed (mixed with TCA, centrifuged, extract neutralized and submitted to SPE) and immediately analyzed (0 h). Other aliquots were selected and stored at room-temperature in order to let them spoil. Selected portions of these aliquots were submitted to sample processing after 3, 6, 12 and 24 h.

3.6.2.3

Solid phase extraction of histamine

The extract obtained from the tuna sample was centrifuged for 15 min at 60,000 relative centrifugal force (RCF) at 15°C. A volume of 10.0 mL of the extract was neutralized with an aqueous NaOH solution (0.10 mol L⁻¹) and filtered using a filter paper. The extract was submitted to a solid phase extraction (SPE) passing them through a cartridge containing a cationic adsorbent (Amberlite CG-50). The cartridge was washed several times with acetate buffer (0.2 mol L⁻¹, pH 4.6). Histamine retained on the column was recovered with 0.5 mL of HCl

solution (0.2 mol L^{-1}). The pH of the eluted solution, containing histamine, was adjusted between 3.3 and 3.8. Then an aliquot was added to the aqueous dispersion GQD-amino- Fe^{3+} to measure their effect on the measured photoluminescence. The sample blank was a TCA solution, which was subjected to the same SPE extraction procedure. Recovery tests to evaluate the efficiency of the SPE procedure and selectivity studies in the presence of amino acids were made in the same way.

3.6.2.4

Chromatographic method for the determination of histamine

The HPLC based method used to determine histamine was based on the literature [112]. The method employed chemical derivatization of histamine using OPA. The mobile phase was prepared by mixing 2.72 g of sodium acetate, 180 μL of triethylamine, 3.0 mL of THF in water (final volume 400 mL). The pH 7.2 was adjusted by adding glacial acetic acid. Then, methanol was added to enable 1 L of mobile phase, which was degassed, 30 min, in ultrasound bath at room temperature previously to use at a flow rate of 1.0 mL min^{-1} . The introduction of sample or standard into the HPLC system was made through a 20 μL sample loop. Fluorescence measurements were made at 340/445 nm. Under such conditions, the retention time of histamine in the C18 column was 5.95 min. For HPLC analysis, the histamine stock solution (1000 mg L^{-1}) was prepared in water and used to prepare, by dilution, the analytical standards (from 50 to $400 \mu\text{g L}^{-1}$). The derivatization solution was prepared by mixing 0.44 g of potassium hydroxide, 1.25 g boric acid and 0.01 g of OPA in water. Methanol (75 μL) and 2-mercaptoethanol (75 μL) were added before final volume adjustment (25 mL) with water. Derivatization was made by mixing 500 μL of analytical standard solution or sample solution (after extraction process) with 500 μL of the derivatization solution. After 1 min of reaction, 20 μL were introduced into the HPLC system. HPLC-MS analysis made in tuna fish extracted samples were made with instrumental conditions that includes C18 column temperature of 25°C , injection volume of 2 μL , mobile phase consisting of mixture 0.1% formic acid aqueous solution/acetonitrile (95/5% v/v) at a flow rate of 0.2 mL min^{-1} (isocratic mode). The spraying ionization source was kept at 5 kV, the capillary was kept at

42 V and at 275°C with desolvation temperature of 350°C under sheathing gas (N₂).

3.6.3

Procedures for kanamycin

3.6.3.1

Analytical probes, standard solutions and photoluminescence measurements for kanamycin.

Stock standard solutions were prepared at 1.0×10^{-2} mol L⁻¹ and at 1.0×10^{-3} mol L⁻¹ by the direct dilution of appropriate amounts of kanamycin sulfate or any tested interfering species in ultrapure water. Less concentrated standard solutions were prepared by diluting the stock solutions with water.

Working dispersions of AuNPs-GQDs-amino (analytical probe) were prepared using 1.50 mL of the synthesis dispersion and placed in a 5.00 mL volumetric flask. The blank dispersions had their final volume adjusted only with water. Working dispersions containing kanamycin sulfate or interfering species were allowed to stand at room temperature for 30 min prior to measurement.

Appropriate volumes of kanamycin sulfate were added to the nanoparticle dispersion before its volume adjusted to 5.00 mL with deionized water (the working dispersion). These dispersions were transferred to quartz cuvettes for photoluminescence measurement at 345/425 nm ($\lambda_{ex}/\lambda_{em}$). Blank measurements were made on aqueous dispersions of AuNPs-GQDs-amino without addition of analyte. Signals (L) obtained by the interaction of kanamycin sulfate or interferers species evaluated with the probe were normalized by their respective blank signals (L₀) in order to establish an increasing ratio between the normalized signal as $(L-L_0)/L_0$ vs [kanamycin].

3.6.3.2

Solid phase extraction of kanamycin using MIP

The cartridges used for SPE procedure were prepared using 70 mg of the kanamycin-MIP which were packed inside a 1 mL polypropylene micropipette tip containing a little piece of wool near the tip to work as a membrane allowing the solution to percolate and keeping the MIP particles packing inside the tip.

This SPE process was semi-automatized with the help of a flow system. This cartridge was previously conditioned with water, then washed also using water using the flow system. An aliquot of 40 μL of sample was manually loaded into the SPE cartridge. Then, were added 5 mL of ultrapure water (in each cartridge) with controlled flow of 1 mL min^{-1} . The sample was finally eluted using 1.0 mL aqueous acid solution (pH 3.5 adjusted with HCl 0.01 mol L^{-1}) [110]. The total volume obtained from the elution was adjusted to pH 4.5 with NaOH 0.01 mol L^{-1} and added to the aqueous dispersion (probe) and adjusted to a final volume of 5 mL with ultrapure water. After each extraction step performed with the samples, the cartridge went through a cleanup step with 5 mL of warm water and 5 mL of methanol to ensure complete cleanup of the polymer for use in the subsequent extraction. A single kanamycin-MIP cartridge and a single NIP cartridge were used throughout the development of the work.

3.6.3.3

Sample preparation for analysis of kanamycin in pharmaceutical formulation and yellow fever vaccine

Sample solutions of the pharmaceutical formulations evaluated were prepared using successive dilutions of the original sample. The pharmaceutical formulation tested in this work contains in addition to kanamycin sulfate the following excipients: sodium bisulfite and sodium citrate. Samples of yellow fever vaccine were fortified with kanamycin sulfate at two concentration levels (2.5×10^{-4} and $5.0 \times 10^{-4} \text{ mol L}^{-1}$). The yellow fever vaccine tested contain as excipients: L-alanine, L-histidine, sodium chloride, sorbitol and lactose.

3.6.3.4

Chromatographic method for the determination of kanamycin sulfate

The HPLC method used to determine kanamycin sulfate as a comparative method was based on the literature with some modifications [113]. The method is based on the chemical derivatization of kanamycin using OPA. The mobile phase was composed of a solution of ammonium acetate (0.77 g ammonium acetate was added to 800 mL water then mixed with 40 mL acetic acid and adjusted to 1 L with a mixture of water and acetonitrile (50:50% v/v). The mobile phase flow rate

was 1.0 mL min^{-1} and the introduction volume into the HPLC system was $50 \text{ }\mu\text{L}$ at room temperature. The analyte was monitored by fluorescence with excitation wavelength at 340 nm and emission wavelength at 450 nm . Under such conditions, the retention time of the kanamycin sulfate on the C18 column was 17.2 min .

For the HPLC analysis, the stock solution of kanamycin sulfate (1000 mg L^{-1}) was prepared in water and used to prepare, by dilution, the analytical standards (1 to 10 mg L^{-1}). The derivatization solution was prepared by dissolving 0.054 g of OPA in 2.0 mL of methanol and then adding 2-mercaptoethanol ($40 \text{ }\mu\text{L}$) and diluting to 10 mL with borate buffer solution (0.4 mol L^{-1} ; pH 9.5) protecting the mixture from ambient light. This solution was prepared in the same day of the analysis. The derivatization was made by mixing $400 \text{ }\mu\text{L}$ of standard analytical solution or sample solution with $150 \text{ }\mu\text{L}$ of the derivatization solution. After 10 min of mixing, $50 \text{ }\mu\text{L}$ was introduced into the HPLC system.

3.6.3.5

Study of the catalytic reduction of 4-nitrophenol with AuNPs

The catalytic effect of either AuNPs or AuNPs-GQDs-amino-CTAB were performed as reported in literature [114]. Briefly, in a quartz cuvette, 1.0 mL of an aqueous NaBH_4 solution (0.03 mol L^{-1}) and $40 \text{ }\mu\text{L}$ of the gold nanoparticle dispersion were added to the following reaction mixture: 1.39 mL of water and $300 \text{ }\mu\text{L}$ of 4-NP ($2.0 \times 10^{-3} \text{ mol L}^{-1}$). The decreasing of the intensity of the 4-nitrophenolate ion band was monitored at 410 nm by UV-visible molecular absorption spectrophotometry.

4

Characterization of the nanomaterials

One of the crucial steps in the development of nanosensors is the characterization of the optical and/or electronic properties of the involved nanomaterials. In this work, GQDs, GQDs-amino and AuNPs-GQDs-amino dispersion were investigated as sensing probes. Therefore, these nanomaterials were characterized using different techniques in order to evaluate their size distribution, structural characteristics, their optical absorption profile and their luminescence characteristics. Techniques such as luminescence spectroscopy, spectrophotometry, scanning transmission electron microscopy (STEM), Raman spectroscopy, atomic force microscopy (AFM) and X-ray photoelectron spectroscopy (XPS) were employed.

4.1

Optical properties of the GQDs and GQDs-amino

GQDs from the pyrolysis of citric acid and the GQDs-amino from the pyrolysis of both citric acid and glutathione were produced by dispersing the molten material in different solutions. The photoluminescence of these graphene quantum dots dispersions were evaluated in the absence and in the presence of captopril. The molten organic material (either citric acid or citric acid/GSH mixture) was added in aqueous solutions of different compositions: i) ultrapure water; ii) solution containing $1.0 \times 10^{-3} \text{ mol L}^{-1}$ of CTAB; iii) solution containing 0.25 mol L^{-1} of NaOH; iv) solution containing 0.10 mol L^{-1} of HCl. Compared with the GQDs photoluminescence intensity obtained in pure water (see Table 4.1), the ones achieved in either acid solution or in solution containing the surfactant CTAB were at least three times lower. However, when the synthesis was made in NaOH solution, the measured photoluminescence was about 28 times more intense. In all cases, blue-shifts of about 20 nm, in both spectral bands, were observed. In the case of GQDs-amino, significant signal enhancements (almost three orders of magnitude) were observed in pure water and in basic medium when compared to the signal observed from GQDs in pure water. In these cases, blue-shifts of about 50 nm occurred in both, emission and excitation spectral

bands. Although blue-shifts were observed in acid and in surfactant containing solution, no significant signal improvement, compared to GQDs in water, were observed.

Table 4. 1. Normalized photoluminescence from GQDs and GQDs-amino aqueous dispersions obtained by the pyrolysis, using pure water and using solutions with different solutes (signals normalized by the one obtained from GQDs in pure water).

Nanomaterial	GQDs	GQDs-amino
	$I_{\text{GQDs (solute)}} / I_{\text{GQDs (pure water)}} (\lambda_{\text{exc}}/\lambda_{\text{em}})$	$I_{\text{GQDs-amino (solute or pure water)}} / I_{\text{GQDs in pure water}} (\lambda_{\text{exc}}/\lambda_{\text{em}})$
Solute ^a		
-	1 (380/480)	911 (345/425)
NaOH	28 (370/460)	663 (345/425)
HCl	0.2 (360/470)	1.5 (365/445)
CTAB	0.3 (350/460)	1.3 (345/420)

^a CTAB 1×10^{-3} mol L⁻¹; NaOH 0.25 mol L⁻¹; HCl 0.10 mol L⁻¹.

From the amino-functionalized graphene quantum dots (GQDs-amino) synthesis dispersion (after filtering and dialysis) an aliquot (a few microliters) was taken and added to ultrapure water (10.00 mL final volume) to form a diluted dispersion used to obtain the spectra in the UV-vis. The wide extinction spectrum, with a maximum peak at about 220 nm, is characteristic of semiconductor quantum dots. Spectral features can be attributed to π - π^* transition of C=C of sp² carbon and to the presence of possible amino functional groups at the edge of the quantum dots [115]. The first excitonic band appeared at 345 nm (Fig. 4.1A). The quantum dots aqueous dispersion showed bright blue-violet emission (maximum at 425 nm) under excitation at 345 nm (Fig. 4.1B). The quantum yield of the GQDs-amino was 54.6%, at 25 °C, being estimated by the comparison with the standard fluorophor quinine sulfate (347/448 nm) in sulfuric acid (0.5 mol L⁻¹) [116]. The photoluminescence of GQDs-amino obtained from the mixture of citric acid and GSH (verted in ultrapure water) is about 900 times more intense than the one obtained using pyrolysis of only citric acid, indicating the presence of electron-donating amino groups generated from the residues of GSH after

pyrolysis. The GQDs-amino dispersion was very stable even after six months storage (under refrigeration) exhibiting clear appearance and strong photoluminescence.

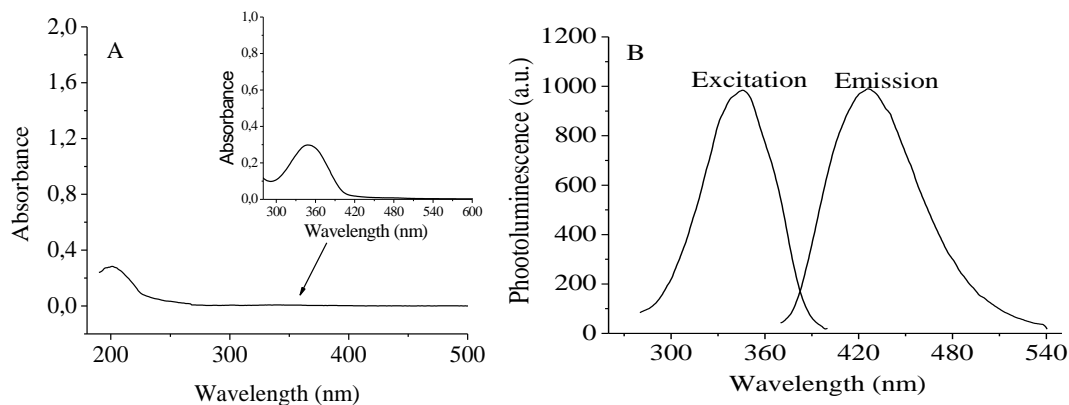


Figure 4.1. (A) Absorption spectra of aqueous dispersion GQDs-amino; (B) Photoluminescence spectrum of excitation and emission GQDs-amino.

4.2

Structural characterizations of the GQDs and GQDs-amino

Two of the synthesized nanomaterials were selected for characterization using field emission scanning electron microscopy (FE-SEM) in transmission mode. Aqueous dispersions of GQDs and GQDs-amino, the ones that produced the most intense photoluminescence, were chosen. The obtained images were processed using the program Image-J in order to obtain the average values for the diameters of the nanomaterials. In the case GQDs, obtained in NaOH solution, it was observed (Fig. 4.2A) the presence of approximately spherical nanomaterials (clusters in some cases) with an average diameter of 5.2 ± 1.2 nm. In contrast, the GQDs-amino (Fig. 4.2B) had a diameter of 27.0 ± 8.3 nm.

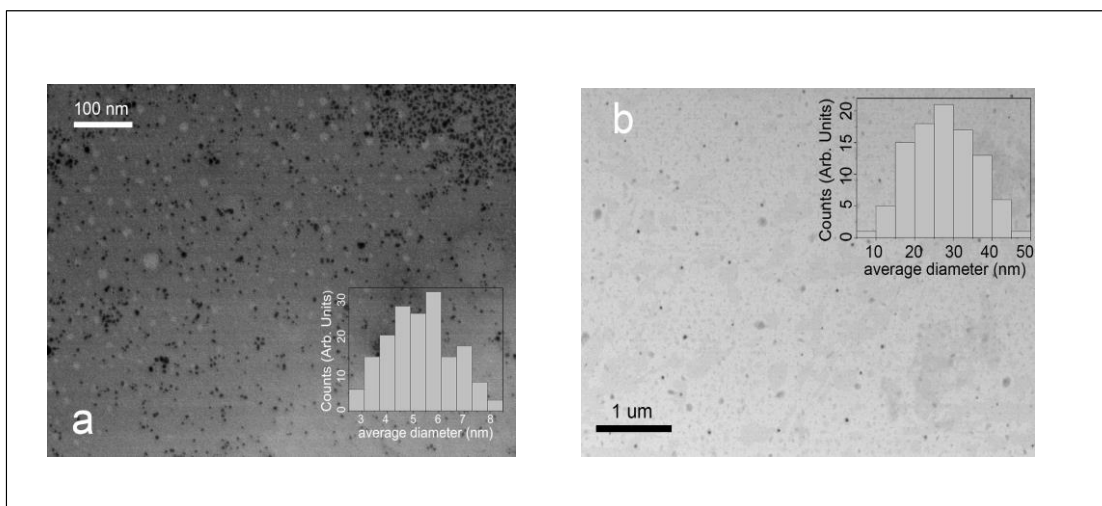


Figure 4.2. FE-STEM images and size distribution of: a) GQDs in NaOH and b) GQDs-amino in pure water.

The Raman spectra of the GQDs, GQDs-amino as well as the one of the GSH and citric acid alone are shown in the Fig. 4.3 GQDs spectrum exhibited typical G- and 2D-bands at 1584 cm^{-1} and 2729 cm^{-1} respectively. The GQDs-amino presented the G-band shifted to lower frequencies (1578 cm^{-1}), typical of quantum confinement of carbon nanostructures with sp^2 hybridization. The values for the 2D- bandwidth remained near 70 cm^{-1} in both cases. The value of the D band associated with defects in GQD could not be precisely determined due to superposition with bands from citric acid and GSH in the same region.

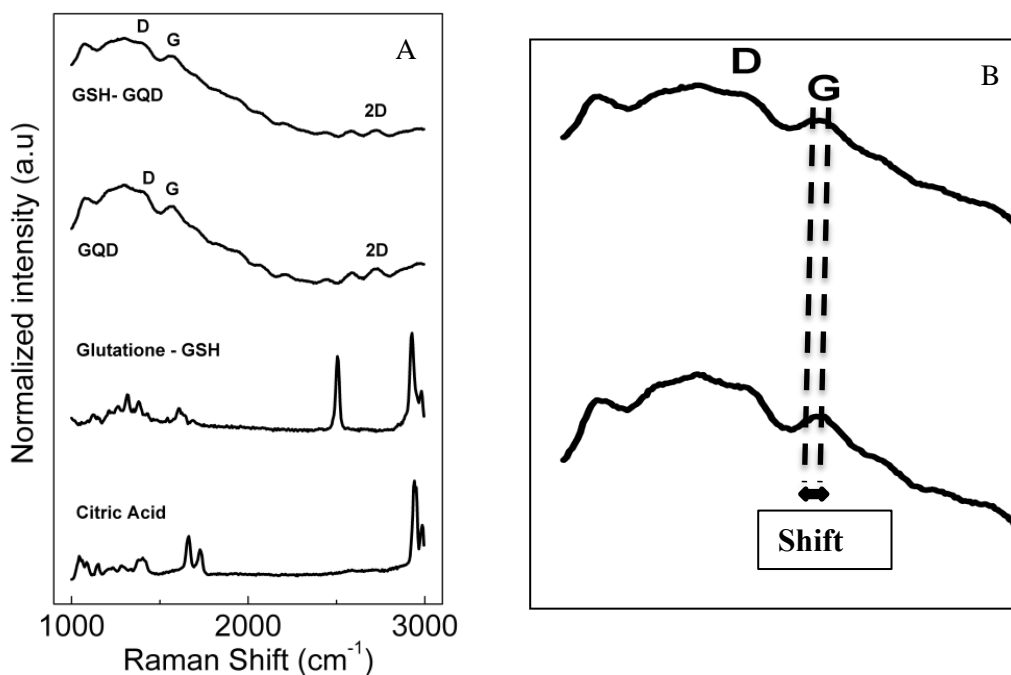


Figure 4.3. A) Raman spectra of GQDs, GQDs-amino, GSH and citric acid (10 times amplification for GSH and citric acid spectra). B) Amplification of the Raman spectra in the range of 1000 to 2000 cm^{-1} .

A second batch of GQDs-amino was synthesized and, after a dialysis process, had their morphology and structure evaluated. The analysis of the synthesized GQDs-amino dispersion resulted in the concentration of 120 mg L^{-1} of total carbon (TC) after 24 h dialysis. From this dialyzed synthesis dispersion, the working dispersions (after 100 times dilution) were prepared (TC of 1.2 mg L^{-1}). Characteristic Raman features (bands D and G) indicated sp^2 carbon in graphitic nanostructures. In Fig. 4.4A the peak near 1586 cm^{-1} is assigned to G band, characteristic to the E_{2g} phonon of sp^2 carbon atoms, and the one near 1358 cm^{-1} can be assigned to the D band. The spectrum presents characteristic of very disordered systems. The produced GQDs-amino had a size distribution in the range of 5 to 50 nm, with an average diameter of 28.4 nm (Fig. 4.4B). In Fig. 4.4C, AFM analysis may reveal that the typical topographic height of the GQDs-amino were in the range of 1.4 to 3.0 nm (about 10 layers of graphene).

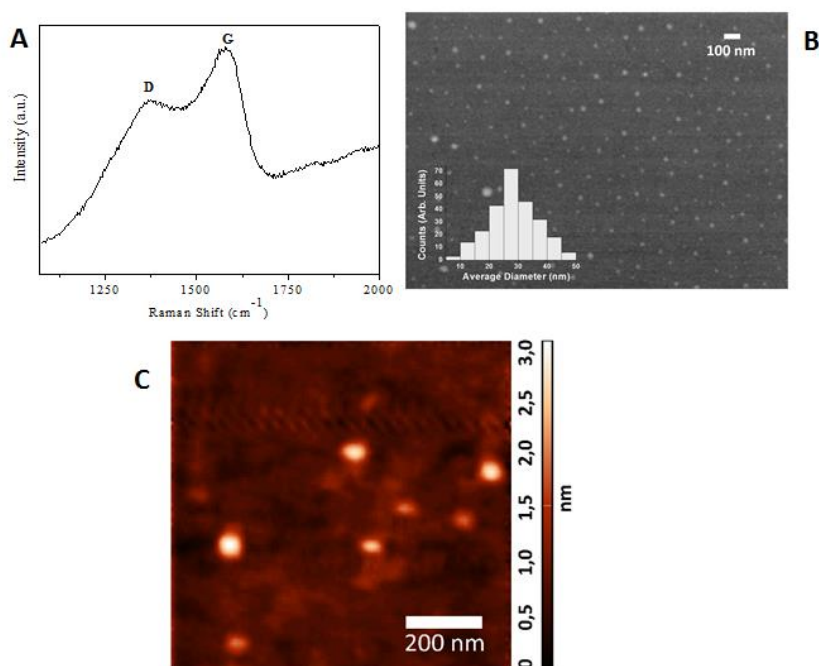


Figure 4.4. Characterization of GQDs-amino: (A) Raman spectra; (B) FE-STEM images and size distribution; (C) AFM topography image.

XPS was used to obtain information that indicated the presence of amino groups in the GQDs structure, as the general survey (Fig. 4.5A) presented characteristic peaks for carbon, oxygen and nitrogen at binding energies of about 285 eV (C1s), 535 eV (O1s) and 400 eV (N1s). The spectrum showed C 1s peaks at 284.6, 286.0 and 288.3 eV (Fig. 4.5B), which can be assigned to the contributions of C-C sp^2 and sp^3 , C-O (C-N) and the C=O respectively. Spectra also shows N1s main peak (Fig. 4.5C) at binding energy 399.8 eV, indicating that the nature of the nitrogen attached to the surface is mainly organic such as the ones typical of amines C–N. The second peak at 401.7 eV corresponds to graphitic bound N. Together with the significant changes in photoluminescence, those XPS spectral features strongly indicated the functionalization of GQDs edges and surface with nitrogen (most probably amino groups) that affects significantly photoluminescence and produced better dispersed nanostructures in water because of the creation of surface charges [115,117].

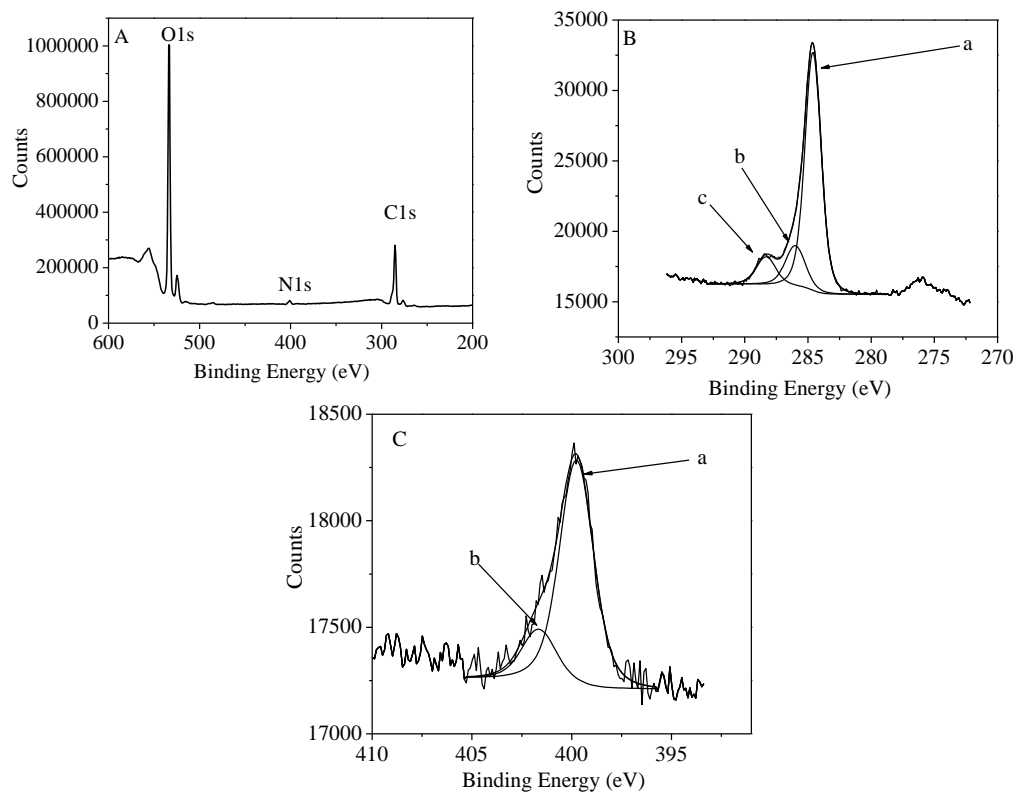


Figure 4.5. (A) XPS general survey scan of GQDs-amino. (B) High resolution C 1s peaks with a, b, and c corresponding to C-C sp^2 e sp^3 , C-N (-O), and COOH groups, respectively. (C) High resolution N 1s peaks with a and b corresponding to C-N piridinic and graphitic respectively.

4.3 Characterization of AuNPs

The dispersed AuNPs synthesized in water by the reduction with NaBH_4 showed extinction profile with a spectral maximum at 507 nm (localized surface plasmon resonance band) that indicated the presence of spherical nanoparticles (Fig. 4.6A). The concentration (C) of AuNPs was estimated using Equation 4.1, where N_T is the total number of Au atoms based on the initial mass of the Au source, V is the volume of the synthesized solution and N_A is the Avogadro constant and N is the number of Au atoms.

$$C = \frac{N_T}{NVN_A} \quad (\text{Equation 4.1})$$

N is estimated by Equation 4.2 [118], where D is the average diameter of the particles, estimated by either STEM or DLS, assuming the density ρ of the

nanoparticles equal to the density of bulk Au whose value is 19.3 g cm^{-3} , M is the Au molar mass.

$$N = \frac{\pi\rho D^3}{6M} \quad (\text{Equation 4.2})$$

The concentration of AuNPs in the dispersion was $3.8 \times 10^{-9} \text{ mol L}^{-1}$ as the average diameter of the AuNPs was $10.9 \pm 3.5 \text{ nm}$ (Fig. 4.6B). Computational processing of the images indicated the aspect ratio of 1.30 ± 0.20 .

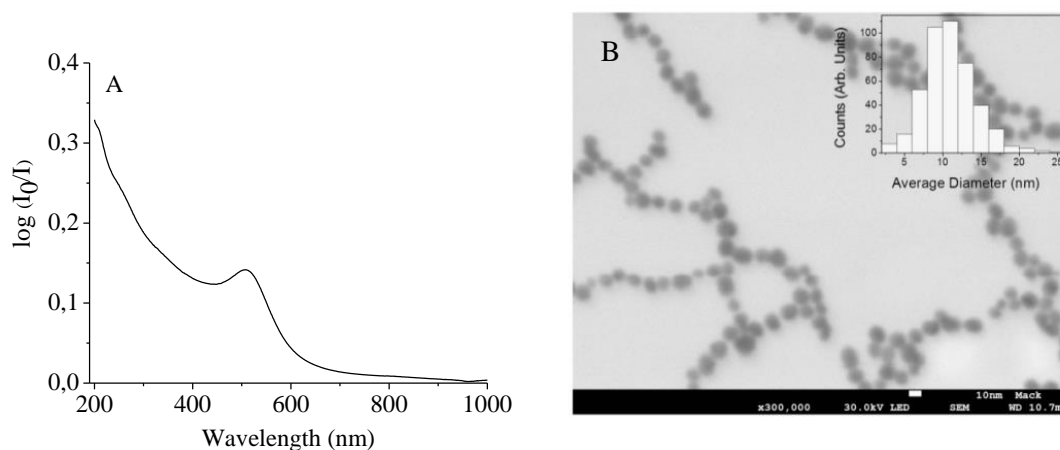


Figure 4.6. (A) AuNPs synthesized from HAuCl_4 (5 fold dilution) with NaBH_4 as the reducing agent (B) FE-STEM images and size distribution of AuNPs aqueous dispersion.

5

Different approaches for sensing captopril based on functionalized graphene quantum dots as photoluminescent probe

Material published as: “*Different approaches for sensing captopril based on functionalized graphene quantum dots as photoluminescent probe*” Toloza CAT, Khan S, Silva RDL, Romani EC, Freire Jr FL, Aucélio RQ, *J. Luminesc.* 2016, 179, 83-92, DOI: 10.1016/j.jlumin.2016.06.055 (See attachment A1).

5.1

Captopril and analytical methods for its determination

Hypertension is the elevation of the blood pressure of the human body that leads to overwork of the heart and blood vessels. Untreated hypertension can cause a number of negative health effects such as chest pain (angina), heart attack, stroke, kidney failure, among others. Antihypertensive drugs act on the human body by lowering blood pressure through a series of actions: (i) opening and enlarging blood vessels, (ii) preventing blood vessel closure and tightening, (iii) reducing the workload of the heart [119]. There are ten types of antihypertensives categorized by the action mechanisms: diuretics, enzyme inhibitors (ACE), angiotensin receptor blockers, alpha-blockers, beta-blockers, calcium channel blockers, angiotensin converting, central adrenergic inhibitors, inhibitors peripheral adrenergic and blood vessel dilators [120].

Captopril, 1 - [(2S) -3-mercapto-2-methyl-L-oxopropyl] -L-proline (Figure 5.1), belonging to the group of antihypertensives, is used in the treatment of hypertension and congestive heart failure that blocks the conversion of angiotensin II from ACE [121], which causes blood vessels to tighten. It was the first ACE inhibitor drug marketed. Although several other ACE inhibitors (such as enalapril, lisinopril, perindopril and ramipril) have been developed, captopril has the lowest cost and therefore is widely indicated in the medical prescription for the general population.

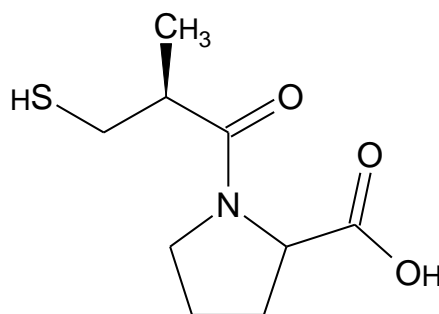


Figure 5. 1. Captopril structure.

Captopril is a slightly yellow or white crystalline powder, easily soluble in alkaline solution, ethanol, chloroform, methanol and water. This drug can be found in medicines at various dosages and trade names.

Most spectro-analytical methods for captopril are based on the long chemical derivatization of the analyte due to the lack of strong chromophore groups in its structure. High-performance liquid chromatography (HPLC) and capillary electrophoresis (EC) using photometric absorption provide LOD values for captopril up to the level of ng mL^{-1} in complex samples such as (plasma and urine) after chemical derivatization of the substance of interest [122]. Some attempts were made to detect captopril and its degradation products using capillary electrophoresis without chemical derivatization, however, poor detection levels (LOD of 1.0 mg mL^{-1}) were achieved.

A simple spectrophotometric method was developed for the determination of captopril in pharmaceutical products [123]. The method was based on the reacting 2,6-dichloroquinone-4-chlorimide in dimethylsulfoxide with captopril. The yellow color reaction product was measured at 443 nm with LOD of $0.66 \mu\text{g mL}^{-1}$. The different experimental parameters that affect color development and stability have been carefully studied and optimized. The proposed method was successfully applied for the analysis of commercial tablets and the results were in agreement with the results obtained in using official and reference spectrophotometric methods. Hydrochlorothiazide, which is often co-formulated with captopril, did not interfere with the assay. A highly sensitive fluorescence method for the determination of captopril in the pure form and tablet dosage form was proposed by El-Didamony *et al.*, The method was based on the oxidation of captopril by Ce (IV) in the presence of sulfuric acid with subsequent monitoring of Ce(III) ion fluorescence (256/354 nm). All variables affecting the reaction conditions, such as Ce (IV) concentration, type and concentration of acid, reaction

time, solvent dilution, temperature and heating time were carefully studied and optimized. Under the experimental conditions used, a good linear relationship was obtained between the fluorescence intensity and captopril concentration. The accuracy of the method was satisfactory and the relative standard deviation values did not exceed 1.1%. No interference was observed from the excipients and additives which are generally presented in formulation. The proposed method was successfully applied in pharmaceutical formulations with recoveries in the range of 99.8-100.2%. The results of the analysis are in agreement with those obtained by the official method [124].

A fluorimetric method was developed by Al-Ghanman *et al.*, [125] for the determination of three pharmaceutical compounds containing thiol groups including captopril. In this method, the drugs were treated with 1,2-naphthoquinone-4-sulfonic acid which was reduced to 1,2-dihydroxynaphthalene-4-sulfonic acid and which has maximum fluorescence intensity between 480 to 318 nm. The method was sensitive in the concentration range of 0.5-4.5 $\mu\text{g mL}^{-1}$ with a detection limit of 0.05 $\mu\text{g mL}^{-1}$ ($S/N = 2$). The results obtained with the developed method were compared favorably with the results obtained by the pharmacopoeia method.

Khan *et al.*, in 2014 developed a method for the determination of captopril based on the photoluminescence amplification of the 2-mercaptopropionic modified CdTe QDs. At adjusted experiential conditions, the calibration model (the Langmuir binding isotherm) was linear up to $4.8 \times 10^{-4} \text{ mol L}^{-1}$ with constant binding equilibrium of $3.2 \times 10^4 \text{ L mol}^{-1}$ and LOD of $2.7 \times 10^{-7} \text{ mol L}^{-1}$ (59 ng mL^{-1}). The approach was tested in the determination of captopril in pharmaceutical formulations and the results were in agreement with those obtained using a comparative method [121].

The goal of the work presented in this chapter is to propose different approaches to quantify captopril using GQDs are presented and compared. The GQDs aqueous dispersions were prepared by the pyrolysis of GSH and citric acid producing amino functionalized GQDs (indicated in the text as GQDs-amino) and used with and without the presence of Fe^{3+} . Analytical responses in the presence of captopril were found in terms of three different photoluminescence variations: i) signal quenching, ii) spectral red-shifting of the GQDs-amino signal and iii) the

switching on of the previously switched-off photoluminescence of GQDs-amino- Fe^{3+} .

5.2

Results and Discussion

5.2.1

Preliminary studies of the interaction between captopril and graphene quantum dots

Addition of captopril (final concentration of $5.0 \times 10^{-5} \text{ mol L}^{-1}$) to the working dispersions of GQDs and GQDs-amino were made to evaluate the effect on the optical response. It was observed that the presence of captopril did not affect neither the photoluminescence intensity nor the spectral position of the GQDs dispersion in basic medium. The interaction between captopril and GQDs were also tested in water either in absence or in the presence of HCl or CTAB and no spectral variation was observed. In contrast, for the GQDs-amino dispersions, captopril has caused the quenching (25%) and red-shift ($\Delta\lambda$ of 7 nm) of the quantum dots spectral band. The same experiment was made in the presence of NaOH, HCl or CTAB and a similar effect, although much less significant, was observed.

Experiments were also made using Fe^{3+} as a mediator of the quantum-dots/captopril interaction since Liu *et al.* have demonstrated the useful luminescence switching on/off sensing quantitative approach of GQDs in the presence of Fe^{3+} to determine phosphate containing metabolites [69]. As observed by Liu *et al.*, in the present work, the addition of Fe^{3+} quenched, due to electron-transfer, the photoluminescence from both GQDs and GQDs-amino. However, the quenching effect was more effective for the GQDs-amino with photoluminescence reduced to 10% of the original intensity when final concentration of Fe^{3+} was $1.3 \times 10^{-4} \text{ mol L}^{-1}$. A spectral red-shift from 425 to 440 nm was also observed. When captopril was added (at $5 \times 10^{-5} \text{ mol}^{-1}$ final concentration) part of the original quantum dots photoluminescence was restored (39% of the original intensity), with no reversion of the previously observed spectral shifting, i.e., the signal enhancement occurred and the spectral maximum remained at 440 nm. Such behavior indicated a probable captopril and Fe^{3+} interaction on the surface of the GQDs-amino, otherwise, if captopril had

removed Fe^{3+} from the quantum dots, a spectral shifting towards the original spectral maximum (425 nm) would be observed.

5.2.2

GQDs-amino photoluminescence quenching and spectral displacement induced by captopril

5.2.2.1

Stability of photoluminescence signal in function of time and pH

Experimental parameters were studied aiming conditions for stable and intense photoluminescence from GQDs-amino aqueous dispersions in order to enable a reliable and intense analytical response in the presence of captopril. First, the volume of the GQDs-amino synthesis dispersion to be used in the working dispersion (probe) was adjusted to enable a signal response close to the maximum instrument detection scale (80% of the maximum signal) in order to achieve a large working detection range. The chosen condition was 50 μL of working dispersion in a final probe volume of 5.00 mL (pH around 4.7).

The intensity of the photoluminescence was studied in function of time (measured every 5 min up to 60 min at room temperature). The measured signal from the aqueous dispersion of GQDs-amino was stable within the studied range (random variation below 2%). The signal stability of the GQDs-amino probe was also evaluated after the addition of captopril ($5.0 \times 10^{-5} \text{ mol L}^{-1}$). The photoluminescence signal was measured each 5 min (up to 60 min) after the mixing of captopril (at room temperature). The photoluminescence response was promptly quenched achieving a signal level that was stable during the whole monitored time. This result indicated faster response and a more stable behavior when compared to the general stability of aqueous working probes based on semiconductor quantum dots, which takes, sometimes, more than 20 min to achieve stabilization of photoluminescence intensity after the addition of an analyte, usually requiring pH buffering, such as the work of Khan *et al.* using 2-MPA-CdTe quantum dots aqueous probes to determine captopril [121].

The signal intensity measured from the GQDs-amino probes were also monitored in function of the pH of the aqueous dispersion (from 2.3 to 4.7). The pH 4.7 is the original one of the probe with the lower pH values adjusted by the addition of HCl 0.01 mol L^{-1} . In the absence of captopril, it was observed that the

intensity of the photoluminescence signal was not affected by the variation of the pH within the studied range. However, there was a red-shifting (up to 20 nm) as the pH of the dispersion was decreased. When captopril was added ($5.0 \times 10^{-5} \text{ mol L}^{-1}$), the signal quenching is somehow less effective at pH values below 3.3 (constant quenching effect of about 2% from pH 3.3 down to pH 2.3) than the one observed at pH 4.7 (10% signal quenching) as can be found in Fig. 5.2.

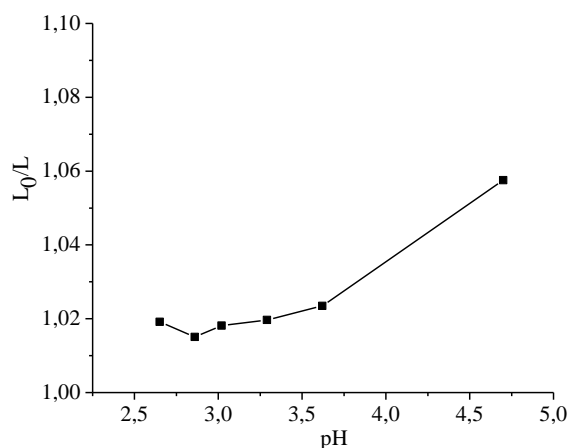


Figure 5. 2. Study of pH (adjusted with HCl 0.01 mol L^{-1}) to evaluate the effect of the photoluminescence quenching of GQDs-amino in the presence of $5.0 \times 10^{-5} \text{ mol L}^{-1}$ captopril, where L_0 and L are the photoluminescence measurements before and the addition of analyte.

Captopril has two pK_a values ($pK_a = 3.7$ concerning the carboxylic group and $pK_a = 9.8$ concerning the thiol group). A more significant fraction of captopril becomes protonated at more acidic pH (above pH 3) due to the carboxylic group, which indicated the importance of the deprotonation of the analyte to enable the interaction between captopril and GQDs-amino. The amino groups, that are believed to be in the surface of the GQDs-amino (due to the use of GSH during synthesis) are protonated, thus enabling an interaction with captopril. In such conditions, thiol groups (from captopril and GSH) remain protonated. A spectral red-shifting of 5 nm was observed as the pH value is decreased from 4.7 to 3.3 and for pH values in the more acid range (down to 2.3) no spectral shifting occurred (Fig. 5.3).

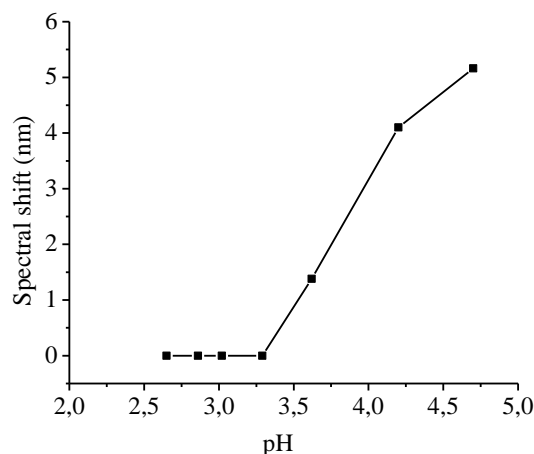


Figure 5.3. Spectral shift observed from GQDs-amino the in the presence of of captopril ($5.0 \times 10^{-5} \text{ mol L}^{-1}$) in function of pH (adjusted with HCl 0.01 mol L^{-1}).

Furthermore, tests were carried to evaluate the signal stability of the probe dispersions at higher values of pH (from 4.7 to 11.3), adjusting the pH with NaOH 0.01 mol L^{-1}). For the GQDs-amino dispersion in absence of captopril, the photoluminescence intensity was constant and similar to the ones observed in more acidic conditions and no spectral shift was observed. In the presence of captopril ($5.0 \times 10^{-5} \text{ mol L}^{-1}$), the magnitude of quenching is about 10% remaining constant up to about pH 9.0, then, becoming less significant at higher pHs (Fig. 5.4A). When compared to the photoluminescence maximum emission wavelength in the absence of captopril, a spectral red-shift of about 6 nm was observed at pH values 5.5 to 7.0, decreasing to about 5 nm from pH 8.0 up the pH 9.5. At more basic pH range, from 9.5 up to pH 11.3, spectral shifting is no longer observed. It is interesting to point out that at pH above 9.5, the thiol group becomes protonated (Fig. 5.4B).

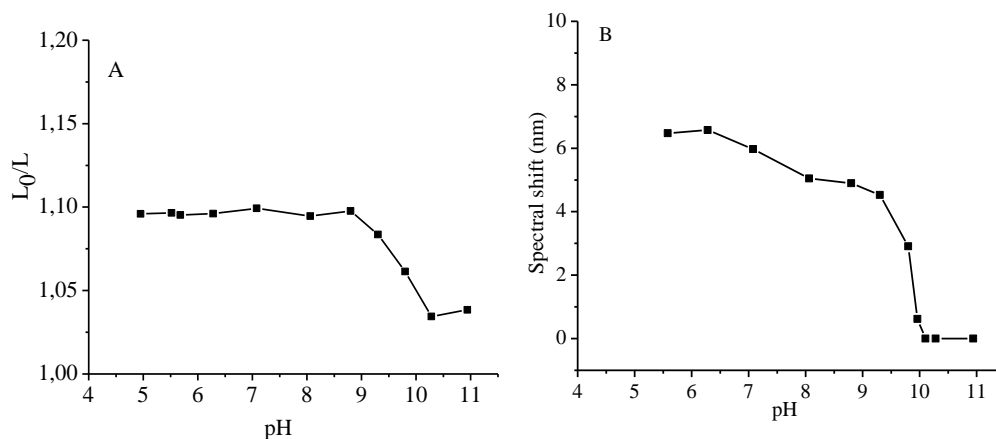


Figure 5. 4. Effect of pH (adjusted with NaOH 0.01 mol L^{-1}) of the GQDs-amino aqueous dispersion: (A) quenching of signal of GQDs-amino in the presence of captopril ($5.0 \times 10^{-5} \text{ mol L}^{-1}$), where L_0 and L are the photoluminescence measured before and after the addition of analyte. (B) relative spectral shift ($\lambda_0 - \lambda$) of the photoluminescence maximum of the in the presence of captopril ($5.0 \times 10^{-5} \text{ mol L}^{-1}$), where λ_0 and λ are the wavelength measured before and the addition of analyte.

5.2.2.2

Effect of Temperature

The effect of temperature on the photoluminescence intensity from the GQDs-amino aqueous probe was studied in the temperature range from 18 to 45°C. The results showed an inverse relationship between signal intensity and temperature (47% decreasing in the temperature range) with no spectral shift. This behavior might be attributed to non-radiative energy loss. A similar study was made using dispersions containing captopril ($5.0 \times 10^{-5} \text{ mol L}^{-1}$) as show in Fig. 5.5A. The quenching effect of captopril was more effective at temperatures from 18°C to 25°C becoming steadily less effective as the temperature is increased until no quenching was produced by captopril at 45 °C. Such a behavior indicates that static quenching is dominant. In Fig. 5.5B it is possible to observe a red-shift (of about 2 nm) as the temperature increased from 18°C to 45°C. This indicates that the interaction between captopril and the GQDs-amino suffers a decrease in the energy gap of π - π transition. Photoluminescence intensity decreases due to the instability of the GSH modified nanomaterial as the increasing in temperature affects the energy transfer between the analyte and the quantum dots. Therefore the temperature control is very critical, which for all measurements of photoluminescence for captopril detection was set to 25°C.

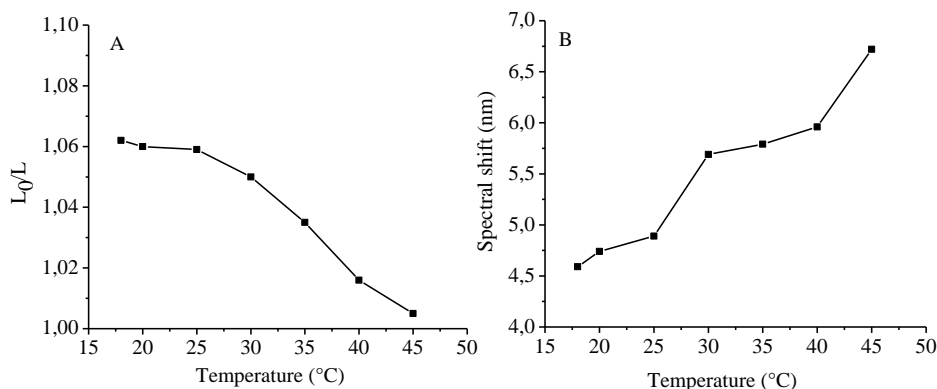


Figure 5.5. Effect of temperature on the photoluminescence from aqueous GQDs-amino probe: (A) the quenching effect in the presence of $5.0 \times 10^{-5} \text{ mol L}^{-1}$ captopril, where L_0 and L are the photoluminescence measurements before and the addition of captopril and (B) the spectral red-shift in the presence of $5.0 \times 10^{-5} \text{ mol L}^{-1}$ of captopril.

A study was conducted to evaluate reversibility of the photoluminescence quenching of GQDs-amino due to temperature increasing. For this purpose, measurements of photoluminescence were performed at 20°C and then at 45°C , where photoluminescence was reduced to about $64.8 \pm 0.5\%$ of the signal observed at 20°C . It was interesting to note that bringing temperature back again to 20°C , the restored signal magnitude was almost complete ($98.2 \pm 0.4\%$ of the signal measured before the temperature cycle), showing that the effect of temperature on the quantum dots is fairly reversible. The experiment was also made aiming to evaluate the signal reversibility of quantum dots in the presence of captopril ($5.0 \times 10^{-5} \text{ mol L}^{-1}$). The application of the temperature cycle, measuring the signal at 20°C then at 45°C and again at 20°C , have demonstrated the reversibility of signal as well as the reversibility of the spectral shift.

5.2.2.3

Photoluminescence time-decay

For the GQDs-amino, a multi-exponential decay was observed with different relative amplitudes (value in parenthesis) as follows: 1.5 ns (5.8); 5.6 ns (58.4); 11.6 ns (35.8). The weighted average lifetime, obtained using the relative amplitude as weighing factor, was 7.5 ns. The quantum dots luminescence average lifetime do not vary significantly in the presence of captopril (Fig. 5.6). This is an indication that the disturbance that results in signal quenching does not occur at the luminophore excited state. Therefore, signal quenching should be due

an interaction that makes the probe not capable to be photo-excited when bounded with captopril.

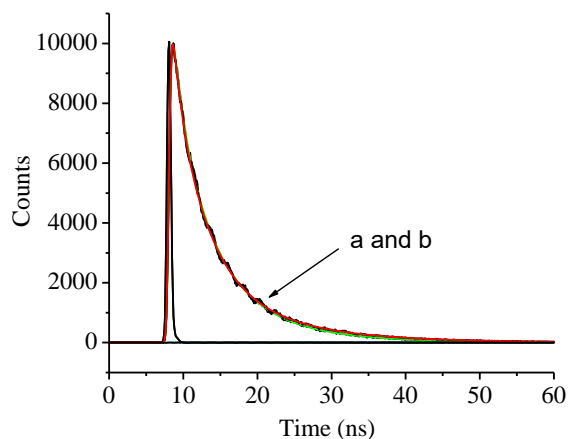


Figure 5.6. Photoluminescence time decay of: A) (a) GQDs-amino and (b) GQDs-amino in the presence of captopril ($5.0 \times 10^{-5} \text{ mol L}^{-1}$).

5.2.2.4

Analytical sensing of captopril using GQDs-amino aqueous probe.

Under the chosen experimental conditions to measure the GQDs-amino photoluminescence (Table 5.1), it was found that two different effects were produced when captopril interacted with the probe: signal quenching effect and spectral shift. Thus, both effects were studied in order to establish a quantitative relationship with the captopril. For the photoluminescence quenching, the Stern-Volmer model was used to establish the relationship between the photoluminescence of the probe (L) in the presence of captopril, normalizing with the probe signal in absence of captopril (L_0), with the increasing concentration of the analyte. When the spectral shifting was used for quantitative purposes, its magnitude was directly related to the concentration of analyte.

Table 5. 1. Experimental conditions for the GQDs-amino probe and GQDs-amino-Fe³⁺ probe used for the sensing of captopril.

Experimental Parameter	Chosen Value	
	GQDs-amino	GQDs-amino-Fe ³⁺
Type of quantum dots		
pH	4.5 to 5 (original pH of the dispersion)	3.3-3.8
Volume of synthesis dispersion	30 μ L in 3.00 mL probe dispersion	30 μ L in 3.00 mL probe dispersion
Concentration of Fe ³⁺	-	3.0×10^{-4} mol L ⁻¹
Photoluminescence signal acquisition after mixing of captopril	After 3 min	After 25 min
Temperature	25°C	25°C

In Fig. 5.7A, the probe photoluminescence quenching and spectral shift generated by captopril is shown (1.2×10^{-5} to 1.7×10^{-4} mol L⁻¹ final concentration of analyte in the dispersion). The analytical curve that correlates the signal quenching (in the form of L_0/L) with the concentration of analyte is shown in Fig. 5.7B. There is a linear response in the studied analyte concentration range ($R^2 = 0.991$) and the calibration equation was $L_0/L = 3.47 \times 10^3$ [captopril] + 0.97. The LOD and limit of quantification (LOQ) values were 4.2×10^{-6} mol L⁻¹ and 1.4×10^{-5} mol L⁻¹, respectively. LOD and LOQ were calculated based on the captopril concentration that produced a photoluminescence decreasing of three times (LOD) and ten times (LOQ) the standard deviation of the probe signal in absence of captopril.

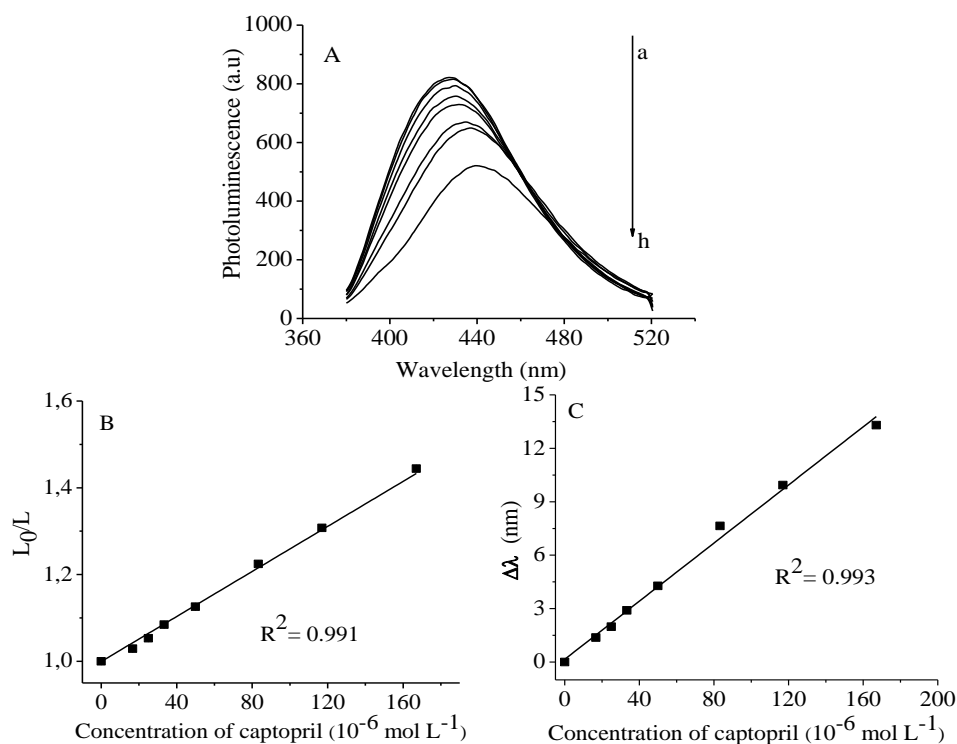


Figure 5.7. (A) Photoluminescent spectral response from the GQDs-amino probe for different concentrations of captopril: (a) 0; (b) 1.7×10^{-5} ; (c) 2.5×10^{-5} ; (d) 3.3×10^{-5} ; (e) 5.0×10^{-5} ; (f) 8.3×10^{-5} ; (g) 1.2×10^{-4} and (h) 1.7×10^{-4} mol L⁻¹. (B) Stern-Volmer curve. (C) analytical curve based on the spectral red-shift.

In order to explore the quantitative potential of the spectral shift, the analytical curve was constructed using the net spectral shifting ($\Delta\lambda$), measured at the maximum of the shifted band and related to the one of the original spectrum in absence of captopril. The analytical curve can be seen in Fig. 5.7C, where linear behavior was found ($R^2 = 0.993$) with equation $\Delta\lambda = 8.157 \times 10^4 [\text{captopril}] + 0.16$. The LOD and LOQ were 1.3×10^{-6} mol L⁻¹ and 4.4×10^{-6} mol L⁻¹, respectively, using $3 s\lambda_{0 \text{ max}}/m$ and $10 s\lambda_{0 \text{ max}}/m$, where $s\lambda_{0 \text{ max}}$ is the standard deviation of maximum wavelength measurement of the probe in absence of captopril and m is the sensitivity of the curve.

5.2.3

GQDs-amino-Fe³⁺ switch on/off photoluminescence probe for captopril

As Fe^{3+} was added to the GQDs-amino aqueous probe (in absence of captopril) the photoluminescence quenching occurred with a red-spectral shifting (Fig. 5.8A). The quenching effect in the presence of Fe^{3+} has been explained by the capability of GSH to coordinate with Fe^{3+} , causing the efficient electron transfer from the GQDs-amino to Fe^{3+} , thus preventing the radiant relaxation of the quantum dots [69]. As captopril is gradually added on this system, the photoluminescence is restored, showing a useful switching on/off property that can be used for quantitative purposes. The photoluminescence enhancement is probably a result of the complex formed at the surface of the GQDs-amino, between Fe^{3+} and the sulfur of the thiol group of captopril producing energy transfer, which increased photoluminescence system. This is supported by the fact that the maximum spectral wavelength of the GQDs-amino system is not restored when photoluminescence increased upon the addition of captopril (Fig. 5.8B).

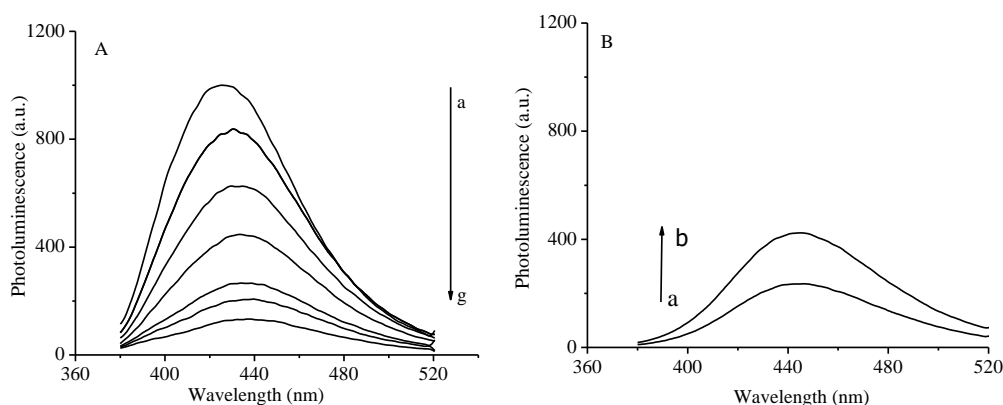


Figure 5.8. GQDs-amino photoluminescence spectrum with excitation at 345 nm: A) GQDs-amino with addition of Fe^{3+} : (a) 0 mol L^{-1} ; (b) 1.7×10^{-5} ; (c) 3.3×10^{-5} ; (d) 5.0×10^{-5} ; (e) 6.7×10^{-5} ; (f) 1.0×10^{-4} ; and (g) $1.3 \times 10^{-4} \text{ mol L}^{-1}$ and B) GQDs-amino- Fe^{3+} after edition of captopril: (a) 0 mol L^{-1} to (b) $1.0 \times 10^{-4} \text{ mol L}^{-1}$.

5.2.3.1

Captopril response in the GQDs-amino and Fe^{3+} probe

Studies were conducted to find a proper proportion between Fe^{3+} and captopril aiming the most significant signal restoration considering a specific amount of captopril added to the probe. The GQDs-amino probe was prepared in the same way for the probe without Fe^{3+} (with 50 μL of synthesis dispersion in 5.00 mL water), then, different volumes of a $\text{Fe}^{3+} 0.10 \text{ mol L}^{-1}$ standard were used.

Each dispersion was fortified with a fixed amount of captopril ($5.0 \times 10^{-5} \text{ mol L}^{-1}$). The reaction was allowed to proceed for 30 min before signal measurement.

The results have shown that as the Fe^{3+} concentration increased, the signal restoration induced by captopril also increased until maximum restoration occurred when Fe^{3+} was $3.0 \times 10^{-4} \text{ mol L}^{-1}$. The signal became saturated at $3.5 \times 10^{-4} \text{ mol L}^{-1}$ of Fe^{3+} , then, at higher concentrations of Fe^{3+} , gradual photoluminescence quenching was again observed. The described behavior might be explained based on the creation of Fe^{3+} sites on the surface of the GQDs-amino until saturation, when maximum interaction with captopril was achieved. As free Fe^{3+} became in excess in the aqueous system, these ions would interact with captopril, preventing them to interact directly with the GQDs-amino- Fe^{3+} . It is important to point out that as the signal restoration is not followed by a spectral maximum restoration towards the original maximum wavelength (blue-shifting is not observed) it is believed that captopril interact with the Fe^{3+} forming a complex, ruling out the possibility of captopril is withdrawing the Fe^{3+} coordinated with the nanoparticle. Based on such results, the concentration of Fe^{3+} added to the probe was fixed at $3.0 \times 10^{-4} \text{ mol L}^{-1}$.

5.2.3.2

Stability of photoluminescence signal in function of time

In order to evaluate the signal stability produced by the switching on/off probe, a study was made first by evaluating the optical response after the mixing of Fe^{3+} without further addition of captopril. The photoluminescence produced by the quantum dots was monitored from 5 to 120 min after the mixing of Fe^{3+} at room-temperature (Fig. 5.9A). Results indicated that the signal quenching achieved maximum effect after 20 min. Then the measured signal remained constant up to 120 min (random standard deviation value of less than 3%). When captopril ($5.0 \times 10^{-5} \text{ mol L}^{-1}$) was added to the system, the restoration increased drastically after only 5 min (Fig. 5.9B), then, slowly increasing until stabilization was achieved after 20 min, remaining constant up to 120 min (random signal variation of no more than 2%).

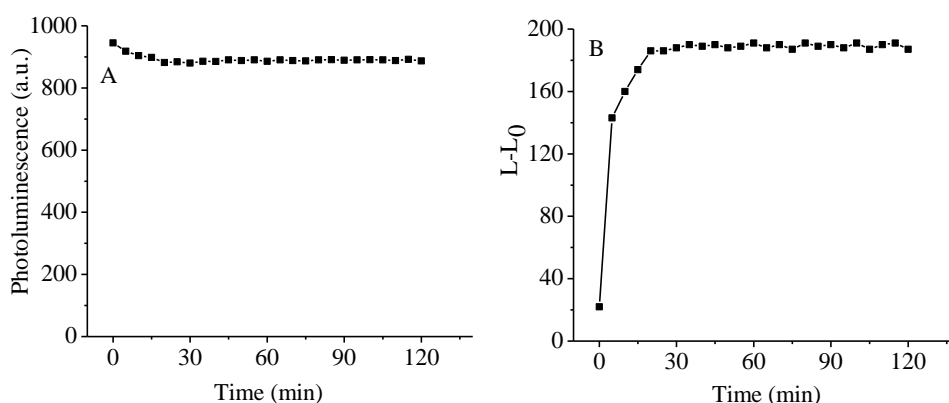


Figure 5.9. Photoluminescence intensity studies in function of time: A) GQDs-amino dispersion after addition of Fe^{3+} ($3.0 \times 10^{-4} \text{ mol L}^{-1}$) B) GQDs-amino- Fe^{3+} dispersion after addition of captopril ($5.0 \times 10^{-5} \text{ mol L}^{-1}$).

5.2.3.3

Photoluminescence time-decay

Photoluminescence time decay was measured under different situations. Taking as reference the lifetime of 7.52 ns (weighted value obtained from the GQDs-amino dispersion), when Fe^{3+} was incorporated in the aqueous system, the lifetime value changes to 10.02 ns, which is a weighted value considering the following lifetimes and relative amplitudes of the luminophores that produced the multiexponential decay: 0.8 ns (1.7); 3.7 ns (29.5); 13.0 ns (68.8). This is an indication that the surface modification (leading to the quenching) first occurs in nanoparticles that present shorter lifetimes as the relative amplitude of the nanoparticles with longer lifetimes increased. After incorporating captopril into the system containing GQDs-amino- Fe^{3+} a similar lifetime (10.00 ns) was obtained, which is a weighted value considering the following lifetimes and relative fractions: 0.8 ns (1.9); 3.8 ns (29.7); 13.0 ns (68.4) (Fig. 5.10).

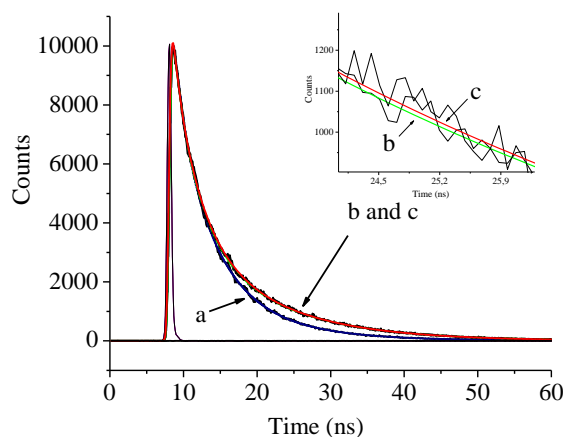


Figure 5.10. Photoluminescence time decay of: (a) GQDs-amino, (b) GQDs-amino-Fe³⁺ and (c) GQDs-amino-Fe³⁺ plus addition of captopril ($5.0 \times 10^{-5} \text{ mol L}^{-1}$).

5.2.3.4 Effect of temperature

Further tests were performed to evaluate the effect of temperature, in the range from 18 to 45°C, on the photoluminescence intensity of GQDs-amino-Fe³⁺ probe in absence of captopril (L_0) as seen in Fig. 5.11A. In this case, the photoluminescence decreased as the temperature increased and the restoration of the original signal was not reversible as the cycle is reversed, with the temperature brought back to 18°C. The irreversibility of the quenching is probably due to the irreversible size increasing of graphene quantum dots that leads to the decreasing of photoluminescence. Comparing the results with the one obtained with GQDs-amino, it is clear that Fe³⁺ plays a crucial role in the agglomeration of the quantum dots.

The interaction study concerning GQDs-amino-Fe³⁺ probe with captopril was also made in function of the temperature (Fig. 5.11B). It could be noticed a proportional signal restoration (measured as $L-L_0$) up to 30°C, indicating that the fraction of the remaining smaller nanoparticles are still optically responsive to the presence of captopril up to such temperature. As the temperature increased to 45°C, signal restoration is less efficient as there was less available smaller

nanoparticles to produce signal restoration as they interact with captopril. The effect was also not reversible as the temperature cycle is reversed.

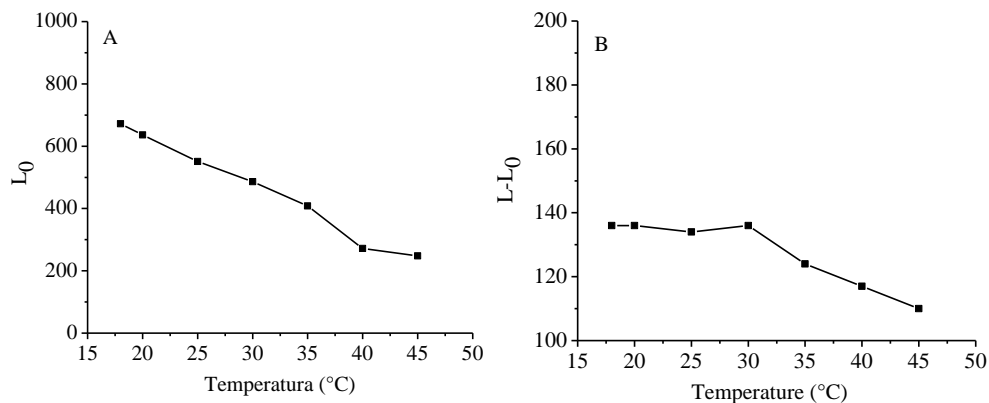


Figure 5.11. Effect of temperature on the photoluminescence GQDs-amino-Fe³⁺ aqueous dispersion: (A) absence of captopril and (B) presence of captopril ($5.0 \times 10^{-5} \text{ mol L}^{-1}$).

5.2.3.5

Analytical sensing of captopril using the switching on/off GQDs-amino-Fe³⁺ aqueous probe

The sensing of captopril using the GQDs-amino-Fe³⁺ probe was evaluated using the adjusted conditions (Table 4.2). It can be observed, in Fig. 5.12A, that the photoluminescence intensity gradually increases as the captopril concentration increased. The analytical curve was constructed using the net photoluminescence ($L - L_0$) as shown in Fig. 5.12B. The linear response ($R^2 = 0.995$) covered the wide range (two orders of magnitude) up to $3.8 \times 10^{-4} \text{ mol L}^{-1}$ (final concentration). The equation model of the calibration curve was $(L - L_0) = 2.24 \times 10^6 [\text{captopril}] + 24.7$. The LOD ($1.4 \times 10^{-6} \text{ mol L}^{-1}$) was calculated from the captopril concentration that produced a photoluminescence intensity equal to $3 sL_0/m$, where sL_0 was the standard deviation ($n=10$) of L_0 and m is the sensitivity of the curve. Similarly, the LOQ ($4.8 \times 10^{-6} \text{ mol L}^{-1}$) was calculated using $10 sL_0/m$.

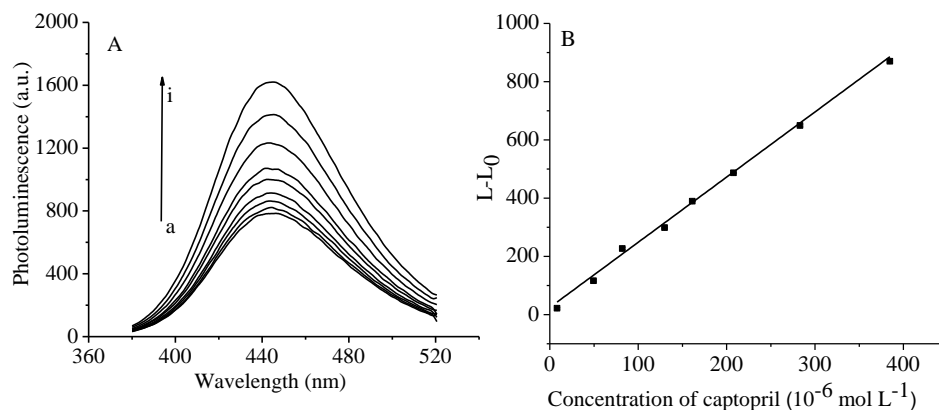


Figure 5. 12. A) Photoluminescence from the GQDs-amino-Fe³⁺ probe with increasing concentrations of captopril: (a) 0 (b) 8.3×10^{-6} , (c) 5.0×10^{-5} , (d) 8.2×10^{-5} , (e) 1.3×10^{-4} , (F) 1.6×10^{-4} , (g) 2.1×10^{-4} , (h) 2.8×10^{-4} , (i) 3.9×10^{-4} mol L⁻¹. B) analytical curve based on the photoluminescence enhancement induced by captopril.

5.2.4

Effect of coexisting substances

A study was carried out to evaluate the selectivity of the method developed in the determination of captopril from the monitoring of the photoluminescent response of the work dispersion of GQDs-amino-Fe³⁺ with different substances. The substances chosen were commonly found in the pharmaceutical formulations of captopril. As can be seen in Table 5.2, the substances tested did not generate significant variations in the photoluminescent signal (less than 3%) at the concentrations evaluated. Therefore, these substances at the indicated concentration levels do not interfere during the probing of captopril.

Table 5. 2. Effect of co-existing substances on the photoluminescence of GQDs-amino and GQDs-amino-Fe³⁺ aqueous dispersion.

Coexisting substances	Concentration (10 ⁻⁵ mol L ⁻¹)	Photoluminescence variation (%)	
		GQDs-amino	GQDs-amino-Fe ³⁺
Lactose	500	-1.8	-1.2
Silicon ioxide	500	-1.5	+1.1
Hydrochloro-thiazide	1000	-2.9	-1.2
Citric acid	100	- 1.1	- 0.3
Ascorbic acid	100	- 0.9	- 0.6
SDS	100	-1.4	-1.2
β- cyclodextrin	100	+0.9	+1.3

5.2.5 Comparative sensing performance

The performances of the captopril sensing approaches are indicated in Table 5.3. The achieved LOD values were in the same order of magnitude no matter the sensing probe used. In addition, the linear ranges and precisions are also comparable. The intermediary precisions were accessed by coefficient of variation obtained of the signal measurements from ten probe dispersions containing 5.0×10^{-5} mol L⁻¹ of captopril.

Table 5. 3. Analytical figures of merit for the captopril sensing using the GQDs-amino probe and the GQDs-amino-Fe³⁺ probe.

	Probe		
	GQDs-amino	GQDs-amino-Fe ³⁺	GQDs-amino-Fe ³⁺
Type of effect	Spectral shifting	Signal quenching	Signal enhancement
Linear range ^a (mol L ⁻¹)	4.4 × 10 ⁻⁶ to 1.7 × 10 ⁻⁴	1.4 × 10 ⁻⁵ to 1.7 × 10 ⁻⁴	4.8 × 10 ⁻⁶ to 3.8 × 10 ⁻⁴
R ²	0.993	0.991	0.995
LOD (mol L ⁻¹)	1.3 × 10 ⁻⁶	4.2 × 10 ⁻⁶	1.4 × 10 ⁻⁶
Intermediary Precision	2.9	1.7	3.1

^a LOQ value up to the highest concentration of the linear response.

All three sensing approaches were used to determine captopril in laboratory simulated samples aiming to evaluate the potential practical use of these probes (Table 5.4). In this case, the recovery tests were made at three different concentration levels: 3.2 × 10⁻⁵ mol L⁻¹, 5.0 × 10⁻⁵ mol and 1.1 × 10⁻⁴ mol L⁻¹ of captopril (final concentration in the probe). Recoveries in simulated samples (captopril dissolved in water) were between 95.4 to 112.3%, which are satisfactory considering the level of captopril in the probe. The results indicated that in a simple sample matrix, the detection performance was equivalent no matter the sensing approach.

When analyzing the real pharmaceutical formulation, the sensing approach based on the signal quenching of the GQDs-amino is affected (recovery of about 50%) probably by the presence of one of the water soluble excipient that prevent the captopril to interact with the quantum dots. In contrast, the recoveries achieved using either the spectral shifting of the GQDs-amino and the signal enhancement of the GQDs-amino-Fe³⁺ switch on/off probe was close to 100%.

Table 5. 4. Recovery (n =3) results for captopril using three different sensing probes using laboratory simulated samples and one real pharmaceutical formulation sample.

Sample	Expected value	Recovery (%) GQDs-amino (spectral shifting)	Recovery (%) GQDs-amino (signal quenching)	Recovery (%) GQDs-amino-Fe ³⁺ (signal enhancement)	Recoveries (%) by the reference method ^c
Simulated Sample	3.2×10^{-5} mol L ⁻¹	95.4 ± 2.1	96.2 ± 2.8	105.1 ± 2.8	102.5 ± 3.2
Simulated Sample	5.0×10^{-5} mol L ⁻¹	100.7 ± 0.7	101.7 ± 1.3	112.3 ± 1.3	106.4 ± 2.2
Simulated Sample	1.1×10^{-4} mol L ⁻¹	105.1 ± 0.7	110.1 ± 2.1	102.3 ± 1.2	98.3 ± 1.9
Pharmaceutical formulation ^a	25 mg ^b	101.9 ± 1.7	46.9 ± 4.1	94.7 ± 1.6	97.8 ± 2.3

^a Captopril concentration in the probe: 1.1×10^{-4} mol L⁻¹

^b Captopril quantity indicated in the pharmaceutical formulation instructions.

^c The Ellman's method.

The group of results obtained for the samples (simulated samples and pharmaceutical formulation) using the methods proposed from GQDs-amino (spectral shifting) and GQDs-amino-Fe³⁺ (signal enhancement) were evaluated in relation to the group of results obtained through the Ellman's Method (spectrophotometric determination) and also agreed according to analysis of variance (single-factor ANOVA with 95% confidence level and n1 = n2 = 3). Fexperimental = 1.72 (spectral shifting) and 2.56 (signal enhancement) < Fcritical = 4.30).

5.3

Partial conclusion

The aqueous dispersion of GQDs-amino and GQDs-amino-Fe³⁺ have been employed as probes for the determination of captopril. The GQDs-amino probe has its photoluminescence quenched and red shifted by captopril enabling an analytical response with LOQ at the 10⁻⁶ mol L⁻¹ level. As the quantification of captopril was made by measuring spectral shifting, the selectivity was guaranteed

in a pharmaceutical formulation matrix. In addition, the switching on/off GQDs-amino-Fe³⁺ probe also enabled good recoveries in the analysis of pharmaceutical formulations. The proposed approaches are very simple and cheaper because it avoids chemical derivatization of captopril. The use of GQDs is a green analytical approach as no toxic reagent is used. Therefore, it was shown a potential competitive assay compared to the ones already reported in literature.

6

Photoluminescence suppression effect caused by histamine on amino-functionalized graphene quantum dots with the mediation of Fe^{3+} , Cu^{2+} , Eu^{3+} : Application in the analysis of spoiled tuna fish

Material published as: “*Photoluminescence suppression effect caused by histamine on amino-functionalized graphene quantum dots with the mediation of Fe^{3+} , Cu^{2+} , Eu^{3+} : Application in the analysis of spoiled tuna fish*”, Toloza CA, Khan S, Silva RLD, Romani EC, Larrude DG, Louro SRW, Freire Jr., FL, Aucélio RQ. *Microchem. J.*, 2017, 133, 448-459. DOI: 10.1016/j.microc.2017.04.013 (see attachment A2).

6.1

Histamine and analytical methods for its determination

Histamine (Fig. 6.1) is produced by the decarboxylation of the amino acid histidine via microbial or enzymatic processes [126] and it plays important role in the central nervous system, acting as a neurotransmitter in regulating sleep and controlling body temperature. In addition, histamine is partly responsible for gastric acid release functions, stimulant effects linked to schizophrenic processes and multiple sclerosis. Concerning food safety, the intake of histamine may cause food poisoning [127,128]. This is critical in fish and fish-derived products (especially in fishes of family *scombroidae*) [129] and in wines [130], where levels of histamine in spoiled samples may be higher than 500 mg kg^{-1} , causing nausea, vomiting, diarrhea and allergies [131], since at temperatures above 16°C , histidine undergoes bacterial-induced decarboxylation, which converts histidine to histamine. Thus, as histamine is a biomarker for quality control during food production, storage and transportation, a simple and selective method to determine histamine is highly desired [132].

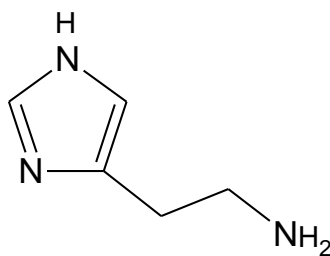


Figure 6.1. Histamine structure.

A colorimetric method was proposed for the determination of captopril based on the reaction between the imidazole ring with the *p*-sulphonate phenyldiazonium ion [133], leading to percent recoveries above 91% in samples containing the analyte at the concentration range of 1-60 mg/100 g. The relative standard deviation in the new assay ranged from 2.61 - 9.63%. The detection limit was 1 mg/100 g.

In a recent review of the analytical approaches for the analysis of biogenic amines (including histamine) in food samples [134] several examples of the use of liquid chromatography, thin layer chromatography, capillary zone electrophoresis (CZE) for the determination of biogenic amines in a variety of foods and products including wine, fish, seafood, orange juice, beer, cheese, sausage and fermented meat products, as well as dairy products and even in lake water was proposed. In some cases, the chromatographic method was coupled to a fluorescence laser induced mass spectrometer for the detection and identification of the analytes. The limit of detection of these methods was in the $\mu\text{g g}^{-1}$ range. The analytical procedure involved a type of selective extraction (liquid extraction, solid phase extraction, or microextraction - SPE and SPME, for example) prior to chromatographic analysis in order to further improve LOD.

HPLC with fluorimetric detection has been used to determine histamine after chemical derivatization with *o*-phthalaldehyde or dansyl chloride, resulting in limit of detection down to 10 ng g⁻¹ in fish samples [135,136]. Capillary electrophoresis with fluorimetric detection has also been used to separate histamine from other biogenic amines allowing detection of quantities down to 0.250 μmol [137]. In such cases, the histamine needs to be converted into a derivative that absorbs visible light so that it can produce a measurable signal. In general, the reagents used for this are expensive and toxic, with a chemical

derivatization procedure and in most cases are complicated to reproduce when analyzing more complex matrices. Thus, analytical approaches that do not require the prior chemical modification of histamine are desirable because of the minimization of the complexity and cost of analyzes. A HPLC based method for the determination of histamine in wines was developed measuring fluorescence after derivatization of histamine using OPA [112]. The method presented LOD of 0.25 mg L^{-1} with precision (repeatability and intermediate accuracy) below 6.0%. The method was applied to determine the histamine content in Cabernet Sauvignon wines and presented values between 1.2 and 5.7 mg L^{-1} .

Ion mobility spectrometry (IMS) was used for the determination of histamine content in tuna samples. In IMS measurements, the relationship between the ion intensity histamine fragment ($K_0 = 2.73 \text{ cm}^2 \text{ V}^{-1} \text{ s}^{-1}$) and the sum of all the ions in the mobility spectrum served to quantify the level of histamine in fish samples. Thus, a fast, simple and inexpensive method was developed for determination of histamine in tuna [138]. Analytical results were compared with measurements by HPLC with fluorescence detection, which is considered the standard method. Production of histamine versus storage time at room temperature (25-29 °C) was followed by both methods and a good correlation was found between them.

In this chapter, aqueous dispersions of amino-functionalized QDs (produced in the presence of GSH) and modified with different metal ions (Fe^{3+} , Eu^{2+} and Cu^{2+}) have been tested for the determination of histamine (based on the photoluminescence quenching caused by histamine). The QDs modified with Fe^{3+} was used as probe aiming the sensitive determination of histamine in Tuna fish samples where selectivity was guaranteed by a pH adjustment of sample solution followed by solid cationic phase extraction.

6.2

Results and Discussion

6.2.1

Studies of the interaction between QDs-amino and metal ions.

6.2.1.1

The effect of cations on the photoluminescence of QDs-amino

Photoluminescence intensity of quantum dots is sensitive to interactions with chemical species through a myriad of mechanisms [9]. Chemical groups generated at the surface and borders of the GQDs, during synthesis with the amino containing precursor (GSH), become sites to coordinate with metal ions. Thus any change in photoluminescence in GQDs-amino in the presence of cations might be a result of the relative ability of these ions to coordinate with these chemical groups and to the tendency of these ions to withdraw electrons from the semiconductor nanostructure, in a reduction process. The photoluminescence suppression effect generated by some cations present (at final concentration of $1.0 \times 10^{-4} \text{ mol L}^{-1}$) in the aqueous dispersion of GQDs-amino (in acid pH) was evaluated. The ions used in these tests were Cd^{2+} , Cu^{2+} , Eu^{3+} , Fe^{3+} , Fe^{2+} , Ni^{2+} , Pb^{2+} and Zn^{2+} and the results were presented as the ratio of the original luminescence of the nanomaterial dispersion (L_0) and the signal measured from the dispersion after addition of the ion (L) (Fig. 6.2). For Fe^{2+} , Pb^{2+} , Cd^{2+} , Zn^{2+} and Ni^{2+} no signal suppression effect was found as the L_0/L value was close to unity. All of these ions present weak tendency to receive electrons (negative standard reduction potentials). The ions Fe^{3+} and Cu^{2+} (the ones with positive standard reduction potentials) decreased the original optical signal produced by the nanomaterial dispersion by, respectively, 88% and 14%. The capability to generate quenching was proportional to the tendency of these ions to withdraw electrons from the semiconductor nanomaterial ($E^{\circ}_{\text{Fe}^{3+}/\text{Fe}^{2+}} > E^{\circ}_{\text{Cu}^{2+}/\text{Cu}^{+}}$) and the higher electrophilic character of Fe^{3+} ion compared to Cu^{2+} ion. In contrast, Eu^{3+} , that present negative standard reduction potential, also produced photoluminescence quenching (29% of the original intensity) that might be attributed to energy transfer mechanism from GQDs to the rare earth ion. It is important to mention that the addition of Fe^{3+} (the one that produced the strongest quenching) into a dispersion containing the GQDs (the one prepared only with citric acid) does not produce photoluminescence quenching. This indicates the importance of the chemical groups (produced by pyrolysis of GSH) to produce the interaction between the nanoparticle and Fe^{3+} .

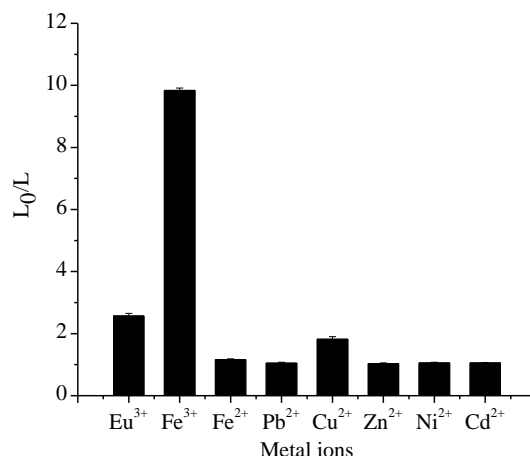


Figure 6.2. Photoluminescence quenching of GQDs-amino by metal ions. The concentration of the metal ions is $1.0 \times 10^{-4} \text{ mol L}^{-1}$. L_0 and L represent the intensities in the absence and presence of tested metal ions.

6.2.1.2

Evaluation of the interaction between histamine and GQDs-amino mediated by Cu^{2+} , Fe^{3+} and Eu^{3+} .

The addition of histamine (at a final concentration of $1.7 \times 10^{-5} \text{ mol L}^{-1}$) in the work dispersion of GQDs-amino was also evaluated and no effect on the measured photoluminescence was observed. The same behavior was found when the addition of histamine was made in the system containing Fe^{2+} , Pb^{2+} , Cd^{2+} , Zn^{2+} or Ni^{2+} . In contrast, the addition of histamine in GQDs-amino dispersions containing Cu^{2+} , Fe^{3+} , Eu^{3+} seemed to produce a further photoluminescence decreasing, indicating that these ions somehow mediate the interaction between histamine and GQDs-amino, probably acting as a bridge connecting them and making possible the energy transfer that reduces the GQDs-amino excitonic recombination efficiency.

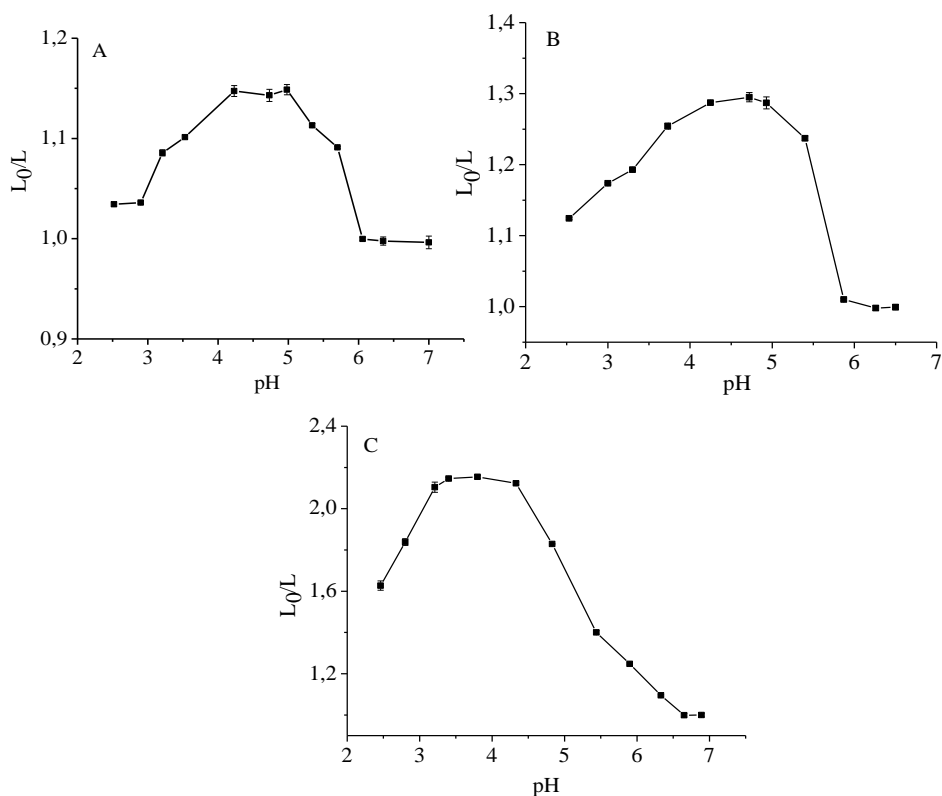


Figure 6.3. Study of pH (adjusted with HCl 0.01 mol L⁻¹ and NaOH 0.01 mol L⁻¹) to evaluate the effect of the photoluminescence quenching of GQDs-amino mediated by A) Cu²⁺; B) Eu³⁺ and C) Fe³⁺ ions in the presence of 5.0×10^{-5} mol L⁻¹ histamine, where L_0 and L are the photoluminescence measurements before and the addition of analyte respectively.

The effect of pH on the interaction of histamine with GQDs-amino under the mediation of Cu²⁺, Fe³⁺, and Eu³⁺ was evaluated (Fig. 6.3). The pH range was initially adjusted using HCl or NaOH 0.01 mol L⁻¹, finding that at pH ranges from 3.2 to 4.0 (Fe³⁺) and 4.3 to 4.9 (Cu²⁺ and Eu³⁺) the effect on photoluminescence was more effective. These pH ranges also provided robust conditions for the measurement of the analytical signal. Results also indicated that the original pH of the working dispersion (pH about 3.4 for the dispersion containing Fe³⁺ and about 4.5 for the ones containing either Cu²⁺ or Eu³⁺) can be used without further adjustment.

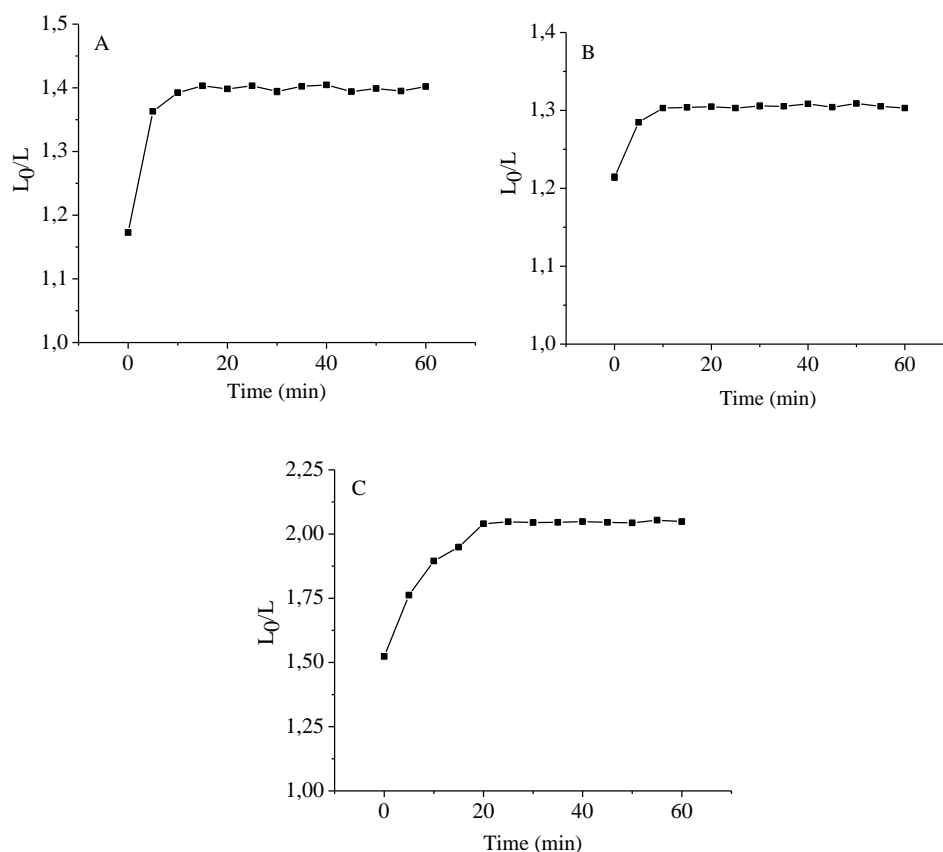


Figure 6.4. Reaction time of the GQD-amino-Mⁿ⁺ dispersion after addition of histamine (1.0×10^{-5} mol L⁻¹), where Mⁿ⁺ is A) Eu³⁺, B) Cu²⁺ and C) Fe³⁺.

The variation of the photoluminescence intensity in function of the time was evaluated after the mixing of histamine in the GQDs-amino dispersion containing Cu²⁺, Fe³⁺ or Eu³⁺ (measurements made every 5 min at room-temperature). In all cases, the GQDs-amino photoluminescence decreased steeply during the first 5 min, with signal stabilization after 20 min (Fig. 6.4) up to at least 60 min (maximum evaluated time). For quantitative batch analysis, this means that reliable measurements would be obtained after 20 min of the addition of histamine. This test was also performed using different final concentrations of histamine (from 5.0×10^{-6} to 6.0×10^{-5} mol L⁻¹) resulting in similar signal decay and stabilization after 20 min. The GQDs-amino photoluminescence after quenching, in the presence of the different ions, is shown at different concentrations of histamine in Fig. 6.5 (Fig. 6.5A in the presence of Fe³⁺, Fig. 6.5B in the presence of Cu²⁺ and Fig. 6.5C in the presence of Eu³⁺). The

photoluminescence intensities were normalized by the signal measured in the absence of histamine (L_0), thus expressing signal changes as L_0/L (inserts in Fig. 6.5).

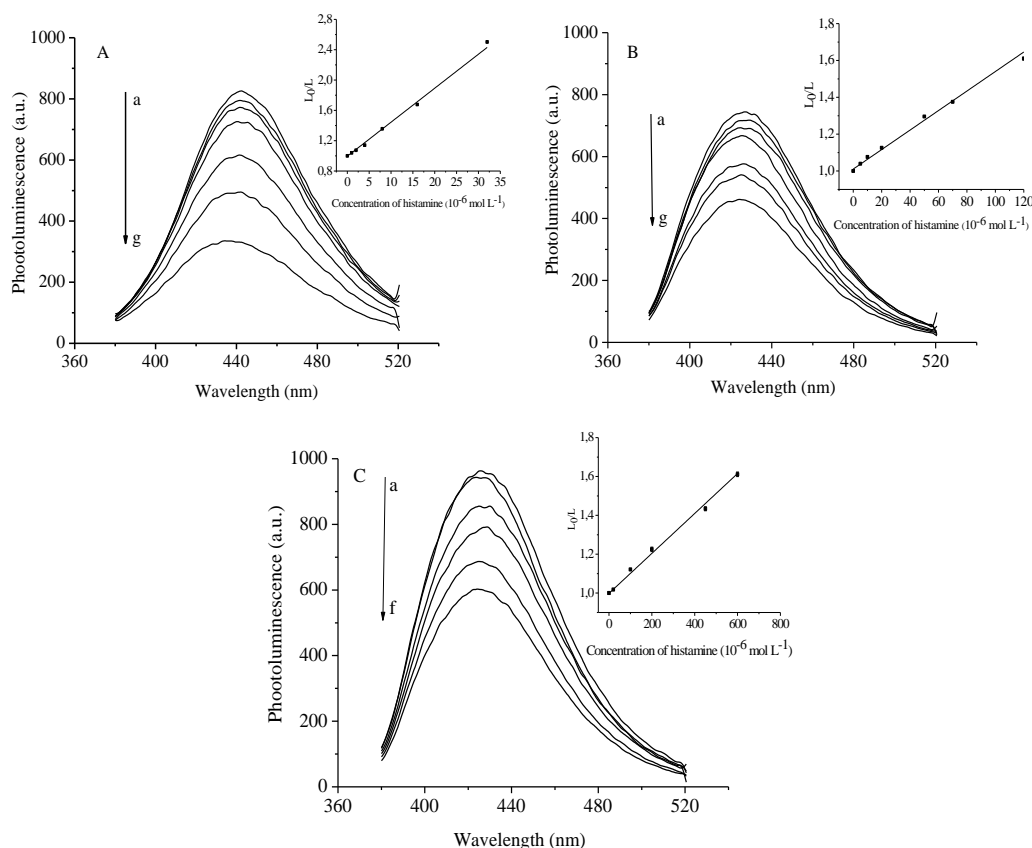


Figure 6.5. Photoluminescent response of the GQD-amino in the presence of increasing concentrations of histamine mediated by: A) Fe^{3+} (a) blank, (b) 4.3×10^{-7} , (c) 2.0×10^{-6} , (d) 4.0×10^{-6} , (e) 8.0×10^{-6} , (f) 1.6×10^{-5} , (g) $3.2 \times 10^{-5} \text{ mol L}^{-1}$. B) Eu^{3+} (a) blank, (b) 5.0×10^{-6} , (c) 1.0×10^{-5} , (d) 2.0×10^{-5} , (e) 5.0×10^{-5} , (f) 7.0×10^{-5} , (g) $1.2 \times 10^{-4} \text{ mol L}^{-1}$. B) Cu^{2+} (a) blank, (b) 2.0×10^{-5} , (c) 1.0×10^{-4} , (d) 2.0×10^{-4} , (e) 4.5×10^{-4} , (f) $6.0 \times 10^{-4} \text{ mol L}^{-1}$ Inserts: The normalized plots for the GQDs-amino photoluminescence quenching mediated by respectively Fe^{3+} , Eu^{3+} , and Cu^{2+} .

The sensitivities of the linearized curves (K_s) indicate the relative binding tendency of histamine with the GQDs-amino- M^{n+} systems following the order: $K_{s(\text{system with Fe}^{3+})} = 4.5 \times 10^4 \text{ L mol}^{-1} > K_{s(\text{system with Eu}^{3+})} = 5.3 \times 10^3 \text{ L mol}^{-1} > K_{s(\text{system with Cu}^{2+})} = 2.7 \times 10^3 \text{ L mol}^{-1}$. These results indicate more favored interaction of histamine with the surface of nanomaterials in the presence of Fe^{3+} , generating a more effective suppression in photoluminescence.

The chemical structure of histamine contains amino groups that can coordinate with the cations on the surface of nanomaterials, forming a complex that produce static luminescence quenching. The coordination of the cation on the

surface of the GQDs is evidenced by the significant increase of the GQDs-amino extinction peak with small red shift ($\Delta\lambda$) of 7 nm in the presence of Cu^{2+} (Fig. 6.6A), 22 nm in the presence of Eu^{3+} (Fig. 6.6B) and 29 nm (Fig. 6.6C) in the presence of Fe^{3+} . For the system containing Fe^{3+} , it was also observed a new band (charge transfer band) with maximum at 292 nm. The inclusion of histamine ($1.0 \times 10^{-5} \text{ mol L}^{-1}$ final concentration) produces a further small increase in extinction with no significant spectral shift except for the system containing Cu^{2+} , where a further red shift ($\Delta\lambda = 4 \text{ nm}$) is clearly observed.

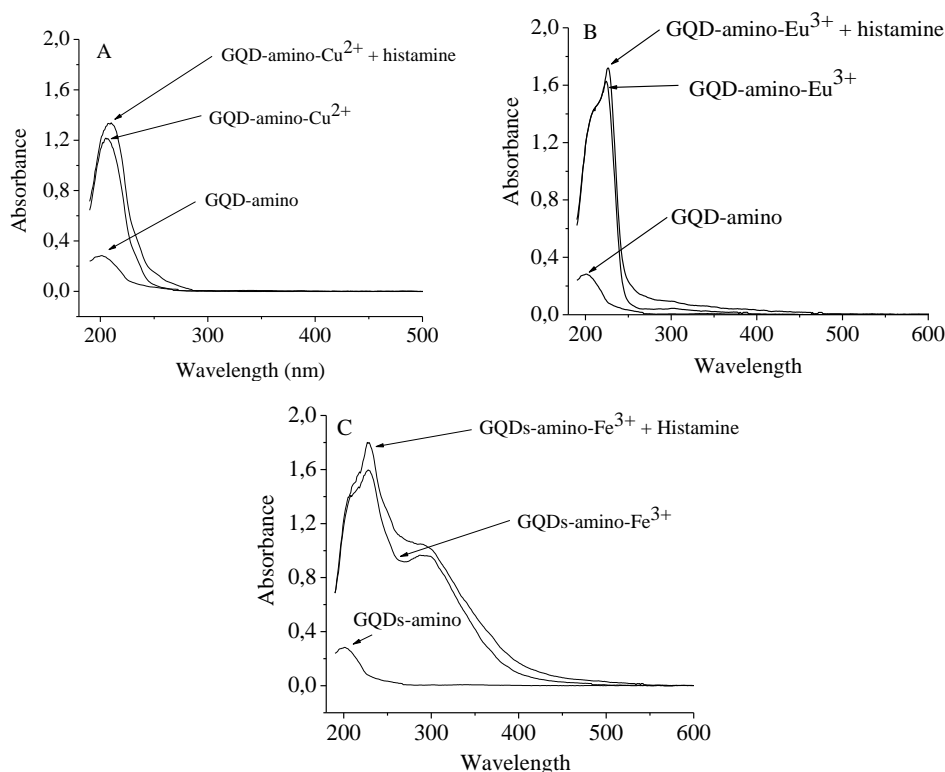


Figure 6.6. UV-vis absorption spectra of GQDs-amino, GQDs-amino- M^{n+} , GQDs-amino- M^{n+} -histamine complex, where M^{n+} is A) Eu^{3+} , B) Fe^{3+} and C) Cu^{2+} .

6.2.1.3

Electrokinetic measurements.

Electrokinetic potential measurements (Table 6.1) have shown that in the absence of metal ions, the GQDs-amino presented negative charge on their surface, which is characteristic of deprotonated carboxylic groups of amino functionalized GQDs in the aqueous medium at pH 4.0-4.5. In the presence of cations (Cu^{2+} at $3.0 \times 10^{-3} \text{ mol L}^{-1}$; Fe^{3+} at $2.0 \times 10^{-4} \text{ mol L}^{-1}$ or Eu^{3+} at $6.0 \times 10^{-4} \text{ mol L}^{-1}$ final concentration), the ζ -potential turned positive, fact that supports the

interaction between GQDs-amino with Cu^{2+} , Eu^{3+} or Fe^{3+} (in this crescent order of positive ζ -potential value). As histamine is added to the system, the significant decreasing of the surface positive charge occurred (in relative terms the decrease is more pronounced for the system containing Eu^{3+} and Cu^{2+}), which corroborates that an interaction between the surface of the nanomaterial and histamine occurred.

Table 6. 1. Electrokinetic potential (ζ -potential) values obtained of GQDs-amino in aqueous dispersion and in the presence of Eu^{3+} , Fe^{3+} and Cu^{2+} ions.

Probe	ζ -potential (mV)	
		<i>Histamine</i>
GQDs-amino	- (38.2 ± 2.4)	-
GQDs-amino- Fe^{3+}	+ (27.6 ± 0.8)	+ (10.8 ± 0.7)
GQDs-amino- Eu^{3+}	+ (12.9 ± 2.4)	+ (1.6 ± 0.8)
GQDs-amino- Cu^{2+}	+ (4.3 ± 0.2)	+ (0.3 ± 0.1)

Under the chosen experimental conditions, it is observed that the surface of GQDs-amino- Fe^{3+} probe has the larger value of ζ -potential, which would imply a higher stability of the dispersed nanomaterial in water and the capability to interact with histamine in a wider concentration range as the nanoparticle still present positive charge after the addition of histamine at $5.0 \times 10^{-6} \text{ mol L}^{-1}$.

6.2.1.4

Evaluation of photoluminescence quenching mechanism.

In order to establish the nature of the photoluminescence quenching, lifetime measurements were made on the: i) aqueous dispersion of GQDs-amino, ii) aqueous dispersion of GQDs-amino in the presence of Fe^{3+} and iii) aqueous dispersion of GQDs-amino in the presence of Fe^{3+} with addition of histamine (Fig. 6.7A).

For the GQDs-amino, a two-exponential decay was observed with different relative amplitudes (value in parenthesis) as follows: 5.4 ns (51.1) and 11.2 ns (48.9). The weighted average lifetime, obtained using the relative

amplitude as weighing factor, was 8.2 ns. When Fe^{3+} was incorporated into the system, the lifetime value increased to 11.6 ns, which is the weighted value considering the following lifetimes and relative amplitudes of the two exponential decay: 4.7 ns (24.0) and 13.8 ns (76.0). This indicates that the quenching produced by the interaction of the GQDs-amino and Fe^{3+} first occurs in nanoparticles that present shorter lifetimes as the relative amplitude of the longer lifetimes increased. After the addition of histamine into the system containing GQDs-amino- Fe^{3+} a similar lifetime (11.5 ns) was obtained, considering 4.85 ns (28.6) and 14.1 ns (71.4). The quantum yield (QY) of the GQDs-amino (QY = 54.6%) decreased when Fe^{3+} was added to form GQDs-amino- Fe^{3+} (QY = 14.1%). As histamine is added the QY further decreased (QY = 7.7%). The experiment was made keeping the established concentration proportions of GQDs-amino, Fe^{3+} and histamine.

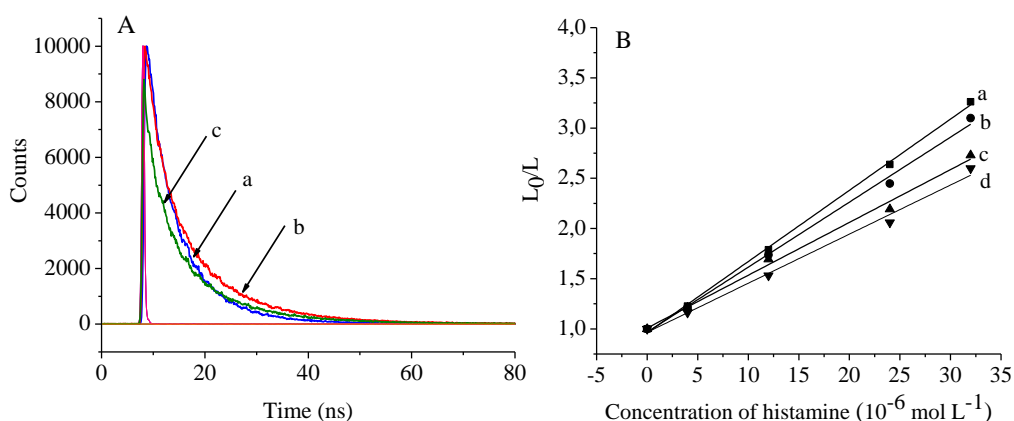


Figure 6.7. A) Photoluminescence time decay of: (a) GQDs-amino; (b) GQDs-amino- Fe^{3+} and (c) GQDs-amino- Fe^{3+} plus addition of histamine ($5 \times 10^{-6} \text{ mol L}^{-1}$); B) Normalized curve for GQDs-amino- Fe^{3+} in the presence of histamine mediated by Fe^{3+} at 20 °C (a) 25 °C (b) 30 °C (c) and 35 °C (d) in aqueous system.

The photoluminescence was studied at different temperatures (from 20 to 35 °C) in order to evaluate the nature of the quenching effect. The optical signal measured from the GQDs-amino decreases as the concentration of Fe^{3+} increased but the binding constant (K_s), given by sensitivity of the L_0/L versus Fe^{3+} concentration curve, decreases from $1.4 \times 10^4 \text{ L mol}^{-1}$ at 20 °C to $7.2 \times 10^3 \text{ L mol}^{-1}$ at 35 °C. Such a result suggests that a static photoluminescence quenching is taking place. When Fe^{3+} is fixed at $2.0 \times 10^{-4} \text{ mol L}^{-1}$ in the GQDs-amino dispersion and the concentration histamine is increased, a further

photoluminescence quenching was observed. However the binding of histamine with GQDs-Fe³⁺, that affect the excitonic recombination, became less effective at higher temperatures as indicated by the decreasing sensitivities of the quenching response curve (Fig. 6.7B). Similar results were found for systems containing Eu³⁺ and Cu²⁺.

6.2.2

GQDs-amino response towards histidine mediated by Cu²⁺, Fe³⁺ and Eu³⁺.

Histamine is produced by the decarboxylation of histidine, thus it is important to evaluate how histidine affect the photoluminescence from these GQDs-amino-Mⁿ⁺ aiming to evaluate their selectivity in detecting histamine in biological samples. The selective response was measured as the ratio between the normalized photoluminescence measured from GQDs-amino-Mⁿ⁺ dispersions after the addition of histamine and the response measured from GQDs-amino-Mⁿ⁺ dispersions fortified with a mixture of both histamine and histidine ($L_0/L_{\text{(histamine)}} / L_0/L_{\text{(histamine + histidine)}}$). For the experiment, the final concentration of histamine was kept constant ($1.0 \times 10^{-5} \text{ mol L}^{-1}$) while the final concentration of histidine was increased (from $1.0 \times 10^{-5} \text{ mol L}^{-1}$ to $1.0 \times 10^{-6} \text{ mol L}^{-1}$) in order to get histamine:histidine molar proportions of 1:0; 1:0.1; 1:1; 1:3; 1:5; and 1:10 with measurements performed in triplicate. The $L_0/L_{\text{(histamine)}} / L_0/L_{\text{(histamine + histidine)}}$ values close to 1 indicated that the presence of histidine did not interfere in the response produced by histamine. In contrast, values less than 1 indicate a further photoluminescence quenching due to the presence of histidine (Table 6.2).

Table 6. 2. Evaluation the interference imposed by histidine in the histamine ($1.0 \times 10^{-5} \text{ mol L}^{-1}$) photoluminescence signal.

Probe	Proportion (histamine / histidine)	$L_0/L_{\text{histamine}} /$
		$L_0/L_{\text{(histamine + histidine)}} \pm S_{\text{ratio}}$
GQDs-amino-Fe ³⁺	1:0	1.00 ± 0.02
	1:0.1	1.01 ± 0.01
	1:1	0.95 ± 0.01
	1:3	0.92 ± 0.02
	1:5	0.87 ± 0.02
	1:10	0.78 ± 0.02
GQDs-amino-Cu ²⁺	1:0	1.00 ± 0.01
	1:0.1	0.93 ± 0.01
	1:1	0.75 ± 0.03
	1:3	0.66 ± 0.02
	1:5	0.52 ± 0.02
	1:10	0.34 ± 0.01
GQDs-amino-Eu ³⁺	1:0	1.00 ± 0.01
	1:0.1	0.95 ± 0.01
	1:1	0.90 ± 0.02
	1:3	0.82 ± 0.03
	1:5	0.73 ± 0.01
	1:10	0.73 ± 0.02

Although the response towards histamine is affected by histidine in all cases, such effect was more pronounced in the GQDs-amino-Cu²⁺ system. At equimolar histamine/histidine proportion, $L_0/L_{\text{(histamine)}} / L_0/L_{\text{(histamine + histidine)}}$ the decreasing was about 25% while for the other two systems, changes were around 5%. These results, especially for GQDs-amino-Eu³⁺ and GQDs-amino-Fe³⁺, showed their relative preference in interacting with histamine rather than with histidine. When histidine was 10 times more concentrated than histamine, the

$L_0/L_{\text{(histamine)}} / L_0/L_{\text{(histamine + histidine)}}$ values measured for the GQDs-amino- Fe^{3+} and GQDs-amino- Eu^{3+} decreased respectively 22% and 27%. For GQDs-amino- Cu^{2+} , the decreasing was 66%, reflecting the ability of Cu^{2+} , on the surface of the nanomaterial, to better coordinate with histidine (less selective towards histamine) than Fe^{3+} and Eu^{3+} .

6.2.3

Analytical characteristics of the GQDs-amino- Fe^{3+} for sensing histamine

Compared to the other two systems, the GQDs-amino- Fe^{3+} aqueous dispersion suffered the largest photoluminescence quenching in the presence of histamine still maintaining a positive charge on the surface of the nanoparticle (that would promote interaction in a wider range of concentration of histamine). Thus, the GQDs-amino- Fe^{3+} aqueous dispersion was selected as a probe to the quantitative determination of histamine.

Photoluminescence was measured after the addition of increasing amounts of histamine into the GQD-amino- Fe^{3+} probe (prepared with 0.1% v/v of the GQDs-amino stock solution and 2.0×10^{-4} mol L^{-1} of Fe^{3+} at pH 3.4) as shown in Fig. 6.5A. The normalized analytical curve (L_0/L vs concentration of histamine) was linear ($R^2 = 0.995$) in the range from the limit of quantification (LOQ) up to 3.2×10^{-5} mol L^{-1} (final concentrations of histamine in the probe) with equation model of $L_0/L = 4.5 \times 10^4 [\text{histamine}] + 0.999$. The LOQ value was 4.2×10^{-7} mol L^{-1} of histamine (absolute value of 233 ng) in the dispersion. The LOQ was calculated as the amount of histamine equivalent to reduction of ten times the standard deviation ($n = 10$) of the probe signal measured in the absence of histamine. Intermediary precision was evaluated by performing measurements (at 345/435 nm) from two sets of ten independent probes (each set containing one level of histamine). Precision was the standard deviation of the L_0/L ratio: $s_{L_0/L} = L_0/L \times [(s_{L_0}/L_0)^2 + (s_L/L)^2]^{1/2}$. In percent values, for histamine at 3.0×10^{-6} mol L^{-1} , precision was 1% while 2% was obtained at 2.0×10^{-5} mol L^{-1} .

6.2.4 Selectivity studies

In order to evaluate the GQD-amino-Fe³⁺ probe optical behavior in the presence of amino acids other than histidine (valine, tyrosine, lysine, phenylalanine, threonine, methionine, cysteine and tryptophan) and in the presence of other important chemical species in biological samples (Ca²⁺, Mg²⁺, Na⁺, K⁺, Zn²⁺, Cl⁻, NO₃⁻) a study was made to measure the degree of signal changing (expressed in percent values) due to the presence of these chemical species (at a final concentration of 5.0×10^{-4} mol L⁻¹ in the probe dispersion). The results showed that, under the experimental conditions established to detect histamine, the dispersion GQD-amino-Fe³⁺ is relatively insensitive to the presence of most of the amino acids tested (less than 2% of variation), except phenylalanine and tyrosine that caused photoluminescence quenching of 3.6 and 2.2% respectively. Cysteine amplified the photoluminescence measured from the probe (about 4.8%), keeping in mind that 5.0×10^{-6} mol L⁻¹ of histamine caused signal quenching of 18 % in the same conditions.

Phenylalanine, tyrosine and cysteine were selected to be mixed with histamine in order to evaluate selectivity of the probe response towards histamine. This was accomplished by comparing the signal measured from the GQD-amino-Fe³⁺ dispersion containing histamine (at 5.0×10^{-6} mol L⁻¹) in absence and in the presence of different concentrations of each one of the selected amino acids. As made before with histidine, the level of interference was evaluated by the $L_0/L_{\text{histamine}} / L_0/L_{\text{(histamine + amino acid)}}$ values. Increasing concentrations of the amino acids were used, covering the histamine:other amino acid molar proportions of 1:1; 1:5; 1:10 and 1:50.

$L_0/L_{\text{histamine}} / L_0/L_{\text{(histamine + amino acid)}}$ values lower than 0.98 were considered an interference due to the further signal quenching promoted by the other amino acid while values higher than 1.02 indicated a significant signal photoluminescence amplification caused the other amino acid on the probe. Results in Table 6.3 indicated no relevant interference from any of the amino acids tested at the histamine: other amino acid molar proportion of 1:5. Interferences were found at higher proportions (1:10 and 1:50) of the tested amino acids with signal quenching promoted by phenylalanine and tyrosine and signal

amplification caused by cysteine. In the latter case, the presence of cysteine minimized the suppression effect generated by histamine still promoting further signal amplification.

During analysis of biological samples, the selectivity towards other biogenic amines can be improved by using a simple solid phase extraction (SPE) with a cation exchange resin (Amberlite - 50 GC) [111]. A study to assess the efficiency of extraction was conducted to evaluate any possibility of analyte losses. The study was made in triplicate using authentic replicates of solutions containing histamine. After addition of trichloroacetic acid 2.5% (used to precipitate proteins biological samples) and adjustment of pH, the solution was passed through the SPE cartridge, in order to retain histamine. The eluted histamine solution had the pH adjusted to about 3.5 (by addition of NaOH 0.01 mol L⁻¹) before adding an aliquot to the dispersion GQD-amino-Fe³⁺. The expected concentration of histamine in the probe was 5.0 × 10⁻⁶ mol L⁻¹ and the results indicated an average loss of analyte of 2.3 ± 0.2%, which was verified by comparing results with the ones achieved using a standard histamine solution (5.0 × 10⁻⁶ mol L⁻¹) which has not been submitted to the SPE procedure.

To evaluate the efficiency of extraction with the cation exchange resin in separating histamine from other amino acids, additional studies were performed to compare the photoluminescence effect caused by the extracted solution containing histamine (5.0 × 10⁻⁶ mol L⁻¹ probe final concentration) and the extracted solution containing a mixture of histamine and tyrosine or phenylalanine or cysteine in molar proportions of 1:1; 1:10 and 1:50. After neutralizing it, the extract was added to the GQD-amino-Fe³⁺ dispersion and the produced photoluminescence was not higher than 3% in mixtures containing up to 10 times more of the other amino acid. As the proportion of tyrosine, phenylalanine or cysteine increased to 50 times, the signal quenching was up to 6% stronger than the one expected for histamine alone (Table 6.3). These results indicated that most of tyrosine, phenylalanine and cysteine were removed in the clean-up step of the SPE procedure.

Table 6. 3. Evaluation of the quenching effect of histamine ($5.0 \times 10^{-6} \text{ mol L}^{-1}$) in the presences of amino acids

Amino acid	Proportion (histamine/amino acid)	$L_0/L_{\text{histamine}} /$
		$L_0/L_{\text{(histamine + amino acid)}} \pm S_{\text{ratio}}$
Phenilalanine	1:1	1.00 ± 0.01
	1:5	$0,98 \pm 0.01$
	1:10	$0,97 \pm 0.02$
	1:50	0.94 ± 0.02
Tyrosine	1:1	1.01 ± 0.01
	1:5	0.98 ± 0.02
	1:10	0.97 ± 0.03
	1:50	0.95 ± 0.02
Cysteine	1:1	1.00 ± 0.01
	1:5	1.02 ± 0.02
	1:10	$1,03 \pm 0.03$
	1:50	1.09 ± 0.03

6.2.5

Application in tuna fish samples

The method was tested in the determination of histamine in samples of fresh tuna fish. Initially, recovery studies were performed from sample extracts fortified with histamine at three concentration levels (25, 75 and 150 mg kg^{-1}). Samples (5.0 g) were homogenized with 25 mL of trichloroacetic acid (2.5%) and fortified with the standard histamine solution in order to obtain the desired analyte concentration. After fortification, the samples were submitted to the SPE procedure and, after pH adjustment, an aliquot added to the GQDs-amino- Fe^{3+} probe. Blank experiments were made with non-fortified homogenized samples that resulted in non-significant changes in the probe signal. Recoveries of histamine were close to the expected value (Table 6.4), confirming the selectivity of the method considering the sample matrix.

Table 6. 4. Recovery results (n =3) for histamine fortified fresh tuna fish samples.

Fortification histamine (mg kg ⁻¹)	Recovery ± RSD (%)
50	110.1 ± 2.5
75	106.0 ± 1.7
150	98.2 ± 1.2

The proposed probe was also tested in determination of histamine in real spoiled samples of tuna fish, after letting them to degrade for different periods of time. The results (Table 6.5) indicated the increasing in histamine concentration as function of the time they were kept at room-temperature. The relatively large standard deviation (triplicate analysis) may be explained by non-homogenous distribution of histamine in the selected fish parts (depending upon the proportion of white and dark muscles different histamine levels are expected [139]). A further experiment using HPLC-MS have shown that histamine is the major component of the sample extract eluted after the SPE procedure (Fig. 6.8), which confirms the selectivity of the SPE towards histamine despite the presence of other biogenic amines in the tuna fish sample.

Table 6. 5. Application of method developed for the determination of histamine in three samples of tuna fish after up to 24 h of storage at room temperature.

Storage time (h)	Sample 1	Sample 2	Sample 3
	Concentration of histamine (mg kg ⁻¹)		
0	38.7 ± 2.4	42.2 ± 3.0	56.0 ± 3,3
3	156.2 ± .5	126.3 ± 5.2	143.1 ± 4.7
6	243.1 ± 8.2	295.6 ± 9.2	290.6 ± 7.5
12	398.9 ± 12.5	425.9 ± 22.5	466.9 ± 15.8
24	986.2 ± 39.2	1022.3 ± 36.5	1100.3 ± 45.4

The histamine content in two independent spoiled tuna fish samples (after 8 h storage at room-temperature) were also determined by HPLC method with fluorescence detection after analyte chemical derivatization with OPA. The results

achieved by the chromatographic method were 340.7 mg kg^{-1} (sample 1) and 479.1 mg kg^{-1} (sample 2) while the results obtained using the proposed method were 349.8 mg kg^{-1} and 494.9 mg kg^{-1} respectively for sample 1 and sample 2. A comparative statistical test (two-tailed Student's t-test) indicated no significant difference between the results achieved by these different methods ($t_{\text{calculated}} = 1.99$ for sample 1 and 1.56 for sample 2 with a $t_{\text{critical}} = 2.78$, at a 95% confidence limit for $n_1 = n_2 = 3$).

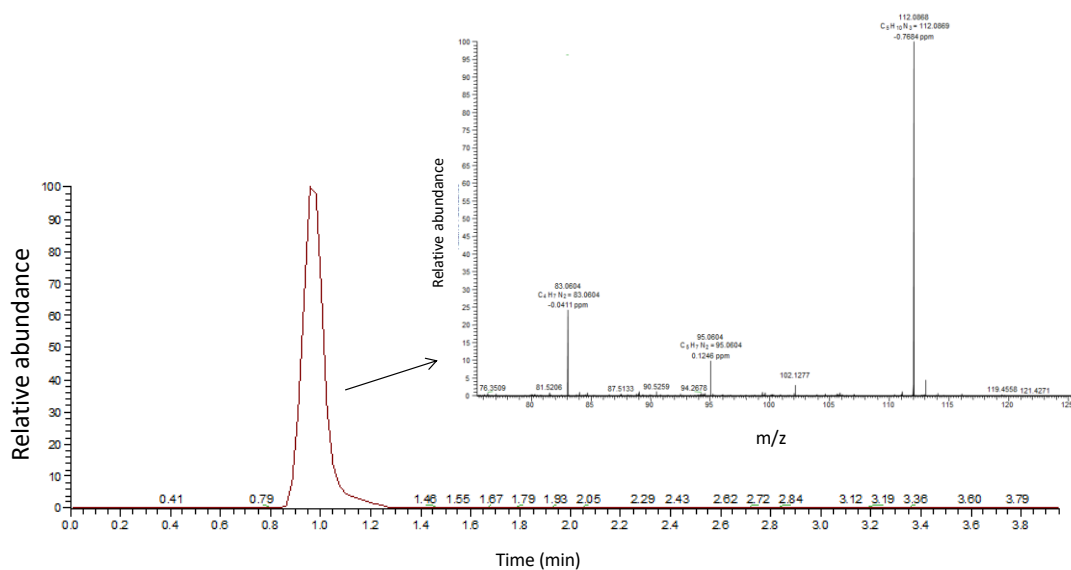


Figure 6.8. Liquid chromatogram of a tuna fish spoiled sample extract showing the main histamine peak at about 1 min retention time. (B) Mass spectrum of the histamine peak.

6.3 Partial conclusions

The photoluminescence quenching of GQDs-amino were achieved in the presence of histamine when mediated by Eu^{3+} , Fe^{3+} and Cu^{2+} in aqueous system. Coordination of the metal ions (M^{n+}) with amino and carboxylate groups on the surface of the quantum dots was indicated by UV-vis absorption. Further signal quenching (of static nature) was observed as histamine interacted with the GQDs-amino- M^{n+} system. The stronger effect was observed when interaction was mediated by Fe^{3+} , thus the GQDs-amino- Fe^{3+} was used as analytical probe for the determination of histamine. The feasibility of the method to monitor histamine in spoiled tuna fish samples was demonstrated by a recovery experiment in controlled analyte fortified samples as well as in a comparative study made with

spoiled samples. The absolute LOQ was 233 ng of histamine, intermediary precision of the method was under 2% and selectivity towards histamine was achieved by solid phase extraction (SPE) using a cation exchange resin. The LOQ of the developed method was 0.05 mg kg^{-1} (considering the sample), which is at least one order of magnitude lower than the reported one achieved by HPLC and CE using chemical derivatization [130,135]. The proposed method is simpler and can be used as an alternative to the ones based on chromatography after chemical derivatization.

7

Determination of kanamycin using photoluminescent amino-functionalized graphene quantum dots coupled with gold nanoparticles in organized medium and solid phase extraction using an aminoglycoside-selective molecular imprinted polymer

Manuscript submitted to *J. Pharm. Biomed. Anal.*

7.1

Kanamycin and analytical methods for its determination

Kanamycin A, 2-(aminomethyl)-6-[4,6-diamino-3-[4-amino-3,5-dihydroxy-6-(hydroxymethyl) tetrahydropyran-2-yl]oxy-2-hydroxycyclohexoxy]-tetrahydropyran-3,4,5-triol, is a polybasic aminoglycoside antibiotic that has activity against a variety of pathogenic bacteria. There are different structures of kanamycin sulfate being the main component denominated kanamycin A (Fig. 7.1). It is produced by the fermentation using certain strains of *Streptomyces kanamyceticus*, being very effective against a broad spectrum of Gram-negative and Gram-positive bacteria. Because it is poorly absorbed by the gastrointestinal mucosa, kanamycin is most commonly used parenterally (intramuscularly and intravenously) reaching peak serum levels after 1 h of dosing. Its therapeutic indications are usually for infections caused by staphylococci, *Mycobacterium tuberculosis* and enterobacteria. It is indicated primarily for systemic (septicemia) or localized infections (meningitis, urinary tract infections). Because of that it has been extensively used, as kanamycin sulfate, in human [140] and veterinary medicine as well as a preserving agent for medicines and vaccines.

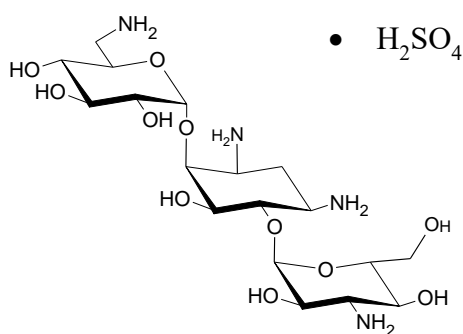


Figure 7. 1. Kanamycin sulfate structure.

Analytical methods for the determination of kanamycin in several matrices are available using traditional analytical techniques. Spectrophotometric methods, coupled or not with separation methods [141], and gas chromatographic methods [142] requires chemical derivatization of kanamycin to either promote relevant absorption in the UV-vis or to make it volatile. Immunoassay methods are usually not sensitive enough for trace analysis [143,144]. However, HPLC with absorption photometric detection [145] or fluorimetric detection is the dominant technique. In these cases, pre-column or post-column chemical derivatization of kanamycin (with phenylisocyanate or OPA) is required to produce UV-vis absorbing capability. LOD values for kanamycin was in the order of $1 \mu\text{g mL}^{-1}$. HPLC methods using detection based on changes of refractive index [146], mass spectrometry [147], amperometry [148] and dye fluorescence quenching [149] have also been reported for kanamycin.

The official method for the quantification of kanamycin in pharmaceuticals, food and biological fluids is a microbiological one that is time consuming and has low detectability and poor accuracy [150]. Blanchaert *et al.*, [151] developed a HPLC method to determine kanamycin A. The complexation of the analyte with borate was used to allow direct UV detection in 205 nm. Very recently, Sharma *et al.*, developed an easy and portable aptasensor for the quantitative determination of kanamycin by electrochemical impedance spectroscopy, which accompanies the assembly of selected single stranded DNA *in vitro*. Detection was based on specific recognition by kanamycin-aptamer immobilized covalently on the surface of screen printed carbon electrodes. Under optimized experimental conditions, the developed aptasensor exhibited a linear dynamic range from 1.2 to 75 ng mL⁻¹ [152]. Also recently, Khan *et al.* developed a sensitive and selective method for the determination of kanamycin sulfate based on the enhanced photoluminescence of QDs TGA-CdTe. In this approach, a solid phase extraction with a new molecular imprinting polymer, made with kanamycin sulfate as template, was use enabling high selectivity. Under adjusted conditions, the analytical curve of two orders of magnitude was constructed obtaining a LOD of $1.4 \times 10^{-8} \text{ mol L}^{-1}$ [110].

A new trend in detection aminoglycoside (AMG) antibiotics such as kanamycin is using the optical changes observed when they interacts with AuNPs. Silver-coated AuNPs as probes for the determination of AMG in human plasma

(kanamycin A and other three AMGs) by laser desorption and ionization mass spectrometry. The LOD for kanamycin was 130 nmol L^{-1} [153]. The combination of RNA aptamers with AuNPs were used for the determination of kanamycin and other AMG. The aptamers were adsorbed physically on the surface of the AuNPs, stabilizing them in water. The presence of AMG promoted the agglomeration of the AuNPs with the decrease of the transverse LSPR band and increasing the plasmon coupling band due agglomeration. The aqueous dispersion color changing was gradual and proportional to the AMG concentration, which allowed the quantification in the range between 10 and 150 nmol L^{-1} [154].

In 2007 Grace *et al.*, studied the influence of aminoglycosides on the surface plasmon resonance of spherical AuNPs. AuNPs were coated with the aminoglycosides in a reaction medium containing the dissolved antibiotic [155]. Techniques such as UV-vis and infrared spectroscopy, as well as transmission electron microscopy, were used to study the interaction of drugs with the surface of AuNPs. The results showed a strong affinity of the nanoparticles with the nitrogenous groups of the aminoglycosides. In 2009, Wang *et al.* described the use of silver-coated AuNPs as probes for the determination of AMG in human plasma (kanamycin A, neomycin, gentamicin, and paromycin) by laser desorption and ionization mass spectrometry. The LOD for kanamycin was 130 nmol L^{-1} [156].

In 2012, Derbyshire *et al.*, combined RNA aptamers with AuNPs for the determination of kanamycin, paromomycin, dihydrostreptomycin, streptomycin, apramycin, tobramycin, neomycin and gentamicin. The aptamers were adsorbed physically on the surface of the AuNPs-E, stabilizing them in the dispersed form. The presence of the AMG promoted agglomeration of the AuNPs with the decrease of the transversal LSPR band and increase of the plasmonic coupling band by agglomeration, with consequent change in the coloration of the dispersion from pink to blue. This change was gradual and proportional to the AMG concentration, which allowed the quantification of the AMG from the normalized signal variation by the ratio of the intensities measured at 650 nm (agglomeration band) and 530 nm (transverse LSPR band) . This signal (I_{650}/I_{530}) allowed better linearization of the analytical response, which covered the range between 180 and 500 nmol L^{-1} [157].

Quin *et al.*, 2017 proposed a visual detection strategy employing functionalized gold nanoparticles to detect kanamycin in several samples using 4-amino-3-hydrazino-5-mercaptop-1.2.4-triazole functionalized nanoparticles. The limit of quantification was in the range of 0.005 to 0.1 μM and 0.1 to 20 μM , with the detection limit of only 0.004 μM which is well below the level of minimum contamination for kanamycin in milk defined by the European Union. The sensor was also used to detect kanamycin in several actual samples and the results were excellent according to the values measured by HPLC [158].

The modification of surfaces of GQDs may produce optical properties suitable for the selective probing of analytes [159]. The combination of GQDs and AuNPs has been exploited as nanoscale-based platforms for bioanalytical sensing [106]. In this chapter, conditions were studied to produce a nanoparticle system comprising GQDs and AuNPs to be applied as a reliable analytical probe for the determination of kanamycin sulfate in samples such as yellow-fever vaccine.

7.2

Results and Discussion

7.2.1

Preliminary studies

Increasing amounts of the AuNPs synthesis dispersion (50 to 600 μL) were mixed with a fixed volume (1.00 mL) of the working GQDs-amino dispersion before a further 10 fold dilution was made. This resulted in dispersions containing TC of 0.1 mg L^{-1} . The photoluminescence (345/425 nm) measured from these dispersions was affected by the presence of AuNPs, generating a suppression effect as indicated in Fig. 7.2A and, in accordance to literature data, such effect is a result of energy transfer [106]. The subsequent addition of a sole amount of kanamycin sulfate into a GQDs-amino system, previously suppressed by AuNPs, partially restored the GQDs-amino photoluminescence, which indicates an off/on effect that can be potentially useful for quantitative probing of kanamycin and probably for other aminoglycosides (Fig. 7.2B). It is important to mention that the photoluminescence of the GQDs-amino dispersion (without the presence of AuNPs) is not affected by the addition of kanamycin.

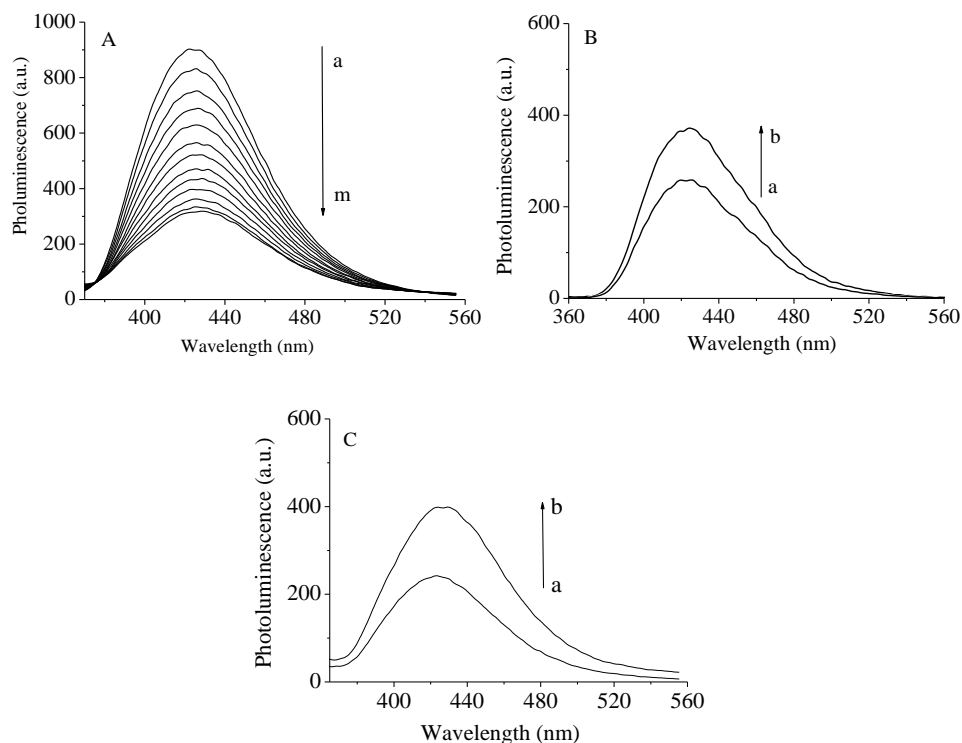


Figure 7.2. Photoluminescence spectra measured at 345/425 nm from: A) GQDs-amino in the presence of increasing amounts of added AuNPs dispersion (in mol L⁻¹): (a) 0; (b) 3.7×10^{-11} ; (c) 7.5×10^{-11} ; (d) 1.2×10^{-10} ; (e) 1.5×10^{-10} ; (f) 1.9×10^{-10} ; (g) 2.3×10^{-10} ; (h) 2.8×10^{-10} ; (i) 3.0×10^{-10} ; (j) 3.5×10^{-10} mol L⁻¹; (k) 3.8×10^{-10} ; (l) 4.3×10^{-10} and (m) 4.5×10^{-10} . B) Mixture of aqueous dispersions of AuNPs (4.5×10^{-10} mol L⁻¹) and GQDs-amino before (a) and after (b) addition of kanamycin (1.0×10^{-5} mol L⁻¹); C) Dispersion prepared by producing AuNPs by reducing HAuCl₄ directly in an aqueous dispersion of GQDs-amino before (a) and after (b) the addition of kanamycin (1.0×10^{-5} mol L⁻¹).

The next step was to compare the kanamycin effect in restoring photoluminescence from: (i) a mixture of independently prepared aqueous dispersions of AuNPs and GQDs-amino and (ii) from a sole dispersion prepared by reducing gold into AuNPs directly in an aqueous dispersion of GQDs-amino. The quantities of HAuCl₄ used in the synthesis of the AuNPs either in water and or in the GQDs-amino aqueous dispersion were the same. In addition, the quantity of GQDs (estimated by TC) in the dispersion used to synthesize AuNPs was chosen to produce, after dilution, a quantity of GQDs similar to the one of the diluted dispersion prepared from the mixture of the independent aqueous dispersions of AuNPs and GQDs-amino. The first observation is that the photoluminescence quenching effect caused by the AuNPs was similar in both cases. Secondly, it was observed that the addition of kanamycin (1.0×10^{-5} mol L⁻¹ final concentration) produced a more effective photoluminescence restoration

(about 30% better) from the dispersion of AuNPs prepared in the presence of GQDs-amino, system indicated from now on as AuNPs-GQDs-amino, as seen in Fig. 7.2C in contrast to Fig. 7.2B. Therefore, considering that both systems contained the same amounts of the AuNPs precursor and total carbon, the one obtained by synthesis of AuNPs directly into the GQDs dispersion produced a more effective response towards kanamycin.

7.2.2

Study of the conditions to produce the AuNPs-GQDs-amino analytical probe for kanamycin.

Studies were carried out to obtain AuNPs-GQDs-amino synthesis conditions that would lead to an analytical probe able to produce the highest signal restoration effect towards kanamycin. In order to do that, the amount of HAuCl₄ (AuNPs precursor) added into the synthesis reactor was kept constant (75 μmol) and the final volume of the synthesis medium inside the reactor (including the added solution containing 0.33 mmol of the reducing agent) was always 250 mL with the pH was around 6.0 to 6.5 (original pH and not controlled). The photoluminescence restoration test was made by selecting a fixed volume of each of these synthesis dispersions to be diluted (5 fold) with water before the addition of 25 nmol of kanamycin.

First, the addition of HAuCl₄ was made in the reactor containing water with different amounts of the original synthesis GQDs-amino dispersion (GQDs-amino varying from 0.1 to 1.0 % v/v, equivalent to TC values from 0.12 to 1.2 mg L⁻¹). The results showed that the photoluminescence restoration induced by kanamycin from the obtained AuNPs-GQDs-amino probes (probe was prepared using five-fold dilution of these synthesis AuNPs-GQDs-amino dispersions in water) sharply increased, being more effective with 0.3 % v/v (TC of 0.36 mg L⁻¹) and 0.5 % v/v (TC of 0.60 mg L⁻¹) of the synthesis GQDs-amino dispersion as seen in Fig. 7.3A. As the GQDs amount was increased to 1.0% (TC of 1.2 mg L⁻¹) a decreasing (about 35 %) in the restoration effect was observed. It seems that higher amounts of GQDs-amino not bound to AuNPs interacts with kanamycin (not producing signal variation) leading to less of the aminoglycoside to interact with the AuNPs to trigger of the signal restoration effect.

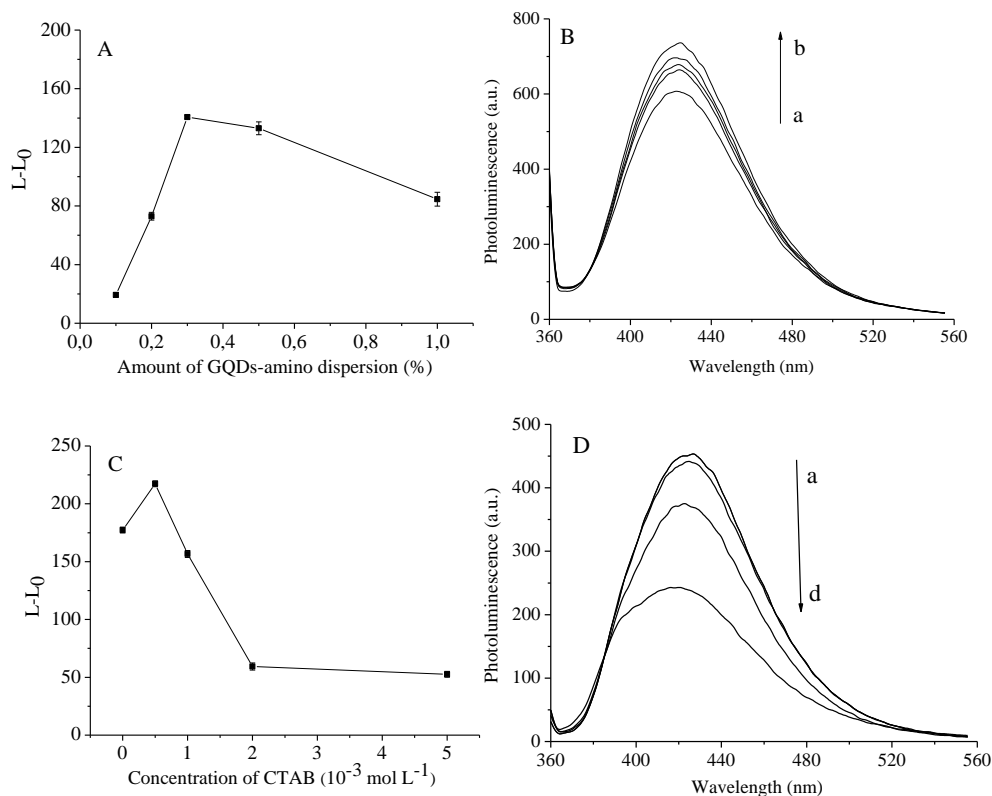


Figure 7.3. A) Evaluation of the amount of GQDs-amino dispersion in the preparation of the synthesis of the AuNPs-GQDs-amino probe and B) Photoluminescence spectra of the AuNPs-GQDs-amino dispersion synthesized in the presence of CTAB at concentrations of: (a) 0 (b) 2.0×10^{-3} , (c) 5.0×10^{-3} , (d) 1.0×10^{-3} and (d) $5.0 \times 10^{-4} \text{ mol L}^{-1}$ (final concentration in the synthesis dispersion). C) Evaluation of the effect of CTAB concentration on the probe response towards a kanamycin (concentration in the working dispersion of $1 \times 10^{-5} \text{ mol L}^{-1}$). D) Photoluminescence spectra from the AuNPs-GQDs-amino probe with increasing concentrations of CTAB: (a) 0 (b) 1.0×10^{-4} , (c) 4.0×10^{-4} , (d) $7.0 \times 10^{-4} \text{ mol L}^{-1}$ (final concentration in the probe).

The presence of a cationic surfactant (CTAB) in the reactor mixture was also evaluated as it might serve as a nucleation to facilitate the approximation the surface negative charged AuNPs and the negative charged GQDs-amino as seen by zeta potential (ζ -potential) values in Table 7.1, obtained by electrokinetic potential measurements at the original pH of these dispersions (at pH 6.0 to 6.5). The ζ -potential of the nanoparticles obtained by the reduction of HAuCl_4 directly in the GQDs-amino (AuNPs-GQDs-amino) is also negative (almost the sum of the ζ -potential of the independent AuNPs and GQDs-amino nanoparticles). As the cationic surfactant CTAB was included in the reaction mixture, the surface charge magnitude of the system turns positive (Table 7.1). It is plausible that the positive charged CTAB heads help to bring together AuNPs and GQDs-amino, also

surrounding the formed nanostructure. Besides, by CTAB pairing, it is produced a bilayer of surfactants that surrounds the AuNPs, producing a positive charge structure (Fig. 7.4). The photoluminescence intensity measured from the AuNPs-GQDs-amino-CTAB increased about 20% as the CTAB added in the reactor was $5.0 \times 10^{-3} \text{ mol L}^{-1}$ ($1 \times 10^{-4} \text{ mol L}^{-1}$ after dilution for photoluminescence measurement). As the concentration of surfactant was increased up to 10 times, the measured photoluminescence decreased yet being still more intense from the synthesized AuNPs-GQDs-amino in absence of CTAB (Fig. 7.3B).

Table 7. 1. Electrokinetic potential (ζ -potential) values obtained of nanostructures under different conditions.

Probe	ζ -potential (mV)
AuNPs	$-(10.5 \pm 0.6)$
GQDs-amino	$-(53.7 \pm 2.3)$
AuNPs-GQDs-amino	$-(66.5 \pm 3.6)$
AuNPs-GQDs-amino-CTAB	$+(57.1 \pm 0.8)$
AuNPs-GQDs-amino-CTAB + kanamycin $1.0 \times 10^{-6} \text{ mol L}^{-1}$	$+(41.5 \pm 1.8)$
AuNPs-GQDs-amino-CTAB + kanamycin $5.0 \times 10^{-6} \text{ mol L}^{-1}$	$+(22.3 \pm 0.6)$
AuNPs-GQDs-amino-CTAB + kanamycin $1.0 \times 10^{-5} \text{ mol L}^{-1}$	$+(9.9 \pm 0.3)$

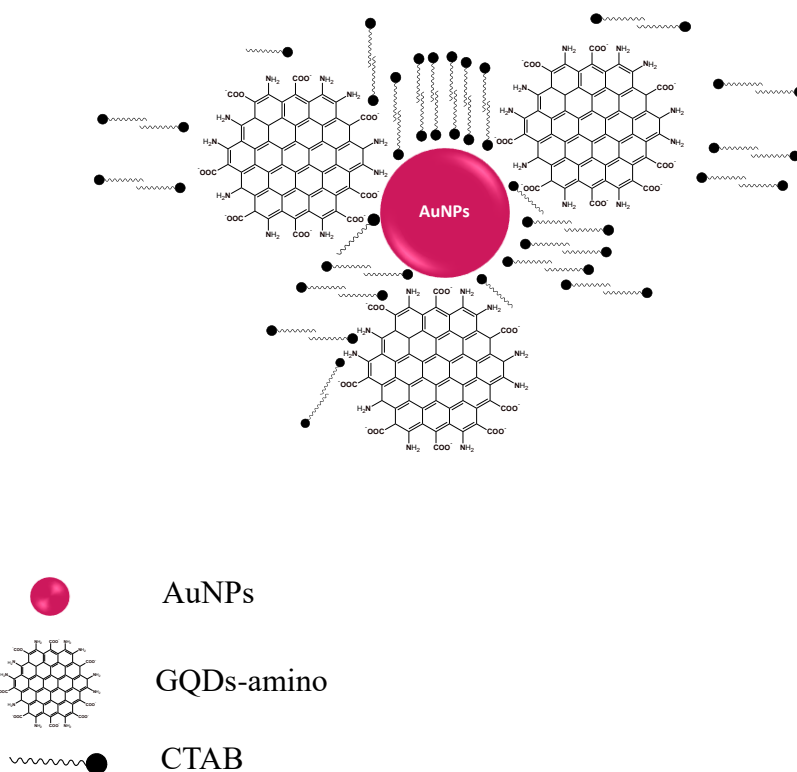


Figure 7.4. Proposal of interaction between AuNPs and GQDs-amino mediated by CTAB.

Dynamic light scattering measurements were performed to evaluate the produced nanoparticles generating histograms related to the mean diameter of the aqueous dispersions of AuNPs synthesized shown in Fig. 7.5. It is possible to observe that there is a change in the dimensions of the nanomaterials when they were obtained under different reaction conditions. AuNPs that were synthesized in aqueous medium showed a size distribution with a mean diameter of 14.7 ± 5.8 nm but when the AuNPs was produced in the presence of 5.0×10^{-4} mol L⁻¹ CTAB (below its critical micelle concentration or CMC which is about 1×10^{-3} mol L⁻¹ in water) an increasing in the mean hydrodynamic diameter was observed (21.1 ± 7.0 nm) which can be related to the redshift ($\Delta\lambda$) of 15 nm of the AuNPs LSPR band maximum (522 nm) compared to the 507 nm maximum of the AuNPs synthesized in the absence of surfactant (Fig. 7.6). In the case of the synthesis of AuNPs in a dispersion of GQDs-amino, the average diameter of the synthesized nanoparticles was 31.7 ± 8.2 nm, two times the one of the AuNPs obtained by reaction in water (Fig. 7.5). The result shows that GQDs-amino is probably helping the nucleation and growth of the nanostructure, which is corroborated by

the redshift of the AuNPs LSPR band maximum (528 nm). Finally, when AuNPs were obtained in the aqueous dispersion of GQDs-amino also containing CTAB (below CMC) a significant further increase in the hydrodynamic mean diameter of the nanostructure (AuNPs-GQDs-amino-CTAB) was observed (39.2 ± 8.2 nm) as well as a strong red shifting of the AuNPs LSPR band (542 nm as seen in Fig. 7.6) that reflects the increasing of the size of the AuNPs core.

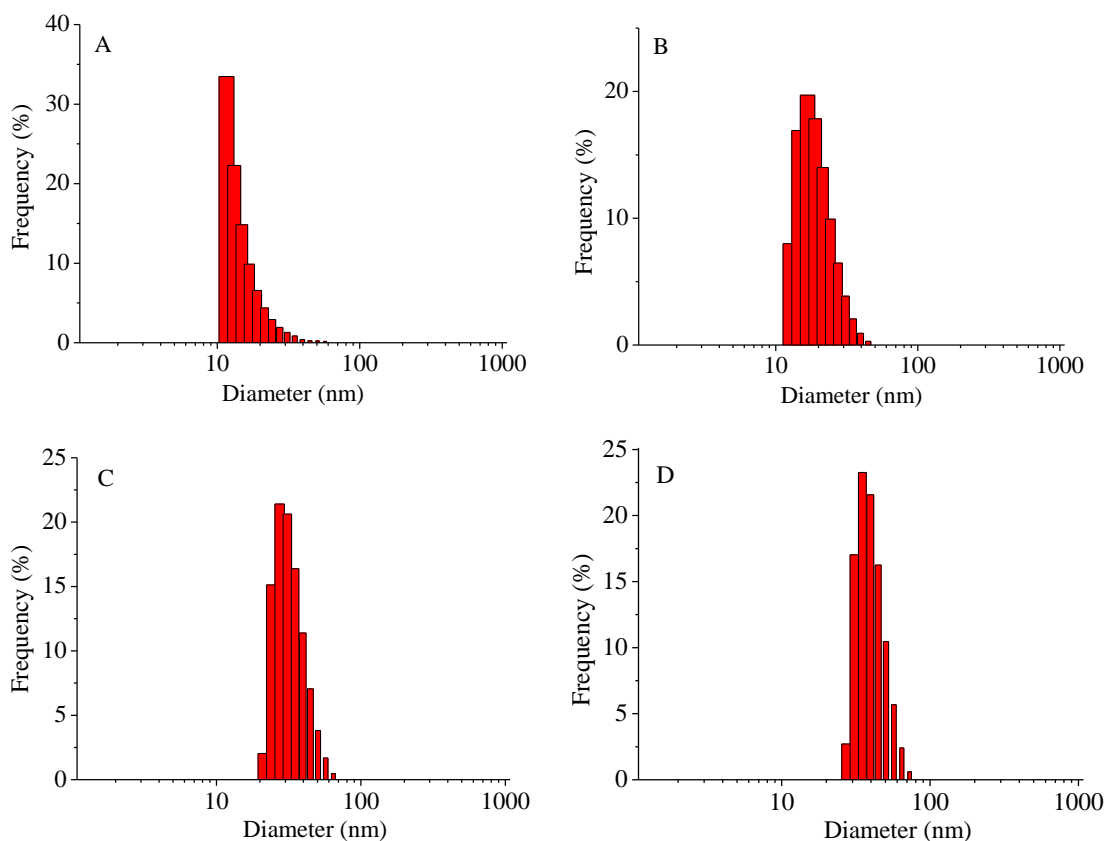


Figure 7.5. Histograms regarding the size distribution obtained by DLS of the synthesized AuNP dispersions: (A) control AuNPs (B) AuNPs in CTAB 5.0×10^{-4} mol L⁻¹, (C) AuNPs-GQDs-amino, (D) AuNPs- GQDs-amino in CTAB 5.0×10^{-4} mol L⁻¹.

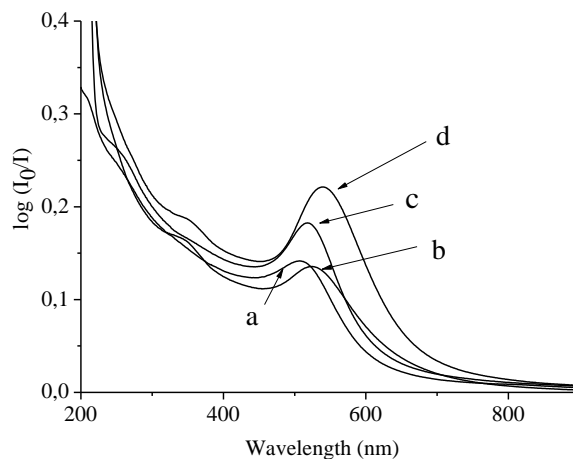


Figure 7.6. UV-vis spectra of dispersions (5 fold dilution): (a) control AuNPs in ultrapure water (b) AuNPs-GQDs-amino, AuNPs in CTAB $5.0 \times 10^{-4} \text{ mol L}^{-1}$, (c) AuNPs in CTAB $5.0 \times 10^{-4} \text{ mol L}^{-1}$, (d) AuNPs-GQDs-amino in CTAB $5.0 \times 10^{-4} \text{ mol L}^{-1}$.

The CTAB surface modification of the AuNPs-GQDs-amino also affected how kanamycin interacted with the nanostructure (Fig. 7.3C). As kanamycin sulfate is added to the system, the significant decreasing of the surface positive charge occurred, which shows that the kanamycin contra-ion (SO_4^{2-}) is pairing with the positive heads of CTAB, allowing the penetration of kanamycin (protonated at the pH of the medium of about 6.0) inside surfactant palisades, interacting with the AuNPs-GQDs-amino nanostructure and restoring the photoluminescence of the GQDs-amino. It is also possible that by penetrating the surfactant palisade, kanamycin may dislodge a CTAB, replacing it in the surface of the nanoparticle. The ability of kanamycin to restore photoluminescence from the AuNPs-GQDs-amino nanostructure was studied in function of the concentration of CTAB inside the reactor producing the nanostructures. It was observed that the presence of CTAB below CMC (at $5.0 \times 10^{-4} \text{ mol L}^{-1}$) promoted a kanamycin-induced signal restoration of around 30% more efficient when compared to that observed when the nanostructure was synthesized in absence of CTAB. In such conditions, the interaction between the protonated kanamycin and the core of the nanostructure is mediated by the less polar carbon chain of the surfactant linked to the AuNPs-GDQs-amino. As the concentration of surfactant in the reactor was increased to values above the CMC (surfactant concentration from 2×10^{-3} to $5 \times 10^{-3} \text{ mol L}^{-1}$) the photoluminescence restoration became less efficient, about 30 % of the signal restoration achieved in AuNPs-GQDs-amino

dispersions synthesized in absence of CTAB. At such relatively high concentrations, a large fraction of the protonated kanamycin is probably included inside CTAB reverse micelles, rendering them to interact with the AuNPs-GQDs-amino-CTAB nanostructures. The excess of free CTAB cations (in equilibrium with the organized structures) may also affect, by electrostatic effect, the electron-hole recombination responsible for the photoluminescence as can be seen in Fig. 7.3D that shows the decreasing of the original AuNPs-GQDs-amino when a very large amounts of CTAB are added in a AuNPs-GQDs amino dispersion.

The concentration of AuNPs-GQDs-amino-CTAB was estimated using Equation 1 and equation 2 using the mean particle diameter the one estimated by FE-STEM. Thus, the concentration of AuNPs-GQDs-amino-CTAB in the dispersion was $1.4 \times 10^{-10} \text{ mol L}^{-1}$, since the mean diameter of these materials was $32.9 \pm 3.6 \text{ nm}$ (Fig. 7.7A). Computational processing of the images indicated the aspect ratio of 1.30 ± 0.20 (Fig. 7.7B).

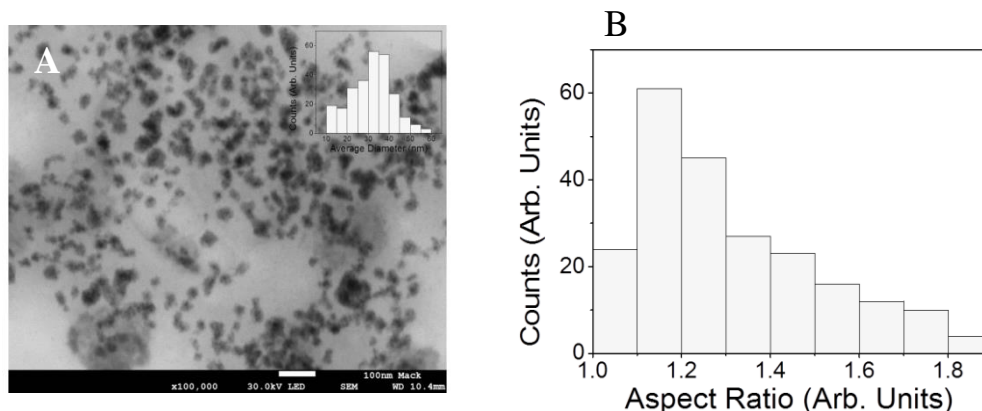


Figure 7.7. (A) FE-STEM images and size distribution of AuNPs-GQDs-amino-CTAB aqueous dispersion. Histograms referring to the process of images of AuNPs-GQDs-amino-CTAB (B) Aspect ratio and (C) Circularity.

A kinetic study modeled by the reduction reaction of 4-NP by NaBH_4 (at 25°C) was carried out to compare the catalytic effect of AuNPs and AuNPs-GQDs-amino (both obtained in a reaction medium containing $5.0 \times 10^{-4} \text{ mol L}^{-1}$ of CTAB) and also the effect caused by the GQDs-amino on reactivity. This reduction reaction was chosen as 4-NP has 2 absorption peaks (at 226 and 317 nm) and after the addition of the NaBH_4 , the band at 317 nm immediately shifted to 410 nm due to the generation of 4-nitrophenolate anion (Fig. 7.8). In the absence of AuNPs, the band at 410 nm remains unchanged indicating that the

produced 4-nitrophenolate ion cannot be reduced by NaBH_4 itself. As it is well known, AuNPs act as a catalyst to enable the reduction of 4-nitrophenolate anion by NaBH_4 forming 4-aminophenol [114]. Due to the large excess of NaBH_4 , the reaction rates can be assumed to be independent related to this reagent thus, the experiment is setup in such a way that the first order rate kinetics (under pseudo-first order conditions) can be used to model the catalytic effect of the nanoparticles. In this way, rate constants can be calculated from the decreasing of the intensity of the 4-nitrophenolate band at 410 nm (monitored at time intervals of 1 min for a total time of 120 min).

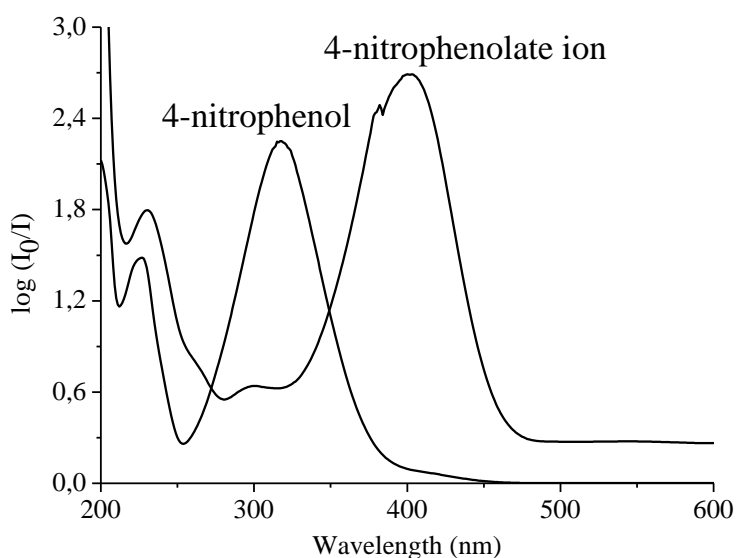


Figure 7. 8. UV-vis spectra of 4-nitrophenol and 4-nitrophenolate ion.

The catalytic effect on the reduction reaction of 4-NP was observed in the presence of either AuNPs-CTAB or AuNPs-GQDs-amino-CTAB. The reaction rate constant was 1.4 times larger for the system catalyzed by AuNPs-GQDs-amino ($1.3 \times 10^{-3} \text{ s}^{-1}$ for AuNPs and $1.8 \times 10^{-3} \text{ s}^{-1}$ for and AuNPs-GQDs-amino) as seen in Fig. 7.9. The higher catalytic efficiency observed for AuNPs-GQDs-amino-CTAB might be partially explained by the increasing of the hydrodynamic radius of this nanomaterial compared to the AuNPs-CTAB produced in absence of GQDs-amino, which increases the surface activity of the nanoparticles as this reaction mechanism is supposed to involve hydrogen adsorption/desorption on the

surface of the AuNPs [114]. No catalytic effect was produced by GQDs-amino alone.

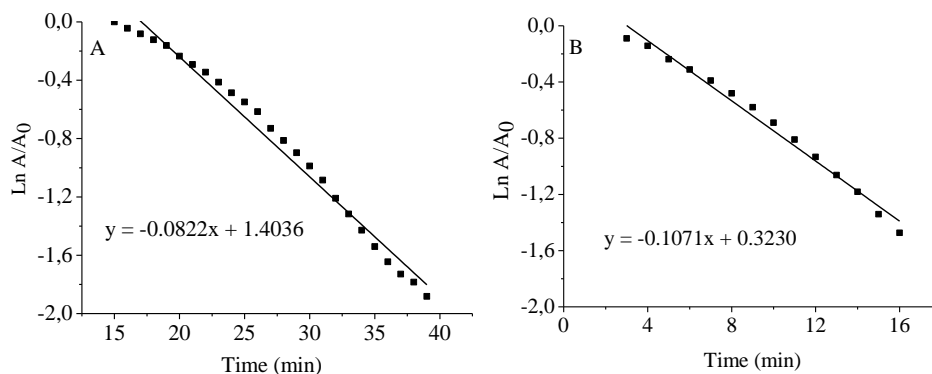


Figure 7. 9. Time profile of the absorbance of 4-phenolate ion absorption (measured at 410 nm) in the presence of: A) AuNPs-CTAB and B) AuNPs-GQDs-amino-CTAB, both sintetized in CTAB ($5 \times 10^{-4} \text{ mol L}^{-1}$ final concentration).

7.2.3

Optimized experimental parameters for the analytical probe

7.2.3.1

Amount of AuNPs-GQDs-amino-CTAB of the probe

As the conditions to produce the synthesis dispersion of the AuNPs-GQDs-amino-CTAB were adjusted, a study was performed to find the experimental conditions to produce the working dispersion of AuNPs-GQDs-amino-CTAB (probe) used as the analytical determine kanamycin.

The photoluminescence amplification effect caused by the presence of kanamycin ($5.0 \times 10^{-6} \text{ mol L}^{-1}$ final concentration) was evaluated in dispersions containing different amounts of AuNPs-GQDs-amino-CTAB. The amount of nanoparticles was varied by mixing different volumes of the synthesis dispersion of AuNPs-GQDs-amino-CTAB (0.2 to 2.0 mL) before adjusting final volume of the probe to 5.0 mL (Fig. 7.10A). The results showed the improvement of the photoluminescence amplification as the quantity of the nanomaterial in the working dispersion (final volume of 5.0 mL) was increased, reaching a maximum response with 1.4 and 1.6 mL of synthesis dispersion. When higher quantities of

nanomaterial were added (volumes greater than 1.6 mL) the signal generated by kanamycin sharply decreased, possibly indicating that the excess of nanomaterial may have induced aggregation affecting quantum confinement, thus reducing photoluminescence. In order to obtain high sensitivity and robust conditions for signal amplification, 1.5 mL was the chosen volume of the nanomaterial synthesis dispersion added to produce the 5.0 mL probe.

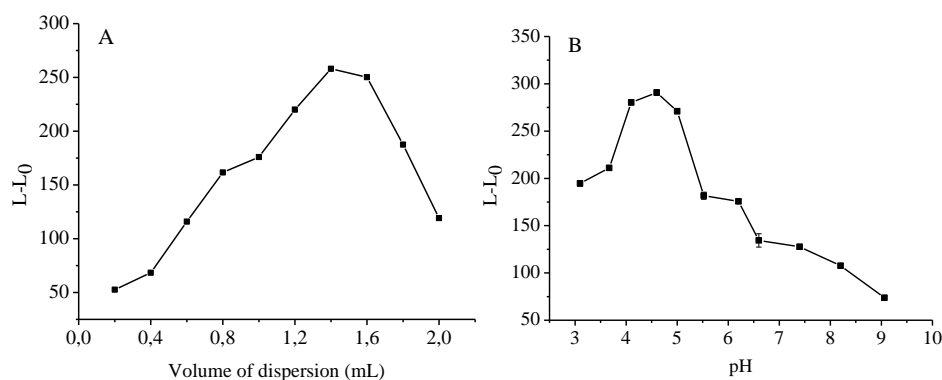


Figure 7.10. A) Effect of amount of the AuNPs-GQDs-amino-CTAB on the photoluminescence intensity (measured as $\Delta L = L - L_0$, where L_0 and L are respectively the photoluminescence of the quantum dots dispersion before and after the addition of $5.0 \times 10^{-6} \text{ mol L}^{-1}$ of kanamycin). B) Influence of the pH on the photoluminescence amplification (measured as $L - L_0$, where L_0 is AuNPs-GQDs-amino dispersion in the absence of kanamycin and L in the presence of kanamycin at $5.0 \times 10^{-6} \text{ mol L}^{-1}$).

7.2.3.2

Influence of pH on the photoluminescence amplification induced by kanamycin.

The effect of pH of the probe is crucial to enable the interaction between kanamycin (apparent $pK_a = 7.2$ [160]) and the AuNPs-GQDs-amino-CTAB nanostructures. The pH was varied in the range of 3.0 to 9.0 by addition of small quantities of either NaOH (0.01 mol L^{-1}) or HCl (0.01 mol L^{-1}) aqueous solutions. The tests were carried out measuring photoluminescence from the probe in the presence and in absence with of kanamycin ($5.0 \times 10^{-6} \text{ mol L}^{-1}$). The signal profile (Fig. 7.10B) indicated a more sensitive response (larger restoration of the photoluminescent signal) in the pH range from 4.0 to 5.0. In such range, these results are consistent with the existence of a pre-functional and anion binding site

for aminoglycoside that does not protonate significantly [161]. Therefore, the ideal pH value selected for the further experiment was fixed at 4.5.

7.2.3.3

Stability of photoluminescence intensity and reaction time.

Under the chosen conditions for the probe, the stability of the photoluminescent intensity measured from it before the addition of kanamycin sulfate was evaluated in function of time (signal measurements made every 10 min in a time interval of 120 min) and photoluminescence was found to be stable during this period (random signal variation of variation less than 2%) as indicated in Fig. 7.11A. The photoluminescence from the probe was also monitored as a function of the time after the addition of a fixed amount of kanamycin (5.0×10^{-6} mol L⁻¹ final concentration). Measurements were taken every 2 min after the addition of kanamycin up to 120 min. The photoluminescence increased achieving maximum after 20 min becoming then stable (random signal variation of variation less than 2%) up to 120 min (Fig. 7.11B). For the analytical method, it was established that all measurements would be made after 20 min of the addition of kanamycin in the probe.

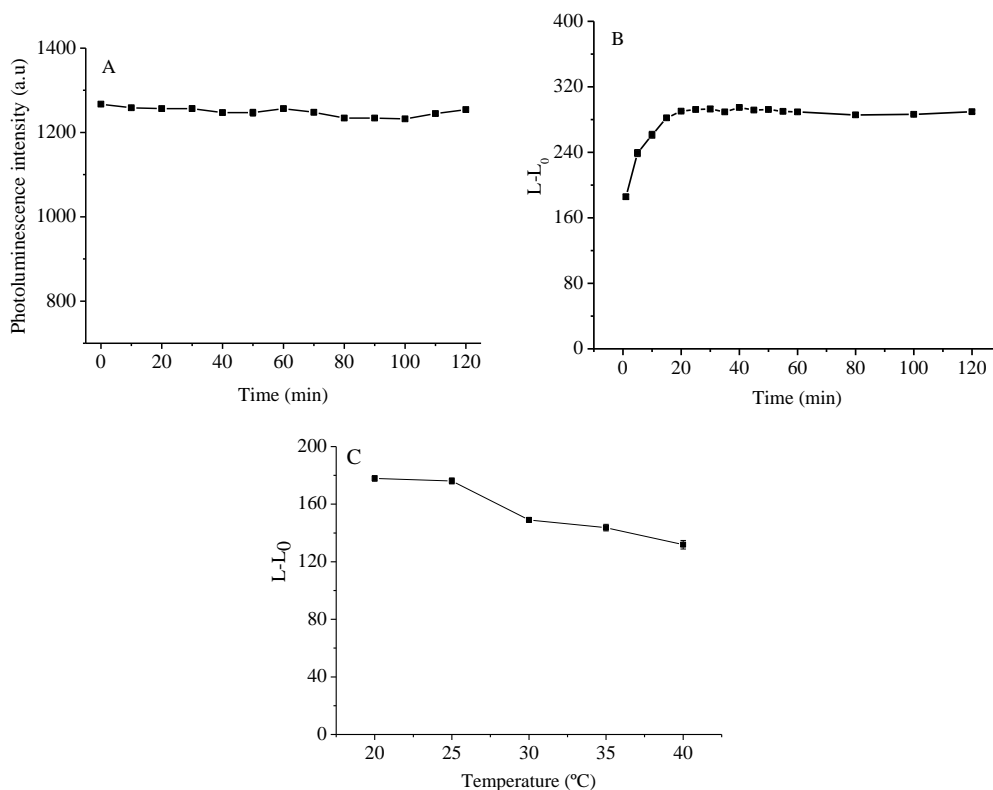


Figure 7. 11. A) Stability of the photoluminescence intensity of the AuNPs-GQDs-amino-CTAB dispersion. B) Stability of the photoluminescence of the AuNPs-GQDs-amino-CTAB after mixing kanamycin (final concentration in dispersion $5.0 \times 10^{-6} \text{ mol L}^{-1}$). C) Effect of the temperature on the photoluminescence enhancement of the aqueous AuNPs-GQDs-amino-CTAB working dispersion after addition of kanamycin ($3.0 \times 10^{-6} \text{ mol L}^{-1}$ final concentration).

7.2.4 The nature of the photoluminescence

The effect of the temperature of the increasing of the photoluminescence induced by the interaction with kanamycin sulfate was studied in the temperature range from 20 to 40 $^{\circ}\text{C}$ (with temperature interval of 5 $^{\circ}\text{C}$). A constant net signal ($L-L_0$), where L is the luminescence induced by the addition of kanamycin in the probe and L_0 is the original luminescence intensity of the probe) was found between 20 and 30 $^{\circ}\text{C}$ (Fig. 7.11C), so the temperature was found to be a fairly robust parameter in such interval. It was also found at higher temperatures the interaction between the probe and the analyte is affected since restoration signal is less efficient. Such a behavior might indicate that there is some kind of bonding between kanamycin and nanoparticle that is disrupted at higher temperatures.

A study was also carried out to evaluate the reversibility of the AuNPs-GQDs-amino-CTAB photoluminescence suppression induced by kanamycin due to the increase in temperature. For this purpose, photoluminescence measurement was performed at 20°C after addition of kanamycin (3.0×10^{-6} mol L⁻¹) then, the probe temperature was brought to 40°C to perform a new photoluminescence measurement. It was observed that when this system temperature was cooled-down to 20°C, the magnitude of the signal was restored almost completely ($98.9 \pm 0.6\%$ of the signal measured before the temperature cycle), showing that the reversibility of the interaction disruption between kanamycin and nanoparticle due to the variation of temperature.

An additional study was carried out to monitor the interaction of the nanoparticle with analyte (kanamycin sulfate). Measurements were made by molecular absorption spectrophotometry to evaluate the optical response of the nanomaterials obtained in the presence of kanamycin sulfate (final concentration in the probe of 5.0×10^{-6} mol L⁻¹). In Fig. 7.12A and 7.12B optical responses respectively for the AuNPs for the AuNPs-GQDs-amino dispersions (both prepared in CTAB) before and after the addition of kanamycin are shown. The results showed that the presence of kanamycin sulfate, in both cases, generated an increasing in the nanoparticle LSPR band, indicating that kanamycin (that do not absorb significantly in the studied spectral range) interacts with AuNPs. Such a result may be explained by the strong affinity of the nanoparticles to the nitrogen groups of the aminoglycosides as demonstrated by previous work using UV-vis, infrared spectroscopy and transmission electron microscopy [155].

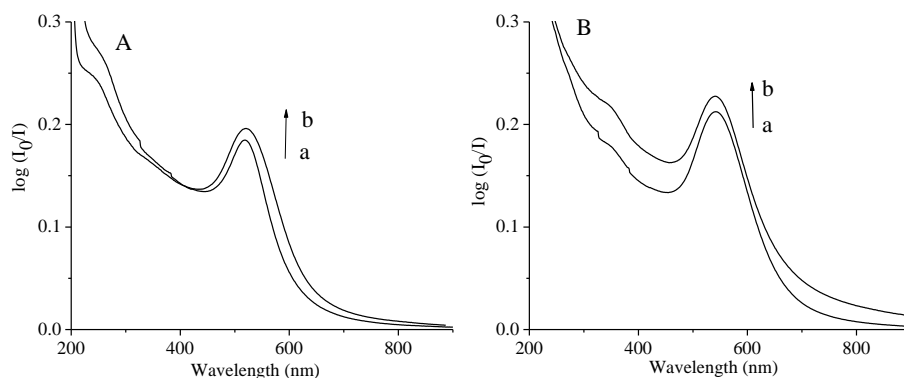


Figure 7. 12. UV-vis extinction spectra (5-fold dilution) of the: A) AuNPs in CTAB $5.0 \times 10^{-4} \text{ mol L}^{-1}$ and B) AuNPs-GQDs-amino in CTAB $5.0 \times 10^{-4} \text{ mol L}^{-1}$ before (a) and after (b) the addition of kanamycin sulfate (final concentration on the probe $5.0 \times 10^{-6} \text{ mol L}^{-1}$).

7.2.5

Analytical characteristics of the AuNPs-GQDs-amino-CTAB aqueous probe for the sensing kanamycin sulfate

The quantification of kanamycin sulfate using the probe based on AuNPs-GQDs-amino-CTAB was made using the chosen conditions described in Table 7.2. It can be seen in Fig. 7.13A that the probe photoluminescence is gradually increased as the higher quantities of kanamycin are added. The evaluation of the probe response was made through an analytical curve constructed using the relative net photoluminescence $((L-L_0)/L_0)$ as shown in Fig. 7.13B. The linear response ($R^2 = 0.998$) covered a wide range (three orders of magnitude) up to $1.0 \times 10^{-5} \text{ mol L}^{-1}$ (final concentration of kanamycin in the probe). The analyte curve equation was $(L-L_0)/L_0 = 5.51 \times 10^{-3} [\text{kanamycin}] + 8.0 \times 10^{-4}$. The limit of detection (LOD) was $6.0 \times 10^{-8} \text{ mol L}^{-1}$, calculated $3s_b/m$, where s_b was the combination standard deviation of $(L_0-L_0)/L_0$ ($n = 10$) and m is the sensitivity of the curve. The limit of quantification ($2.0 \times 10^{-7} \text{ mol L}^{-1}$) was calculated using $10s_b/m$.

Table 7. 2. Experimental conditions for the AuNPs-GQDs-amino probe used for the quantification of kanamycin sulfate.

Experimental parameter	Optimized value
Type of quantum dots	AuNPs-GQDs-amino-CTAB
pH	4.0 to 5.0
Time required to perform measurement	30 min
Volume of synthesis dispersion	1.5 mL
Temperature	25 °C
Final volume	5 mL

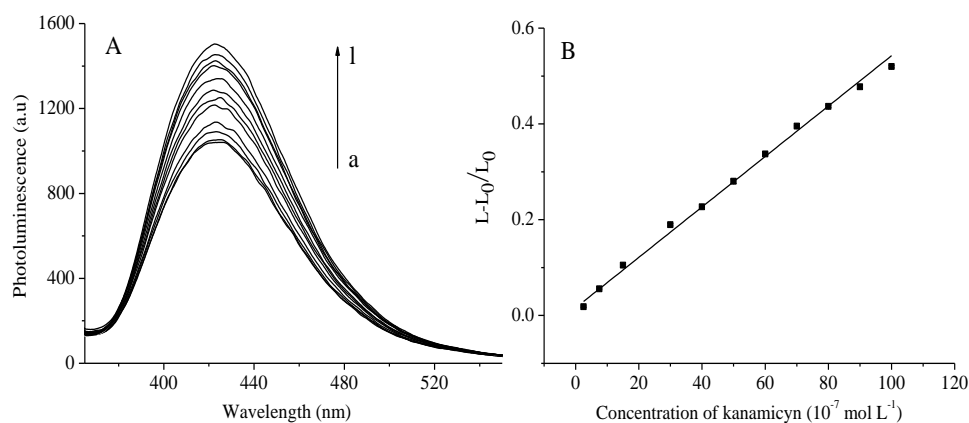


Figure 7. 9. A) Photoluminescence from the AuNPs-GQDs-amino-CTAB probe with increasing concentrations of kanamycin: (a) 0 (b) 2.5×10^{-7} , (c) 7.5×10^{-7} , (d) 1.5×10^{-6} , (e) 3.0×10^{-6} , (f) 4.0×10^{-6} , (g) 5.0×10^{-6} , (h) 6.0×10^{-6} , (i) 7.0×10^{-6} mol L⁻¹, (j) 8.0×10^{-6} , (k) 9.0×10^{-6} mol L⁻¹, (l) 1.0×10^{-5} mol L⁻¹. B) Analytical curve based on the photoluminescence enhancement of AuNPs-GQDs-amino-CTAB (expressed as $L-L_0/L_0$ in function of the concentration of kanamycin).

The precision of the method (intermediate precision) was evaluated by performing measurements (at 345/435 nm) from two sets of ten independent probes (each set containing one different kanamycin concentration). The precision was evaluated as the standard deviation of the $L-L_0/L$ ($s_{L-L_0/L}$) (Equation 7.1), where L and L_0 are the photoluminescence values of the probe before and after the addition of kanamycin respectively, and s_L and s_{L_0} are the standard deviations of L and L_0 respectively. For a kanamycin concentration of 1.0×10^{-6} mol L⁻¹

intermediate precision was 1.2%, whereas for a concentration of $5.0 \times 10^{-6} \text{ mol L}^{-1}$ it was 1.7%. The instrumental precision was evaluated from ten measurements of single probe dispersion containing a fixed concentration of kanamycin. The results were 0.7% and 1.1% for respectively $1.0 \times 10^{-6} \text{ mol L}^{-1}$ and $5.0 \times 10^{-6} \text{ mol L}^{-1}$ final concentration of kanamycin.

$$S_{\frac{L-L_0}{L}} = \frac{(L-L_0)}{L} \sqrt{\left(\frac{S_L + S_{L_0}}{L-L_0}\right)^2 + \left(\frac{S_L}{L}\right)^2} \quad (\text{Equation 7.1})$$

7.2.6

Selectivity studies and solid phase extraction with a cartridge packed with a molecularly imprinted polymer

A study was made to evaluate the optical behavior of the probe based on AuNPs-GQDs-amino-CTAB in the presence of the selected substances which are commonly found in pharmaceutical formulations containing kanamycin and in yellow fever vaccine. In order to do that, it was evaluated the degree of the signal variation (expressed in percent values) measured from the probe due to the presence of these chemical species (at a final concentration of $5.0 \times 10^{-4} \text{ mol L}^{-1}$). The results show that under the same experimental conditions established for the detection of kanamycin sulfate, the dispersion of AuNPs-GQDs-amino-CTAB is not significantly affected by the presence of sodium citrate, sodium bisulfite, sorbitol, lactose and sodium chloride (signal variation in the probe of less than 2%), which can be explained in the case of the salts (sodium citrate, sodium bisulfite and sodium chloride) by the formation of a bilayer between the possible tail of the amine groups present in the CTAB and the anions produced by the dissociation in aqueous medium of these salts getting trapped and avoiding their interaction with nanomaterials. In the case of the excipients sorbitol and lactose, they have structures which have weak functional groups (-OH) which do not favor effective interaction with the probe. However, for histidine and alanine, a small amplification of the photoluminescent signal from the probe occurred (respectively 4.6% and 2.7%). These amino acids, that present pK_{a1} (referring to the carboxylic group) of about 2 and pK_{a2} (referring to the amino group) of about

9, tend to be predominantly uncharged at the pH of probe (4.0 to 5.0) thus penetrating into the palisades of the nanomaterial system and interacting with the AuNPs-GQDs core. It is important to point out that for kanamycin, at a concentration two orders of magnitude smaller, the signal amplification was 28%.

A study to evaluate the analyte extraction efficiency, using a solid phase cartridge packed with a kanamycin imprinted polymer produced by a sol-gel synthesis [120], was conducted in order to guarantee that complex samples could be analyzed without systematic error. The study was performed in triplicate using authentic replicas of solutions containing kanamycin. Samples were loaded into the SPE cartridge to retain kanamycin, which was then cleansed with water before elution with an acidic aqueous solution (pH 3.5 adjusted by the addition of 0.01 mol L⁻¹ HCl). The eluted solution had its pH adjusted to about pH 4.5 (by addition of 0.01 mol L⁻¹ NaOH) before one aliquot was added to the probe (the AuNPs-GQDs-amino-CTAB working dispersion). The expected concentration of kanamycin sulfate in the probe was 5.0 × 10⁻⁶ mol L⁻¹ and the results indicated an average analyte loss of 2.1 ± 0.5%, which was verified by comparing the results with those, obtained using a standard solution of histamine (5.0 × 10⁻⁶ mol L⁻¹) that was not submitted to the SPE procedure.

The separation efficiency test of the analyte was performed by comparing the effect of the photoluminescent signal caused by the extracted kanamycin solution (final concentration in the probe of 5.0 × 10⁻⁶ mol L⁻¹) in a simulated sample containing the same concentration of kanamycin and in a mixture of interferents already evaluated (sodium citrate, sodium bisulfite, sorbitol, lactose and sodium chloride, histidine and alanine), which may be present in the matrices of the samples of interest (vaccine and pharmaceutical formulations) for this a kanamycin interfering relation in molar ratios of 1: 100 was chosen, obtaining a final concentration in the probe of each of the interferents of 5.0 × 10⁻⁴ mol L⁻¹. After the extract was neutralized and added to the AuNPs-GQDs-amino dispersion, comparison of the two signals showed a recovery of the 97.2% photoluminescent signal. These results indicated that the interferences tested in this study are removed in the process of cleaning the SPE procedure.

7.2.7

Application of the method

The kanamycin sulfate quantification based on the use of the AuNPs-GQDs-amino-CTAB probe was tested by determine kanamycin in a pharmaceutical sample for veterinary use, in a yellow fever vaccine sample and in simulated laboratory sample. In all cases, samples were clean up using the SPE procedure with the cartridge packed with MIP. After analyte elution, the pH was adjusted and an aliquot selected and placed into the AuNPs-GQDs-amino-CTAB working dispersion for photoluminescence measurement.

Vaccine and veterinary samples were also analyzed by a HPLC method (based on chemical derivatization with OPA) in order to provide ground to a statistical comparison made by using a two-tailed Student's t-test (95% confidence limit for $n_1 = n_2 = 3$).

The simulated sample was prepared from a mixture of kanamycin ($5.0 \times 10^{-4} \text{ mol L}^{-1}$) and excipients (sodium citrate, sodium bisulfite, sorbitol, lactose and sodium chloride, histidine and alanine) each one at concentration of $5.0 \times 10^{-2} \text{ mol L}^{-1}$. The recovery in simulated sample was 96.7 ± 2.1 , which was very satisfactory considering the level of kanamycin sulfate in the probe, the concentration of excipients and the effectiveness of the retention and elution of analyte from the MIP stationary phase.

The Brazilian yellow-fever vaccine present kanamycin as one of the conservative agents. However, the French brand, available to be tested in this work, replaces kanamycin for other bacterial growth inhibitor. Therefore, the yellow-fever sample was fortified at two levels: $2.5 \times 10^{-4} \text{ mol L}^{-1}$ (vaccine-1) and $5.0 \times 10^{-4} \text{ mol L}^{-1}$ (vaccine-2) with a known quantity of kanamycin in order to simulate one formulation that contain the target analyte. Tests using non-fortified vaccine samples were performed and no effect on the probe was observed. The determination of kanamycin in the yellow fever vaccine provided recovery close to 100% (Table 7.3) at the two concentration levels tested. For vaccine-1 ($t_{\text{experimental}} = 1.46$) and vaccine-2 ($t_{\text{experimental}} = 1.94$) equivalent results were achieved with the ones obtained by HPLC ($t_{\text{experimental}} < t_{\text{critical}} = 2.12$).

The veterinary pharmaceutical sample was also analyzed and the result obtained using the proposed method was statistically equal to the one obtained using HPLC (Table 7.3) as $t_{\text{experimental}} (1.31) < t_{\text{critical}} (2.12)$.

Table 7. 3. Recovery results (n = 3) for kanamycin sulfate in fortified vaccine samples and a sample of actual pharmaceutical formulation.

Sample	Expected value	HPLC	AuNPs-GQD-amino-CTAB probe
Recovery of kanamycin (%)			
Pharmaceutical sample	250 mg mL ⁻¹	103.1 ± 2.5	106.9 ± 3.7
Fortified vaccine-1	2.5 × 10 ⁻⁴ mol L ⁻¹	102.2 ± 2.2	98.7 ± 3.4
Fortified vaccine-2	5.0 × 10 ⁻⁴ mol L ⁻¹	101.6 ± 3.1	104.9 ± 2.9

The group of experimental results achieved for the samples (vaccine and veterinary formulation) using the proposed method were evaluated against the group of results achieved by using HPLC and they also agreed according to the analysis of variance (ANOVA of a single factor at 95% confidence level and $n_1 = n_2 = 3$): $F_{\text{experimental}} = 1.96 < F_{\text{critical}} = 4.30$).

7.3

Partial conclusions

The aqueous dispersion of AuNPs-GQDs-amino-CTAB nanostructures was found to be a sensitive probe for kanamycin after conditions were adjusted for a reliable and sensitive response towards kanamycin sulfate. The effect of generated amplification on the probe by the presence of kanamycin sulfate is favored at acid pH (4.0 - 5.0), indicating a possible inclusion of the protonated kanamycin within the CTAB palisades that surrounds the nanoparticles. Conditions of synthesis of the AuNPs-GQDs-amino-CTAB nanoparticles were adjusted as well as the ones required to prepare the working dispersion used for quantification. The detection limit value achieved was 3.0×10^{-8} mol L⁻¹ of

kanamycin sulfate in the working dispersion. The use of solid phase extraction using a kanamycin-imprinted polymer ensured the selectivity required to perform analysis in yellow fever vaccine and in formulations containing a diversity of excipients. The proposed approach is simple and does not rely on the use of chemical derivatization procedures.

General Conclusion

The main objective of the use of nanomaterials in analytical chemistry is to explore their peculiar properties to improve detection power, selectivity and separation power. Recently, numerous photoluminescent carbon nanomaterials, such as GQDs, have been explored for their potential use in analytical determination of analytes with poor optical properties in the UV-vis. In this work the GQDs were used to establish photoluminescent probes for the detection of several chemical species. The present work focused on amino-functionalized graphene quantum dots (GQDs-amino) and nanosystems composed by GQDs-amino coupled with gold nanoparticles in CTAB (AuNPs-GQDs-amino-CTAB). These nanomaterials were characterized using different techniques that aimed to find information about their morphology, structure and optical properties. The characterization studies allowed to confirm nanometric size synthesized materials, as well as the presence of graphene from its characteristic Raman bands. Functionalization with amino groups was indicated by XPS. In addition conditions were adjusted to use the aqueous dispersions of these nanomaterials as analytical probes for the determination of captopril, histamine, and kanamycin. However, experimental conditions must be carefully optimized in order to achieve stable signal and repetitive measurements.

GQDs-amino and GQD-amino-Fe³⁺ dispersions were applied as photoluminescent probes for the determination of captopril. In the presence of captopril the GQDs-amino probe suffers a quenching in its photoluminescence and a red shift, on the other hand, in the system mediated by Fe³⁺ ions, captopril generates an increment of the photoluminescence of the probe. In the case of interaction between GQDs-amino and captopril, signal quenching should be due an interaction that makes the probe not capable to be photo-excited when bounded with captopril. As Fe³⁺ was added to the GQDs-amino aqueous probe (in absence of captopril) the photoluminescence quenching occurred. As captopril is gradually added on this system, the photoluminescence is restored, showing a useful switching on/off property that can be used for quantitative purposes. The

photoluminescence enhancement is probably a result of the complex formed at the surface of the GQDs-amino, between Fe^{3+} and the sulfur of the thiol group of captopril producing energy transfer, which increased photoluminescence system.

The increased photoluminescence (GQDs-amino- Fe^{3+}) and signal shift (GQDs-amino) approaches showed a greater analytical potential due to their selectivity over quenching approaches, therefore, it was used for the determination of captopril in pharmaceutical formulation samples. The proposed photoluminescent probes allowed the sensitive and selective determination of captopril in the presence of many substances normally present in pharmaceutical formulations. The simplicity of the approach makes the proposed probe very competitive in relation to those reported in the literature.

Photoluminescence suppression of GQDs-amino was achieved in the presence of histamine when mediated by Eu^{3+} , Fe^{3+} and Cu^{2+} in aqueous system. Coordination of the metal ions (M^{n+}) with amino groups on the surface of the quantum dots was indicated by UV-vis absorption. Further signal quenching (of static nature) was observed as histamine interacted with the GQDs-amino- M^{n+} system. The strongest effect was observed when the interaction was mediated by Fe^{3+} , therefore the GQDs-amino- Fe^{3+} was used as an analytical probe for the determination of histamine. Solid phase extraction with ion exchange resins and their combination with the GQDs-amino- Fe^{3+} probe provide a sensitive and selective approach for the determination of histamine in fish samples.

The intensity of the photoluminescent signal of the GQDs-amino aqueous dispersion coupled with gold nanoparticles in medium containing cetyltrimethyl ammonium bromide (AuNPs-GQDs-amino-CTAB) was amplified in the presence of increasing concentrations of kanamycin. The effect of generated amplification on the probe by the presence of kanamycin sulfate is favored at acid pH (4.0 - 5.0), indicating a possible inclusion of the protonated kanamycin within the CTAB palisades that surrounds the nanoparticles. The results by molecular absorption showed that the presence of kanamycin sulfate in the probe generated an increase in the LSPR band of nanoparticles, indicating that kanamycin (which does not absorb significantly in the studied spectral range) interacts with AuNPs. This result can be explained by the strong affinity of the nanoparticles with the nitrogen groups of the aminoglycosides. The use of solid phase extraction using kanamycin MIP ensured selectivity in the measurements. This approach was

successfully applied for the determination of fortified yellow fever vaccine samples and pharmaceutical formulations.

All the proposed methods are based on the use of the strong photoluminescence of nanomaterials, avoiding the use of complex chemical derivation procedures and allowing simple and sensitive quantification. The use of GQDs is a green analytical approach as their preparation relies on reagents with low toxicity producing photoluminescent nanomaterials that replaces expensive and toxic dyes used in chemical derivatization procedures. The overall performance achieved in this work, indicated that they are very competitive assays compared to the ones already reported in literature.

Future work

In this work functionalized GQDs were synthesized in aqueous dispersion and evaluated as photoluminescent probes for analytical applications. However due to time constrain it was not possible to exhaust all possibilities related to this research. Therefore, some important points should be addressed as:

- ✓ To evaluate new strategies for the preparation of GQDs dispersions using other types of precursors aiming to obtain modifications in the nanomaterials looking to improve selective interaction with target analytes.
- ✓ To adapt the develop methods in flow-injection analysis systems.
- ✓ To use these carbon-based nanomaterials as probes in capillary electrophoresis with fluorimetric detection for the determination of aminoglycosides and other analytes of biological and pharmacological interest.
- ✓ To investigate, in more detail, the mechanism of interaction between the nanomaterials and the analytes studied in this work.
- ✓ To evaluate the degree of functionalization on the edges of the GQDs using characterization tools.
- ✓ Try to separate fractions of GQDs by size and from other carbon-based structures formed during synthesis.
- ✓ To evaluate the cytotoxicity of nanomaterials used in this work.

- [1] SOTOMAYOR, M. D. P. T.; DIAS, I. L. T.; MOREIRA, A. B.; KUBOTA, L. T. Aplicação e avanços da espectroscopia de luminescência em análises farmacêuticas. **Quim Nova**, v.31, n.7, p.1755-1774, Jan 2008.
- [2] KHAN, S. Photoluminescent semiconductor nanoparticles as optical probes for the determination of captopril, histamine, aminoglycosides and thyroxine. Tese de doutorado (Pontifícia Universidade Católica do Rio de Janeiro- PUC Rio), 2013.
- [3] DE FARIAS, P. M. A.; SANTOS, B. S.; LONGO, R. L.; FERREIRA, R.; CÉSAR, C. L. CdS nanoparticles: structural and energetical correlations. **Mat Chem Phys**, v. 89, n. 1, p. 21-27, Jan 2005.
- [4] BELIAN, M. F. Nanopartículas de Sílica com Complexos de Lantanídeos: Sondas luminescentes para aplicações em Imunoensaios Ultra-sensíveis. Dissertação de mestrado (Universidade Federal de Pernambuco-UFPE), 2004.
- [5] LU, J.; YEO, P. S. E.; GAN, C. K.; WU, P.; LOH, K. P. Transforming C60 molecules into graphene quantum dots. **Nat. Nanotechnol**, v. 6, p. 247–252, Feb 2011.
- [6] NURUNNABI, M.; KHATUN, Z.; REECK, G. R.; LEE, D.Y.; LEE, Y. K. Near infra-red photoluminescent graphene nanoparticle greatly expands use in noninvasive biomedical imaging. **Chem. Commun**, v. 49, p. 5079–5081, Apr 2013.
- [7] YE, Z.; TAN, M.; WANG, G.; YUAN, J. Development of functionalized terbium fluorescent nanoparticles for antibody labeling and time-resolved fluoroimmunoassay application. **Talanta**, v. 65, n. 1, p. 206-210, Jan 2005.
- [8] PETRYAYEVA, E.; RUSS, W. A.; MEDINTZ, I. L. Quantum dots in bioanalysis: A review of applications across various platforms for fluorescence spectroscopy and imaging. **Appl. Spectrosc**, v.67, n. 3, p. 215-252, 2013.
- [9] TOLOZA, C. A. T.; KHAN, S.; SILVA, R. L. D.; ROMANI, E. C.; FREIRE JR, F. L.; AUCÉLIO, R. Q. Different approaches for sensing captopril based on functionalized graphene quantum dots as photoluminescent probe. **J. Lumin**, v. 179, p. 83–92, Nov 2016.
- [10] COSTA-FERNANDEZ, J. M; PEREIRO, R.; SANZ-MEDEL, A. The use of luminescent quantum dots for optical sensing. **Trends Anal. Chem**, v. 25, n. 3, p. 207-218, 2006.
- [11] MARSH, J.N.; Partlow, K. C.; Abendschein, D. R.; Scott, M. J.; Lanza, G. M.; Wickline, S. A. Molecular imaging with targeted perfluorocarbon nanoparticles: quantification of the concentration dependence of contrast enhancement for binding to sparse cellular epitopes. **Ultrasound Med. Biol**, v. 33, n. 6, p. 950-958, Apr 2007.
- [12] EFROS, A.L. Interband absorption of light in a semiconductor sphere, **Soviet Phys. Semiconductors**, v. 16 p. 772-775, 1982.
- [13] BRUS. L. E. Electron–electron and electron-hole interactions in small semiconductor crystallites: The size dependence of the lowest excited electronic state. **J. Chem. Phys**, v. 80 p. 4403, 1984.

- [14] XU, Y., SALIM, N. A., BUMBY, C. W., TILLEY, R. D. Synthesis of SnS Quantum dots. **J. Amer. Chem. Soc.**, v. 131, n. 44, p. 15990-15991, Oct 2009.
- [15] MEDINTZ, I. L.; UYEDA, H. T.; GOLDMAN, E. R.; MATTOUSSI, H. Quantum dot bioconjugates for imaging, labelling and sensing. **Nat. Mater.**, v. 4, p. 435-446, Jun 2005.
- [16] ULBRICHT, R.; PIJPERS, J. J. H.; GROENEVELD, E.; KOOLE, R.; DONEGA, C. D.; VANMAEKELBERGH, D.; DELERUE, C.; ALLAN, G.; BONN, M. Loosening Quantum Confinement: Observation of real conductivity caused by hole polarons in semiconductor nanocrystals smaller than the bohr radius, **Nano Lett.**, v. 12, p. 4937-4942, 2012.
- [17] BOEV, V. I.; SILVA, C. J. R.; GOMES, M. J. M. Métodos químicos de síntese de pontos quânticos (QD) de semicondutores. Trabalho publicado no livro Nanoestruturas semicondutoras – Fundamentos y aplicaciones. Editores: SANCHEZ, J. T.; H.; RODRIGUEZ-COPOLLA, H. G.; ARMELLES-REIG (2003)180-194.
- [18] DIAS, D. B. Propriedades opticas de pontos quânticos semicondutores de InAs;GaAs. Trabalho de conclusão de curso: Universidade Tecnológica Federal do Paraná, Apucarana, 2011.
- [19] MURRAY, C. B.; NORRIS, D. J.; BAWENDI, M. G. Synthesis and characterization of nearly monodisperse CdE (E=sulfur, selenium, tellurium) semiconductor nanocrystallites. **J. Am. Chem. Soc.**, v. 115, n. 19, p. 8706-8715, Sep 1993.
- [20] MATOS, C. R. S. Síntese e caracterização de nanopartículas de semicondutores metálicos do tipo II-VI. Dissertação de Mestrado: Universidade Federal de Sergipe, 2012.
- [21] GULLAPALLI, S., BARRON, A. R. Physical Methods in Chemistry and Nano Science. Disponível online: <http://cnx.org/content/col10699/1.17/>.
- [22] MURPHY, C. J.; COFFER, J. L. Quantum Dots: A Primer. **Appl. Spectrosc.**, v.56, n. 1, p. 16A-27A, 2002.
- [23] HSU, P. C.; SHIH, Z. Y.; LEE, C. H.; CHANG, H.T. Synthesis and analytical applications of photoluminescent carbon nanodots. **Green Chem.**, v. 14, p. 917-920, Jan 2012.
- [24] XU, X. Y. RAY, R. GU, Y. L. PLOEHN, H. J. GEARHEART, L. RAKER K.; SCRIVENS, W. A. Electrophoretic analysis and purification of fluorescent single-walled carbon nanotube fragments. **J. Am. Chem. Soc.**, v. 126, p. 12736–12737, 2004.
- [25] BAKER, S. N.; BAKER, G. A. Luminescent carbon nanodots: emergent nanolights. **Angew. Chem. Int. Ed.**, v. 49, n. 38, p. 6726-6744, Sep 2010.
- [26] LIU, R.; WU, D.; LIU, S.; KOYNOV, K.; KNOLL, W.; LI, Q. An aqueous route to multicolour photoluminescent carbon dots using silica spheres as carriers. **Angew. Chem. Int. Ed.**, v. 48, n. 25, p. 4668-4671, Jun 2009.
- [27] KWON, W.; LEE, G.; DO, S.; JOO, T.; RHEE, S. W. Size-controlled soft-template synthesis of carbon nanodots toward versatile photoactive materials. **Small**, v. 10, n. 3, p. 506–513, Sep 2014.
- [28] SUN, W.; DU, Y.; WANG, Y. Study on fluorescence properties of carbogenic nanoparticles and their application for the determination of ferrous succinate. **J. Lumin.**, v. 130, n. 8, p. 1463-1469, Aug 2010.

- [29] WANG, F.; KREITER, M.; HE, B.; PANG, S.; LIU, C.Y. Synthesis of direct white-light emitting carbogenic quantum dots. **Chem. Commun**, v. 46, p. 3309-3311, Apr 2010.
- [30] YANG, S.T.; CAO, L.; LUO, P. G.; LU, F.; WANG, X.; WANG, H.; MEZIANI, M. J.; LIU, Y.; QI, G.; SUN, Y.P. Carbon dots for optical imaging in vivo. **J. Am. Chem. Soc**, v.131, n. 32, p.11308-11309, Jul 2009.
- [31] LI, H.; HE, X.; KANG, Z.; HUANG, H.; LIU, Y.; LIU, J.; LIAN, S.; TSANG, C. H. A.; YANG, X.; LEE, S.T. Water-soluble fluorescent carbon quantum dots and photocatalyst design. **Angew. Chem. Int. Ed**, v. 49, n. 26, p. 4430-4434, Jun 2010.
- [32] ZHU, S.; SONG, Y.; ZHAO, X.; SHAO, J.; ZHANG, J.; YANG, B. The photoluminescence mechanism in carbon dots (graphene quantum dots, carbon nanodots, and polymer dots): Current state and future perspective. **Nano. Res**, v. 8, n. 2, p. 355-381, Nov 2015.
- [33] Wang, X. Cao, L. Lu, F. S. Mezziani, M. J. Li, H. Qi, G. Zhou, B. Harruff, B. A. Kermarrec F. Sun, Y. P. Photoinduced electron transfers with carbon dots. **Chem. Commun**, v. 25, p. 3774-3776, 2009.
- [34] BOURLINOS, A. B.; STASSINOPOULOS, A.; ANGLOS, D.; ZBORIL, R.; KARAKASSIDES, M.; GIANNELIS, E. P. Surface functionalized carbogenic quantum dots. **Small**, v. 4, n. 4, p. 455-458, Apr 2008.
- [35] SUN, Y. P.; ZHOU, B.; LIN, Y.; WANG, W.; FERNANDO, K. A. S.; PATHAK, P.; MEZIANI, M. J.; HARRUFF, B. A.; WANG, X.; WANG, H.; LUO, P. G.; YANG, H.; KOSE, M. E.; CHEN, B.; VECA, L. M.; XIE, S.-Y. Quantum-sized carbon dots for bright and colourful photoluminescence. **J. Am. Chem. Soc**, v. 128, n. 4, p. 7756-7757, May 2006.
- [36] MIRTCHEV, P.; HENDERSON, E. J.; SOHEILNIA, N.; YIP, C. M.; OZIN, G. A. Solution phase synthesis of carbon quantum dots as sensitizers for nanocrystalline TiO₂ solar cells. **J. Mater. Chem**, v. 22, p. 1265-1269, Nov 2012.
- [37] LI, H.; KANG, Z.; LIU, Y.; LEE, S.-T. Carbon nanodots: synthesis, properties and applications. **J. Mater. Chem**, n. 22, p. 24230 - 24253, Aug 2012.
- [38] NOVOSELOV, K. S.; GEIM, A. K.; MOROZOV, S. V.; JIANG, D.; ZHANG, Y.; DUBONOS, S. V. Electric field effect in atomically thin carbon films. **Science**, v. 306, n. 5696, p. 666-669, Oct 2004.
- [39] GEIM, A. K. Graphene: status and prospects. **Science**, v. 324, n. 5934, p. 1530-1534, Jun 2009.
- [40] LI, L. L.; WU, G. H.; YANG, G. H.; PENG, J.; ZHAO, J. W.; ZHU, J. J. Focusing on luminescent graphene quantum dots: current status and future perspectives. **Nanoscale**, v. 5, p. 4015-4039, Jan 2013.
- [41] SHEN, J.; ZHU, Y.; YANG, C. X.; LI, C. Facile preparation and upconversion luminescence of graphene quantum dots. **Chem. Commun**, v. 47, p. 2580-2582, Dec 2011.
- [42] LIU, R. L.; WU, D. Q.; FENG, X. L.; MULLEN, K. Bottom-up fabrication of photoluminescent graphene quantum dots with uniform morphology. **J. Am. Chem. Soc**, v. 133, n. 39, p. 15221-15223, Sep 2011.
- [43] DONG, Y.; CHEN, C.; ZHENG, X.; GAO, L.; CUI, Z.; YANG, H.; GUO, C.; CHI, Y.; LI, C. M. One-step and high yield simultaneous preparation of single-

- and multi-layer graphene quantum dots from CX-72 carbon black. **J. Mater. Chem**, v.22, n. 18, p. 8764–8766, Mar 2012.
- [44] PENG, J.; GAO, W.; GUPTA, B. K.; LIU, Z.; ROMERO-ABURTO, R.; GE, L. H.; SONG, L.; ALEMANY, L. B.; ZHAN, X. B.; GAO, G. H.; VITHAYATHIL, S. A.; KAIPPARETTU, B. A.; MARTI, A. A.; HAYASHI, T.; ZHU, J. J.; AJAYAN, P. M. Graphene quantum dots derived from carbon fibers. **Nano Lett**, v. 12, n. 2, p. 844–849, Jan 2012.
- [45] LIN, L. X.; ZHANG, S. W. Creating high yield water soluble luminescent graphene quantum dots via exfoliating and disintegrating carbon nanotubes and graphite flakes. **Chem Commun**, v. 48, n. 82, p. 10177–10179, Aug 2012.
- [46] LIU, Q.; GUO, B. D.; RAO, Z. Y.; ZHANG, B. H.; GONG, J. R. Strong two-photon-induced fluorescence from photostable, biocompatible nitrogen-doped graphene quantum dots for cellular and deep-tissue imaging. **Nano Lett**, v. 13, n. 6, p. 2436–2441, May 2013.
- [47] FAN, Z. T.; LI, Y. C.; LI, X. H.; FAN, L. Z.; ZHOU, S. X.; FANG, D. C.; YANG, S. H. Surrounding media sensitive photoluminescence of boron-doped graphene quantum dots for highly fluorescent dyed crystals, chemical sensing and bioimaging. **Carbon**, v. 70, p. 149–156, Abr 2014.
- [48] LI, S. H.; LI, Y. C.; CAO, J.; ZHU, J.; FAN, L. Z.; LI, X. H. Sulfur-doped graphene quantum dots as a novel fluorescent probe for highly selective and sensitive detection of Fe³⁺. **Anal. Chem**, v. 86, n. 20, p. 10201–10207, Sep 2014.
- [49] WU, Z.; LI, W.; CHEN, J.; YU, C. A graphene quantum dot-based method for the highly sensitive and selective fluorescence turn on detection of biothiols. **Talanta**, v. 119, n. 15, p. 538–543, Feb 2014.
- [50] ZHU, S.; ZHANG, J.; LIU, X.; LI, B.; WANG, X.; TANG, S. Graphene quantum dots with controllable surface oxidation, tunable fluorescence and up-conversion emission. **RSC Adv**, v. 2, p. 2717–2720, Feb 2012.
- [51] DONG, Y. Q.; SHAO, J. W.; CHEN, C. Q.; LI, H.; WANG, R. X.; CHI, Y. W.; LIN, X. M.; CHEN, G. N. Blue Luminescent Graphene Quantum Dots and Graphene Oxide Prepared by Tuning the Carbonization Degree of Citric Acid. **Carbon**, v. 50, n. 12, p. 4738–4743, Oct 2012.
- [52] PAN, D. Y.; ZHANG, J. C.; LI, Z.; WU, M. H. Hydrothermal route for cutting graphene sheets into blue-luminescent graphene quantum dots. **Adv. Mater**, v. 22, n. 6, p. 734–738, Dec 2010.
- [53] SHEN, J.; ZHU, Y.; YANG, X.; ZONG, J.; ZHANG, J.; LI, C. One-pot hydrothermal synthesis of graphene quantum dots surface-passivated by polyethylene glycol and their photoelectric conversion under near-infrared light. **New J. Chem**, v. 36, n. 1, p. 97–101, Oct 2012.
- [54] HU, C.; LIU, Y.; YANG, Y.; CUI, J.; HUANG, Z.; WANG, Y.; YANG, L.; WANG, H.; XIAO, Y.; RONG, J. One-step preparation of nitrogen-doped graphene quantum dots from oxidized debris of graphene oxide. **J. Mater. Chem. B**, v. 1, p. 39–42, Oct 2013.
- [55] LI, Y.; ZHAO, Y.; CHENG, H. H.; HU, Y.; SHI, G. Q.; DAI, L. M.; QU, L. T. Nitrogen-doped graphene quantum dots with oxygen-rich functional groups. **J. Am. Chem. Soc**, v. 134, n. 1, p. 15–18, Dec 2012.
- [56] TANG, L.; JI, R.; CAO, X.; LIN, J.; JIANG, H.; LI, X.; TENG, K. S.; LUK, C. M.; ZENG, S.; HAO, J.; LAU, S. P. Deep ultraviolet photoluminescence of

- water-soluble self-passivated graphene quantum dots. **ACS Nano**, v. 6, n. 6, p. 5102–5110, May 2012.
- [57] TETSUKA, H.; ASAH, R.; NAGOYA, A.; OKAMOTO, K.; TAJIMA, I.; OHTA, R.; OKAMOTO, A. Optically tunable amino-functionalized graphene quantum dots. **Adv. Mater**, v. 24, n. 39, p. 5333–5338, Oct 2012.
- [58] LUO, P. H.; JI, Z.; LI, C.; SHI, G. Aryl-modified graphene quantum dots with enhanced photoluminescence and improved pH tolerance. **Nanoscale**, v. 5, p. 7361–7367, Jun 2013.
- [59] JIN, S. H.; KIM, D. H.; JUN, G. H.; HONG, S. H.; JEON, S. Tuning the photoluminescence of graphene quantum dots through the charge transfer effect of functional groups. **ACS Nano**, v. 7, n. 2, p. 239–245, Dec 2013.
- [60] LI, M.; WU, W.; REN, W.; CHENG, H. M.; TANG, N.; ZHONG, W.; DU, Y. Synthesis and upconversion luminescence of N-doped graphene quantum dots. **Appl. Phys. Lett**, v. 101, p. 1031071–1031073, Sep 2012.
- [61] FENG, Q.; CAO, Q.; LI, M.; LIU, F.; TANG, N.; DU, Y. Synthesis and photoluminescence of fluorinated graphene quantum dots. **Appl. Phys. Lett**, v. 102, p. 013111-0131114, Jan 2013.
- [62] Zhuo, S.; Shao, M.; Lee, S. T. Upconversion and Downconversion Fluorescent Graphene Quantum Dots: Ultrasonic Preparation and Photocatalysis. **ACS Nano**, v. 6, n. 2, p. 1059-1064, 2012.
- [63] ZHOU, X. J.; ZHANG, Y.; WANG, C.; WU, X. C.; YANG, Y. Q.; ZHENG, B. Photo-Fenton reaction of graphene oxide: a new strategy to prepare graphene quantum dots for DNA cleavage. **ACS Nano**, v. 6, n. 8, p. 6592–6599, Jul 2012.
- [64] LI, Y.; HU, Y.; ZHAO, Y.; SHI, G.; DENG, L.; HOU, Y. An electrochemical avenue to green-luminescent graphene quantum dots as potential electron-acceptors for photovoltaics. **Adv. Mater**, v. 23, n. 6, p. 776–780, Feb 2011.
- [65] LI, L.; JI, J.; FEI, R.; WANG, C.; LU, Q.; ZHANG, J.; JIANG, L.; ZHU, J. A Facile Microwave Avenue to Electrochemiluminescent Two-Color Graphene Quantum Dots. **Adv. Funct. Mater**, v. 22, n. 14, p. 2971-2979, Jul 2012.
- [66] MOHANTY, N.; MOORE, D.; XU, Z.; SREEPRASAD, T. S.; NAGARAJA, A.; RODRIGUEZ, A. A.; BERRY, V. Nanotomy-based production of transferable and dispersible graphene nanostructures of controlled shape and size. **Nat. Commun.** v. 3, n. 844, p. 1-8, May 2012.
- [67] SREEPRASAD, T. S.; RODRIGUEZ, A. A.; COLSTON, J.; GRAHAM, A.; SHISHKIN, E.; PALLEM, V. Electron-Tunneling Modulation in Percolating Network of Graphene Quantum Dots: Fabrication, Phenomenological Understanding, and Humidity/Pressure Sensing Applications. **Nano Lett**, v. 13, n. 4, p.1757-1763, Mar 2013.
- [68] PHAMA, T. A.; KIMB, J. S.; KIMA, J. S.; JEONGA, Y. T. One-step reduction of graphene oxide with l-glutathione. **Colloids Surf. A**, v. 384, n. (1-3), p. 543–548, Jul 2011.
- [69] LIU, J. J.; ZHANG, X. L.; CONG, Z. X.; CHEN, Z. T.; YANG, H. H.; CHEN, G. N. Glutathione-functionalized graphene quantum dots as selective fluorescent probes for phosphate-containing metabolites. **Nanoscale**, v. 5, p. 1810–1815, Jan 2013.
- [70] GEORGAKILAS, V.; OTYEPKA, M.; BOURLINOS, A. B.; CHANDRA, V.; KIM, N.; KEMP, K. C.; HOBZA, P.; ZBORIL, R.; KIM, K. S. Functionalization

- of Graphene: Covalent and Non-Covalent Approaches, Derivatives and Applications. **Chem. Rev.**, v. 112, n.11, p. 6156–6214, Sep 2012.
- [71] HE, Y.; WANG, X.; SUN, J.; JIAO, S.; CHEN, H.; GAO, F.; WANG, L. Fluorescent blood glucose monitor by hemin-functionalized graphene quantum dots based sensing system. **Anal. Chim. Acta**, v. 810, p. 71–78, Jan 2014.
- [72] SAIDI, W. A. Oxygen reduction electrocatalysis using N-doped graphene quantum-dots. **J. Phys. Chem. Lett.**, v. 4, n. 23, p. 4160-4165, Nov 2013.
- [73] YEH, T. F.; TENG, C. Y.; CHEN, S. J.; TENG, H. Nitrogen-doped graphene oxide quantum dots as photocatalysts for overall water-splitting under visible light illumination. **Adv. Mater.**, v. 26, n. 20, p. 3297-3303, May 2014.
- [74] ZHANG, L.; ZHANG, Z. Y.; LIANG, R. P.; LI, Y. H.; QIU, J. D. Boron-doped graphene quantum dots for selective glucose sensing based on the “abnormal” aggregation-induced photoluminescence enhancement. **Anal. Chem.**, v. 86, n. 9, p. 4423-4430, Apr 2014.
- [75] LI, X. M.; LAU, S. P.; TANG, L. B.; JI, R. B.; YANG, P. Z. Sulphur doping: a facile approach to tune the electronic structure and optical properties of graphene quantum dots. **Nanoscale**, v. 6, n. 10, p. 5323-5328, May 2014b.
- [76] LI, X. M.; LAU, S. P.; TANG, L. B.; JI, R. B.; YANG, P. Z. Multicolour light emission from chlorine-doped graphene quantum dots. **J. Mater. Chem. C**, v. 1, n. 44, p. 7308-7313, Sep 2013.
- [77] LIN, L.; SONG, X.; CHEN, Y.; RONG, M.; WANG, Y.; ZHAO, L.; ZHAO, T.; CHEN, X. Europium-decorated graphene quantum dots as a fluorescent probe for label-free, rapid and sensitive detection of Cu^{2+} and L-cysteine. **Anal. Chim. Acta**, v. 891, p. 261-268, Sep 2015;
- [78] ZHU, S.; ZHANG, J.; QIAO, C.; TANG, S.; LI, Y.; YUAN, W.; LI, B.; TIAN, L.; LIU, F.; HU, R.; GAO, H.; WEI, H.; ZHANG, H.; SUN, H.; YANG, B. Strongly green-photoluminescent graphene quantum dots for bioimaging applications. **Chem. Commun.**, v. 47, p. 6858-6860, May 2011.
- [79] PRADHAN, S. K.; XIAO, B.; MISHRA, S.; KILLAN, A.; PRADHAN, A. K. Resistive switching behavior of reduced graphene oxide memory cells for low power nonvolatile device application. **Sci. Rep.**, v. 6, n. 26763, p. 1-9, May 2016.
- [80] FENG, Y.; ZHAO, J.; YAN, X.; TANG, F.; XUE, Q. Enhancement in the fluorescence of graphene quantum dots by hydrazine hydrate reduction. **Carbon**, v. 66, p. 334–339, Jan 2014.
- [81] XU, H.; ZHOU, S.; XIAO, L.; WANG, H.; LI, S.; YUAN, Q. Fabrication of a nitrogen-doped graphene quantum dot from MOF-derived porous carbon and its application for highly selective fluorescence detection of Fe^{3+} . **J. Mater. Chem. C**, v. 3, n. 2, p. 291-297, Oct 2015.
- [82] RAN, X.; SUN, H. J.; PU, F.; REN, J. S.; QU, X. G. Ag Nanoparticle-decorated graphene quantum dots for label-free, rapid and sensitive detection of Ag^+ and biothiols. **Chem. Commun.**, v. 49, p. 1079–1081, Dec 2013.
- [83] RITTER, K. A.; LYDING, J. W. The influence of edge structure on the electronic properties of graphene quantum dots and nanoribbons. **Nat. Mater.**, v. 8, p. 235–242, Feb 2009.
- [84] PONOMARENKO, L. A.; SCHEDIN, F.; KATSNELSON, M. I.; YANG, R.; HILL, E. W.; NOVOSELOV, K. S. Chaotic Dirac billiard in graphene quantum dots. **Science**, v. 320, n. 5874, p. 356–358, Apr 2008.

- [85] SON, Y. W.; COHEN, M. L.; LOUIE, S. G. Half-metallic graphene nanoribbons. **Nature**, v. 444, p. 347–349, Nov 2006.
- [86] LI, X.; WANG, X.; ZHANG, L.; LEE, S.; DAI, H. Chemically derived, ultrasmooth graphene nanoribbon semiconductors. **Science**, v. 319, n. 6867, p. 1229–1232, Feb 2008.
- [87] FUJII, S.; ENOKI, T. Cutting of oxidized graphene into nanosized pieces. **J. Am. Chem. Soc.**, v. 132, n. 29, p. 10034–10041, Jun 2010.
- [88] WANG, F.; GU, Z.; LEI, W.; WANG, W.; XIA, X.; HAO, Q. Graphene quantum dots as a fluorescent sensing platform for highly efficient detection of copper (II) ions. **Sens. Actuator B-Chem**, v. 190, p. 516–522, Jan 2014.
- [89] CHAKRABORTI, H.; SINHA, S.; GHOSH, S.; PAL, S. K. Interfacing water soluble nanomaterials with fluorescence chemosensing: graphene quantum dot to detect Hg^{2+} in 100% aqueous solution. **Mater. Lett.**, v. 97, p. 78–80, Apr 2013.
- [90] FAN, L.; HU, Y.; WANG, X.; ZHANG, L.; LI, F.; HAN, D. Fluorescence resonance energy transfer quenching at the surface of graphene quantum dots for ultrasensitive detection of TNT. **Talanta**, v. 101, p. 192–197, Nov 2012.
- [91] WANG, Y.; ZHANG, L.; LIANG, R. P.; BAI, J. M.; QIU, J. D. Using Graphene Quantum Dots as Photoluminescent Probes for Protein Kinase Sensing. **Anal Chem**, v. 85, n. 19, p. 9148–9155, Sep 2013.
- [92] ZHOU, Y.; QU, Z.; ZENG, Y.; ZHOU, T.; SHI, G. A novel composite of graphene quantum dots and molecularly imprinted polymer for fluorescent detection of paranitrophenol. **Biosens. Bioelectron**, v. 52, p. 317–323, Feb 2014.
- [93] ZHANG, Y.; WU, C.; ZHOU, X.; WU, X.; YANG, Y.; WU, H.; GUO, S.; ZHANG, J. Graphene quantum dots/gold electrode and its application in living cell H_2O_2 detection. **Nanoscale**, v. 5, p. 1816–1819, Jan 2013.
- [94] LI, Z.; SUN, R.; NI, Y.; KOKOT, S. A novel fluorescent probe involving a graphene quantum dot–enzyme hybrid system for the analysis of hydroquinone in the presence of toxic resorcinol and catechol. **Anal. Methods**, v. 6, n. 18, p. 7420–7425, Jul 2014.
- [95] LIU, J. J.; CHEN, Z. T.; TANG, D. C.; WANG, Y. B.; KANG, L. T.; YAO, J. N. Graphene quantum dots based fluorescent probe for turnon sensing of ascorbic acid. **Sens. Actuator. B-Chem**, v. 212, p. 214–21, Jun 2015.
- [96] GUPTA, B. K.; THANIKAIVELAN, P.; NARAYANAN, T. N.; LI, S.; WEI, G.; TAKUYA, H.; ARAVA, L. M. R.; AVISHEK, S.; VIRENDRA, S.; MORINOBU, E.; ANGEL, A. M.; PULICKEL, M. A. Optical bifunctionality of europium-complexed luminescent graphene nanosheets. **Nano Lett**, v. 11, n.12, p. 5227–5233, Nov 2011.
- [97] KANEMOTO, M.; SEKIGUCHI, H.; YAMANE, K.; OKADA, H.; WAKAHARA, A. Eu^{3+} luminescence properties of Eu- and Mg-codoped AlGaIn. **J. Lumin**, v. 166, p. 60–66, Oct 2015.
- [98] ARAI, T.; TIMMERMAN, D.; WAKAMATSU, R.; LEE, D.; KOIZUMI, A.; FUJIWARA, Y. Enhanced excitation efficiency of Eu ions in Eu-doped GaN/AlGaIn multiple quantum well structures grown by organometallic vapor phase epitaxy. **J. Lumin**, v. 158, p. 70–74, Feb 2015.
- [99] BAI, J. M.; ZHANG, L.; LIANG, R. P.; QIU, J. D. Graphene Quantum Dots Combined with Europium Ions as Photoluminescent Probes for Phosphate sensing. **Chem. Eur. J**, v. 19, n. 12, p. 3822–3826, May 2013.

- [100] CHAI, F.; WANG, T.; LI, L.; LIU, H.; ZHANG, L.; SU, Z.; WANG, C. Fluorescent gold nanoprobe for the sensitive and selective detection for Hg²⁺. **Nanoscale Res. Lett**, v. 5, p. 1856–1860, Nov 2010.
- [101] DONG, Y.; WANG, R.; TIAN, W.; CHI, Y.; CHEN, G. “Turn-on” fluorescent detection of cyanide based on polyamine-functionalized carbon quantum dots. **RSC Adv**, v. 4, p. 3701–3705, Nov 2014.
- [102] HUANG, X.; EL-SAYED, M. A. Gold nanoparticles : Optical properties and implementations in cancer diagnosis and photothermal therapy. **J Adv. Res**, v. 1, n. 1, p. 13–28, Jan 2010.
- [103] TOMA, H. E.; ZAMARION, V. M.; TOMA, S. H.; ARAKI, K. The Coordination Chemistry at Gold Nanoparticles. **J. Braz. Chem. Soc**, v. 21, n. 7, p. 1158–1176, Apr 2010.
- [104] TING, S. L.; JING EE, S.; ANANTHANARAYANAN, A.; LEONG, K. C.; CHEN, P. Graphene quantum dots functionalized gold nanoparticles for sensitive electrochemical detection of heavy metal ions. **Electrochim. Acta**, v. 172, p.7–11, Aug 2015.
- [105] JU, J.; CHEN, W. In Situ Growth of Surfactant-Free Gold Nanoparticles on Nitrogen-Doped Graphene Quantum Dots for Electrochemical Detection of Hydrogen Peroxide in Biological Environments. **Anal. Chem**, v. 87, n. 3, p. 1903–1910, Dec 2015.
- [106] HUANG, S.; WANG, L.; HUANG, C.; HU, B.; SU, W.; XIAO, Q. Graphene quantum dot coupled with gold nanoparticle based Boff-on fluorescent probe for sensitive and selective detection of L-cysteine. **Microchim. Acta**, v. 183, n. 6, p. 1855–1864, Jun 2016.
- [107] DONG, Y. Q.; WU, H.; SHANG, P. X.; ZENG, X. O.; CHI, Y. W. Immobilizing water-soluble graphene quantum dots with gold nanoparticles for a low potential electrochemiluminescence immunosensor. **Nanoscale**, v. 7, n. 39, p. 16366–16371, Sep 2015.
- [108] FENG, X.; ZHANG, Q.; ZHINONG, G. Simple one-step synthesis of gold nanoparticles with controlled size using cationic Gemini surfactants as ligands: Effect of the variations in concentrations and tail lengths. **Colloids Surf. A**, v. 417, p. 201–210, Nov 2013.
- [109] MELHUIH, W. H. Quantum efficiencies of fluorescence of organic substances: effect of solvent and concentration of the fluorescent solute. **J. Phys. Chem**, v. 65, n. 2, p 229–235, Feb 1961.
- [110] KHAN, S.; MIGUEL, E. M.; DE SOUZA, C. F.; DA SILVA, A. R.; AUCÉLIO, R. Q. Thioglycolic acid-CdTe quantum dots sensing and molecularly imprinted polymer based solid phase extraction for the determination of kanamycin in milk, vaccine and stream water samples. **Sens. Actuator B-Chem**, v. 246, p. 444–454, Jul 2017.
- [111] LERKE, P. A.; BELL, L. D. A rapid fluorometric method for the determination of histamine in canned tuna. **J. Food Sci**, v. 41, n. 6, p.1282–1284, Nov 1976.
- [112] PRESTES, O. D.; PRESTA, M. A.; KOLSBERG, D. I.; ZANELLA, R.; ROSSATO, S. B.; PENNA, N. G.; HECKTHEUER, L. H. R. Desenvolvimento e validação de um método analítico para a determinação de histamina em vinhos utilizando cromatografia líquida de alta eficiência com detecção por fluorescência. **Quím. nova**, v. 30, n. 1, p. 18–21, Sep 2007.

- [113] ZHOU, Y. X.; YANG, W. J.; ZHANG, L. Y.; WANG, Z. Y. Determination of Kanamycin A in Animal Feeds by Solid Phase Extraction and High Performance Liquid Chromatography with Pre-Column Derivatization and Fluorescence Detection. **J. Liq. Chromatogr. Relat. Technol.**, v. 30, n. 11, p. 1603-1615, Apr 2007.
- [114] SEOUDI, R.; SAID, D. A. Studies on the Effect of the Capping Materials on the Spherical Gold Nanoparticles Catalytic Activity. **W. J. Nano Sci. Eng.**, v. 1, p. 51-61, Apr 2011.
- [115] BLANCO, E.; BLANCO, G.; GONZALEZ-LEAL, J. M.; BARRERA, M. C.; DOMINGUEZ, M.; RAMIREZ-DEL-SOLAR, M. Green and fast synthesis of amino-functionalized graphene quantum dots with deep blue photoluminescence **J. Nanopart. Res.**, v.17, p. 214- , 2015.
- [116] ZANG, Y.; LIU, X.; FAN, Y.; GUO, X.; ZHOU, L.; LV, Y.; LIN, J. One-step microwave synthesis of N-doped hydroxyl-functionalized carbon dots with ultra-high fluorescence quantum yields. **Nanoscale**, v. 8, n. 33, p. 15281-15287, Jul 2016.
- [117] SANDOVAL, S.; KUMAR, N.; ORO-SOLÉ, J.; SUNDARESAN, A.; RAO, C. N. R.; FUERTES, A.; TOBIAS, G. Tuning the nature of nitrogen atoms in N-containing reduced graphene oxide. **Carbon**, v. 96, p. 594-602, Jan 2016.
- [118] LIU, X.; ATWATER, M.; WANG, J.; HUO, Q. Extinction coefficient of gold nanoparticles with different sizes and different capping ligands. **Colloids Surf. B**, v. 58, n. 1, p. 3–7, Jul 2007.
- [119] American Heart Association official website, retrieved in January 2012 from-<http://www.americanheart.org/presenter.jhtml?identifier=593>).
- [120] Heart Center Online document on hypertension and treatment, retrieved in January 2013 - <http://www.heartcenteronline.com/myheartdr/common/artprn>
- [121] KHAN, S.; LIMA, A. A.; LARRUDÉ, D. G.; ROMANI, E. C.; AUCÉLIO, R. Q. Determination of captopril using selective photoluminescence enhancement of 2-mercaptopropionic modified CdTe quantum dots. **Mater. Res. Express.** 1 (2014) 206.
- [122] KÚSMIEREK, K.; CHWATKO, G.; GŁOWACKI, R.; KUBALCZYK, P.; BALD, E. Ultraviolet derivatization of low-molecular-mass thiols for high performance liquid chromatography and capillary electrophoresis analysis. **J Chromatogr. B**, v. 879, n. (17-18), p. 1290–1307, May 2011.
- [123] EL-ENANY, N.; BELAL, F.; RIZK, M. Novel Spectrophotometric Method for the Assay of Captopril in Dosage Forms using 2,6-Dichloroquinone-4-Chlorimide. **Int J Biomed Science**, v. 4, p. 147-154, 2008.
- [124] EL-DIDAMONY, A. M. Spectrofluorimetric Determination of the Hypertensive Drug Captopril Based on Its Oxidation with Cerium (IV). **J. Chin. Chem. Soc.**, v. 56, p. 755-762, 2009.
- [125] AL-GHANNAM, S. M.; EL-BRASHY, A. M.; AL-FARHAN, B. S. Fluorimetric determination of some thiol compounds in their dosage forms. **IL Farmaco** 57 (2002) 625–629.
- [126] BELFILALI, I.; LOUHIBI, S.; MAHBOUB, R.; TOUZANI, R.; EL KADIRI, S.; ROISNEL, T. Study of the histamine copper (II) chloride complex catalytic activity. **Res. Chem. Intermed.**, v. 41, p. 1819–1831, 2015.
- [127] TAO, Z. H.; SATO, M.; HAN, Y. L.; TAN, Z. J.; YAMAGUCHI, Y.; NAKANO, T. A simple and rapid method for histamine analysis in fish and

- fishery products by TLC determination. **Food Control**, v. 22, n. 8, p. 1154-1157, Aug 2011.
- [128] COHEN, G.; RUDNIK, D. D.; LALOUSH, M.; YAKIR, D.; KARPAS, Z. A Novel Method for Determination of Histamine in Tuna Fish by Ion Mobility Spectrometry. **Food Anal. Methods**, v. 8, n. 9, p. 2376–2382, Oct 2015.
- [129] BILGIN, B.; GENÇCELEP, H. Determination of Biogenic Amines in Fish Products. **Food Sci. Biotechnol.**, v. 24, n. 5, p.1907-1913, Oct 2015.
- [130] SIMO, C.; MORENO-ARRIBAS, M. V.; CIFUENTES, A. Ion-trap versus time-of-flight mass spectrometry coupled to capillary electrophoresis to analyze biogenic amines in wine. **J. Chromatogr. A**, v. 1195, n. (1-2), p. 150–156, May 2008.
- [131] LEHANE, L.; OLLEY, J. Histamine fish poisoning revisited. **Int. J. Food Microbio**, v. 58, n. (1-2), p. 1-37, Jun 2000.
- [132] HU, Y.; MA, X.; ZHANG, Y.; CHE, Y.; ZHAO, J. Detection of Amines with Fluorescent Nanotubes: Applications in the Assessment of Meat Spoilage. **ACS Sens**, v. 1, n. 1, p. 22–25, Nov 2016.
- [133] PATANGE, S. B.; MUKUNDAN, M. K.; KUMAR, K. A. A simple and rapid method for colorimetric determination of histamine in fish flesh. **Food Control**, v. 16, n. 5, p. 465–472, Jun 2005.
- [134] BADIA-ERIM F. Recent analytical approaches to analysis of biogenic amines in food samples. **Trends Anal. Chem**, v. 52, p. 239–247, 2013.
- [135] PENG, J. F.; FANG, K. T.; ME, D. H.; DING, B.; YIN, J. Y.; CUI, X. M.; ZHANG, Y.; LIU, J. F. Development of an automated on-line pre-column derivatization procedure for sensitive determination of histamine in food with high-performance liquid chromatography-fluorescence detection. **J. Chromatogr. A**, v. 1209, n. (1-2), p. 70-75, Oct 2008.
- [136] KONAKOVSKY, V.; FOCKE, M.; SOMMERGRUBER, K. H.; SCHMID, R.; SCHEINER, O.; MOSER, P.; JARISCH, R.; HEMMER, W. Levels of histamine and other biogenic amines in high-quality red wines. **Food Addit. Contam. A**, v. 28, n. 4, p. 408-416, Feb 2011.
- [137] MALE, K. B.; LUONG, J. H. T. Derivatization, stabilization and detection of biogenic amines by cyclodextrin-modified capillary electrophoresis–laser-induced fluorescence detection. **J. Chromatogr. A**, v. 926, n. 2, p. 309-317, Aug 2001.
- [138] COHEN, G; RUDNIK, D. D; LALOUSH, M; YAKIR, D; KARPAS, Z. A Novel Method for Determination of Histamine in Tuna Fish by Ion Mobility Spectrometry. **Food Anal. Methods** (2015) 8: 2376–2382.
- [139] WEDAKOON, C. N.; MURATA, M.; SAKAGUCHI, M. Comparison of non-volatile amine formation between the dark and white muscles of mackerel during storage. **Nippon Suisan Gakk. J.**, v. 56, n. 5, p. 809-818, Nov 1990.
- [140] YU, C. Z.; HE, Y. Z.; FU, G. N.; XIE, H.Y.; GAN, W. E. Determination of kanamycin A, amikacin and tobramycin residues in milk by capillary zone electrophoresis with post-column derivatization and laser-induced fluorescence detection. **J. Chromatogr. B**, v. 877, n. 3, p. 333-338, Dec 2009.
- [141] WANG, R.; WANG, R.; GE, B.; JIA, X.; LI, Z.; CHANG, J. Spectral method determination of kanamycin sulfate using both gold nanoparticles and quantum dots. **Anal. Methods**, v. 5, n. 19, p. 5302-5308, Aug 2013.

- [142] TSUJI, K.; ROBERTSON, J. H. Gas-Liquid Chromatographic Determination of Amino-Glycoside Antibiotics: Kanamycin and Paromomycin. **Anal. Chem.**, v. 42, n. 15, p. 1661-1663, Nov 1970.
- [143] DIJKSTRA, J. A.; VOERMAN, A. J.; GREIJANUS, B.; TOUW, D. J.; ALFFENAAR, J. W. C. Immunoassay Analysis of Kanamycin in Serum Using the Tobramycin Kit. **Antimicrob. Agents Chemother.**, v. 60, n. 8, p. 4646-4651, Aug 2016.
- [144] HE, J.; WANG, Y.; ZHANG, X. Preparation of Artificial Antigen and Development of IgY-Based Indirect Competitive ELISA for the Detection of Kanamycin Residues. **Food Anal. Methods**, v. 9, n. 3, p. 744-751, Jul 2016.
- [145] KIM, B. H.; KIM, Y. K.; OK, J. H. Development of liquid chromatographic method for the analysis of kanamycin residues in varicella vaccine using phenylisocyanate as a derivatization reagent. **J. Chromatogr. B**, v. 752, n. 1, p. 173-177, Mar 2001.
- [146] MEGOULAS, N. C.; KOUPPARIS, M. A. Direct determination of kanamycin in raw materials, veterinary formulation and culture media using a novel liquid chromatography-evaporative light scattering method. **Anal. Chim. Acta**, v. 547, n.1, p. 64-72, Mar 2005.
- [147] OERTEL, R.; NEUMEISTER, V.; KIRCH, W. Hydrophilic interaction chromatography combined with tandem-mass spectrometry to determine six aminoglycosides in serum. **J. Chromatogr. A**, v. 1058, n. (1-2), p. 197-201, Nov 2004.
- [148] ADAMS, E.; DALLE, J.; DE BIE, E.; DE SMEDT, I.; ROETS, E.; HOOGMARTENS, J. Analysis of kanamycin sulfate by liquid chromatography with pulsed electrochemical detection. **J. Chromatogr. A**, v. 766, n. (1-2), p. 133-139, Abr 1997.
- [149] YANG, M.; TOMELLINI, S. A. Non-derivatization approach to high performance liquid chromatography-fluorescence detection for aminoglycoside antibiotics based on a ligand displacement reaction. **J. Chromatogr. A**, v. 939, n. (1-2), p. 59-67, Dec 2001.
- [150] MEGOULAS, N. C.; KOUPPARIS, M. A. Direct determination of kanamycin in raw materials, veterinary formulation and culture media using a novel liquid chromatography-evaporative light scattering method. **Anal. Chim. Acta**, v. 547, n. 1, p. 64-72, Aug 2005.
- [151] BLANCHAERT, B.; PODEROS JORGE, E.; JANKOVICS, P.; ADAMS, E.; SCHEPDAEL, A. V. Assay of Kanamycin A by HPLC with Direct UV Detection. **Chromatographia**, v. 76, p. 1505-1512, Mar 2013.
- [152] SHARMA, A.; ISTAMBOULIE, G.; HAYAT, A.; CATANANTE, G.; BHAND,S.; MARTY, J. L. Disposable and portable aptamer functionalized impedimetric sensor for detection of kanamycin residue in milk sample. **Sens. Actuator B-Chem**, v. 245, p. 507-515, Jun 2017.
- [153] WANG, M. T.; LIU, M. H.; WANG, C. R. C.; CHANG, S. Y. Silver-Coated Gold Nanoparticles as Concentrating Probes and Matrices for Surface-Assisted Laser Desorption/Ionization Mass Spectrometric Analysis of Aminoglycosides. **J. Am. Soc. Mass Spectrom**, v. 20, n. 10, p. 1925-1932, Oct 2009.
- [154] DERBYSHIRE, N.; WHITE, S. J.; BUNKA, D. H. J.; SONG, L.; STEAD, S.;TARBIN, J.; SHARMAN, M.; ZHOU, D.; STOCKLEY, P. G. Toggled RNA Aptamers Against Aminoglycosides Allowing Facile Detection of Antibiotics

- Using Gold Nanoparticle Assays. **Anal Chem**, v. 84, n.15, p. 6595–6602, Jul 2012.
- [155] GRACE, A. N.; PANDIAN, K. Antibacterial efficacy of aminoglycosidic antibiotics protected gold nanoparticles - A brief study. **Colloids Surf. A**, v. 297, n. (1-3), p. 63–70, Abr 2007.
- [156] WANG, M-T.; LIU, M-H.; CHRIS WANG, C. R.; CHANG, S. Y. Silver-coated gold nanoparticles as concentrating probes and matrices for surface-assisted laser desorption/ionization mass spectrometric analysis of aminoglycosides. **J. Amer. Soc. Mass Spectrometry**, v. 20, n. 10, p. 1925-1932, Oct 2009.
- [157] DERBYSHIRE, N. et al. Indirect spectrophotometric determination of gentamicina and vancomycin antibiotics based on their oxidation by potassium permanganate. **Cent. Eur. J.Chem**, v. 4, n.4, p.708-722, 2006.
- [158] QIN, L.; ZENG, G.; LAI, C.; HUANG, D.; ZHANG, C.; XU, P.; HU, T.; LIU, X.; CHENG, M.; LIU, Y.; HU, L.; ZHOU, Y. A visual application of gold nanoparticles: Simple, reliable and sensitive detection of kanamycin based on hydrogen-bonding recognition. **Sens. Actuator B-Chem**, v. 243, p. 946–954, May 2017.
- [159] ANHA, N. T. N.; CHOWDHURYA, A. D.; DOONGA, R. Highly sensitive and selective detection of mercury ions using N, S-codoped graphene quantum dots and its paper strip based sensing application in wastewater. **Sens. Actuator B-Chem**, v. 252, p. 1169–1178, Nov 2017.
- [160] NISHI, H.; NAKAMURA, K.; NAKAI, H.; SATO, T. Enantiomer separation by capillary electrophoresis using DEAE-Dextran and aminoglycosidic antibiotics. **Chromatographia**, v. 43, n. (7-8), p. 426–430, Oct 1996.
- [161] TALBOT, P. A. Potentiation of aminoglycoside-induced neuromuscular blockade by protons in vitro and in vivo. **J. Pharmacol. Exp. Ther**, v. 241, n. 2, p. 686–694, May 1987.

11 Attachment

A Published papers

Journal of Luminescence 179 (2016) 83–92



Contents lists available at ScienceDirect

Journal of Luminescence

journal homepage: www.elsevier.com/locate/jlumin



Full Length Article

Different approaches for sensing captopril based on functionalized graphene quantum dots as photoluminescent probe



Carlos A.T. Toloza^a, Sarzamin Khan^a, Renan L.D. Silva^a, Eric C. Romani^b,
F.L. Freire Jr.^b, Ricardo Q. Aucélio^{a,*}

^a Department of Chemistry, Pontifical Catholic University of Rio de Janeiro (PUC-Rio), Rio de Janeiro 22451-900, Brazil

^b Department of Physics, Pontifical Catholic University of Rio de Janeiro (PUC-Rio), Rio de Janeiro 22451-900, Brazil

Graphical Abstract

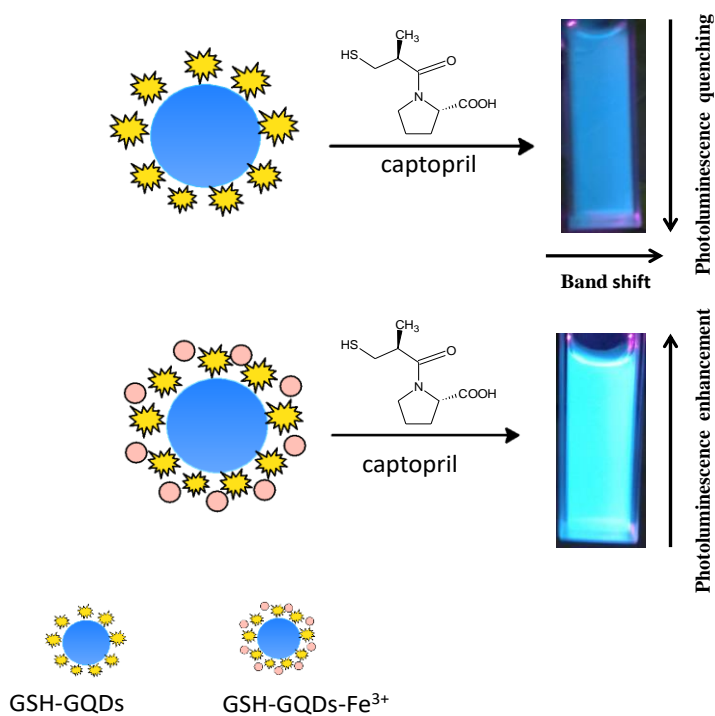


Figure A.1. Published paper: Chapter 4.



Contents lists available at ScienceDirect

Microchemical Journal

journal homepage: www.elsevier.com/locate/microc

Photoluminescence suppression effect caused by histamine on amino-functionalized graphene quantum dots with the mediation of Fe^{3+} , Cu^{2+} , Eu^{3+} : Application in the analysis of spoiled tuna fish



Carlos A.T. Toloza^a, Sarzamin Khan^{a,b}, Renan L.D. Silva^a, Eric C. Romani^b, Dunieskys G. Larrude^d, Sonia R.W. Louro^c, Fernando L. Freire Júnior^c, Ricardo Q. Aucélio^{a,*}

^a Department of Chemistry, Pontifical Catholic University of Rio de Janeiro (PUC-Rio), Rio de Janeiro 22451-900, Brazil

^b Department of Chemistry, University of Swabi, Khyber Pakhtunkhwa, Anbar 23561, Pakistan

^c Department of Physics, Pontifical Catholic University of Rio de Janeiro (PUC-Rio), Rio de Janeiro 22451-900, Brazil

^d MackGraph - Graphene and Nanomaterials Research Center, Mackenzie University, 01302-907 São Paulo, Brazil

Graphical Abstract

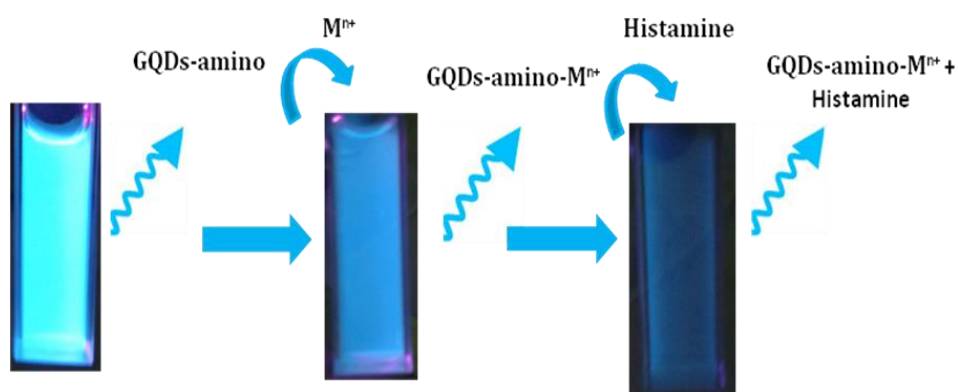
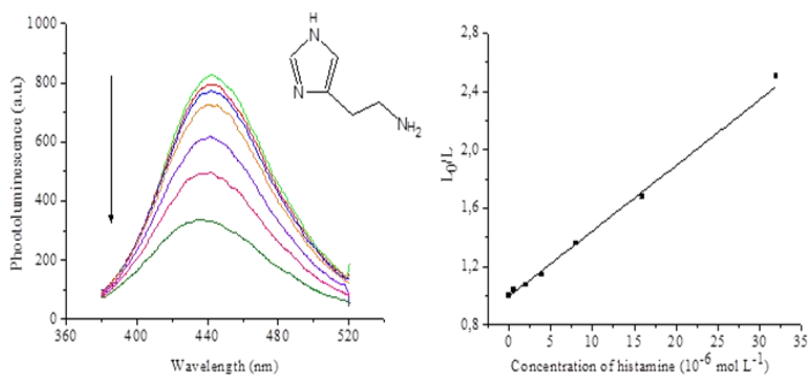


Figure A. 2. Published paper: Chapter 5.

B

Participation in Congress

Oral presentation

Quantum dots de grafeno funcionalizados com glutathione como sonda fotoluminescente para histamina, histidina, cisteína e captopril. In: **38º Reuniao Anual da Sociedade Brasileira de Quimica**, 2015, Águas de Lindóia.

Amino-functionalized graphene quantum dots coupled with gold nanoparticles: a first evaluation as an analytical probe. **46th World Chemistry Congress, 40º Reuniao Anual da Sociedade Brasileira de Química and IUPAC 49th General Assembly**, 2017, São Paulo, Brasil.

Desenvolvimento de métodos analíticos utilizando pontos quânticos de grafeno como sonda fotoluminescente para determinação de analitos do tipo biológicos e farmacológicos. **I Jornada de Pós-Graduação e Pesquisa-DQ/PUC-Rio**, Rio de Janeiro, 2017, Brasil.

Posters

Quantum dots de grafeno funcionalizados com glutathione como sonda fotoluminescente para histamina, histidina, cisteína e captopril. In: **38º Reuniao Anual da Sociedade Brasileira de Quimica**, 2015, Águas de Lindóia.

Estudo da influência de surfactantes catiônicos na fotoluminescência de pontos quânticos de grafeno funcionalizados com glutathione. In: **15º Encontro Regional da Sociedade Brasileira de Quimica**, 2016, Rio de Janeiro.

Quantum dots de grafeno funcionalizados com glutathione mediado por Fe^{3+} como sonda fotoluminescente para a determinação de histamina. In: **17º Encontro Nacional de Química Analítica**, 2016, Florianópolis, Brasil

Determinação da concentração micelar crítica de surfactantes catiônicos utilizando pontos quânticos de grafeno amino-funcionalizados como sonda fotoluminescente. In: **17º Encontro Nacional de Química Analítica**, 2016, Florianópolis, Brasil

Amino-functionalized graphene quantum dots coupled with gold nanoparticles: a first evaluation as an analytical probe. **46th World Chemistry Congress, 40^o Reunião Anual da Sociedade Brasileira de Química and IUPAC 49th General Assembly**, 2017, São Paulo, Brasil.

Determinação de canamicina por extração em fase sólida com um polímero de impressão molecular e detecção com sonda fotoluminescente de pontos quânticos de grafeno acoplados com nanopartículas de ouro. In: **16^o Encontro Regional da Sociedade Brasileira de Química**, 2017, Rio de Janeiro.